SIMULATION AND USE OF A CENTRIFUGAL BIOREACTOR FOR MAMMALIAN CELL AND TISSUE CULTURE

By

CHRISTOPHER JAMES DETZEL

A dissertation submitted in partial fulfillment of
the requirements for the degree of

DOCTOR OF PHILOSOPHY

WASHINGTON STATE UNIVERSITY
School of Chemical Engineering and Bioengineering

AUGUST 2009

To the Faculty of Washington State University:

The members of the Committee appointed to examine the dissertation of CHRISTOPHER JAMES DETZEL find it satisfactory and recommend that it be accepted.

_____
Bernard J. Van Wie, Ph.D., Chair

_____
Cornelius F. Ivory, Ph.D.

_____
Nehal Abu-Lail, Ph.D.

_____
William C. Davis, Ph.D.

ACKNOWLEDGEMENTS

I would first like to thank my committee members; Dr. Bernie Van Wie, Dr. Neil Ivory, Dr. Bill Davis, and Dr. Nehal Abu-Lail, for their willingness to serve on my committee and their support and encouragement throughout my graduate career. As I move on from WSU, I will take with me many memories and lessons which are sure to be invaluable as I progress through my professional career. Thank you.

I especially thank Dr. Van Wie, the Voiland School of Chemical Engineering and Bioengineering, and the NIH Biotechnology Training Program who provided the encouragement and support to pursue a project which I was passionate and excited about. I would also like to thank the Cartilage Repair group at Genzyme, particularly Mike DiMicco and Gloria Matthews, for all the training and support they provided not only during my two internships, but any time I had a question or concern. This made all the difference in my ability and desire to complete the Ph.D. program at WSU.

I would also like to thank Kurt Hutchinson of the College of Engineering and Architecture Engineering Shops for his ability to take my ideas and return modified functional reactors which enhanced my research. Also, I must recognize the Voiland School of Chemical Engineering and Bioengineering office staff; Jo Ann, Diana, and Senja, thank you for helping me with all the little things, without which I would still be stuck at the starting line. This department surely would not be the same without you.

Finally, I must thank my friends and family. Without the many friends I have made along the way I appreciate the times we blew off steam together, as well as the times we spent discussing research. Without you guys, Jeff in particular, my ideas would never have matured into attainable research objectives, thanks for always forcing me to rethink ideas and pushing me

to excel. Last, but certainly not least, my dad Jack, my mom Terry, and my sister Clara I can not thank you enough. You have been an inspiration at various times throughout this process and your continued encouragement and love have provided needed support as I journeyed through what at times seemed an endless amount of school. Mom and Dad, without you none of this would have been possible, thank you.

SIMULATION AND USE OF A CENTRIFUGAL BIOREACTOR

FOR MAMMALIAN CELL AND TISSUE CULTURE

Abstract

by Christopher James Detzel, Ph.D.
Washington State University
August 2009

Chair: Bernard J. Van Wie

Increasing demand for tissue, proteins, and antibodies derived from mammalian cell cultures is limited by low protein yields and growth rates. Host productivity may be increased through genomic modification while volumetric productivity is maximized through novel bioreactor research to increase maximum cell culture density. The centrifugal bioreactor (CCBR) is a novel bioreactor which can be used to increases volumetric productivity by maintaining densities above 10^8 cells/mL using counter-flow centrifugation to immobilize cells.

System rotation necessary for cell immobilization in the CCBR results in Coriolis forces that affect momentum transport. At operating conditions typical of cell culture, 300-1200 RPM and inlet velocities of 4-16 cm/s, Coriolis forces dominate system fluid dynamics and streamlines indicate preferential flow along the leading wall of the reactor to the chamber's widest point, after which fluid transverses the reactor to the trailing wall. This unique flow profile is completely disrupted during cell culture leading to uniform flow through the cell bed creating a well mixed fluidized bed of cells. These phenomena are observed experimentally and in numerical simulation results of the CCBR reactor chamber during operation.

The uniform high cell density fluidized bed in the CCBR is maintained through convective transport of nutrients and metabolites allowing for the development of a hybridoma growth rate kinetic model from low density batch experiments. A model has been developed to predict glucose, lactate, ammonium ion, and monoclonal antibody concentrations during reactor operation within 13%. This model provides a tool to determine necessary dilution rates to ensure the maximum cellular growth rate is maintained at any operational cell density.

Finally, CCBR applicability has been expanded to include adherent cells which can be mechanically stimulated with multiple mechanical forces resulting from the unique method of cell immobilization. Isolated chondrocytes were stimulated with hydrostatic pressure and low shear during 3 weeks cultures, after which a solid tissue construct resulted. When compared with pellet cultures, the CCBR constructs contained similar levels of both glycosaminoglycan and collagen, per weight of DNA. Optimization of mechanical force magnitudes and stimulation regimens will provide a unique model system for the future study of cartilage development and degeneration.

TABLE OF CONTENTS

Page

LIST OF TABLES

CHAPTER II

CHAPTER IV

LIST OF FIGURES

CHAPTER II

Dedication

This dissertation is dedicated to my mother,

my father, and my grandmother

who never had a doubt.

CHAPTER I

Introduction

The demand for complex proteins, particularly monoclonal antibodies (mAbs), for use in therapeutic and diagnostic purposes is rising exponentially, and is forecasted to reach $16 billion in 2010 [1-4]. Many new therapeutics require post-translational modifications such as glycosylation, phosphorylation, and folding which necessitates the use of mammalian hosts to produce functional proteins [5-7]. The use of mammalian hosts such as hybridoma or CHO cells for protein production is hampered by both low cellular growth and protein production rates when compared with traditional bacterial cultures. Combination of these limitations with high dose requirements of protein therapeutics inhibits the ability to achieve demand using current production technologies [1]. To meet the production need a two pronged approach has been suggested: first, increasing specific cellular productivity and second, increasing overall culture volumetric productivity [8, 9]. Cellular productivity can be increased through manipulation of the host genome, while volumetric productivity is a direct reflection of increasing maximum viable cell density within a bioreactor.

There are numerous techniques to produce proteins from mammalian cell culture, each with varying maximum cell densities and their own individual limitations. Batch culture of mammalian cells is restricted by low viability and densities on the order of 10^6 cells/mL which limits overall culture productivity [10-12]. Use of a continuous stirred batch reactor (CSTR) increases overall culture viability due to constant medium flow rates, but cell wash-out at these flow rates limits densities to 10^6 cells/mL [13]. Thus, further increases in cell density and volumetric productivity require a cell retention device or other method to prevent cells from leaving the culture chamber. CSTR density can be increased in this manner to a maximum of

10^7 cells/mL if cells are separated from spent medium and returned to the reactor with the use of a vertical sedimentation column [13, 14]. However, cell density must be increased further in order to meet production needs.

Reactors such as hollow fiber bioreactors (HFBs) and packed bed bioreactors (PBRs) prevent cell wash-out with the use of a porous membranes or packing, respectively. The use of these mechanical cell immobilization techniques increases maximum cell density to 10^8 cells/mL, but membrane fouling, diffusional limitations, and non-uniform gradients lead to heterogeneous product formation and inactive portions of the biomass [3, 7, 15-18].

Another bioreactor capable of exceeding densities of 10^8 cells/mL is the continuous centrifugal bioreactor (CCBR) [19-21]. The CCBR is similar to the Beckman Elutriation System as well as a reactor patented by Kinetic Biosystems, Inc. for wastewater remediation employing high density bacterial cell culture [22, 23]. Diffusional limitations associated with HFBs and PBRs are eliminated by the CCBR as convective transport of nutrients and metabolites to and from cells is the result of the unique method of cell immobilization. The CCBR immobilizes cells by increasing the settling force through centrifugation to offset drag forces resulting from high medium flow rates required to sustain cell viability at such extreme densities.

System rotation provides a centrifugal force which when balanced with drag and buoyant forces acting in the opposite direction will result in cell immobilization. Fluid is supplied to the reactor chamber at the point furthest from the center of rotation, thus both drag and centrifugal force decrease as the distance from the center of rotation is decreased. Due to the conical shape of the CCBR, drag and centrifugal force decrease at the same rate resulting in a uniform density of cells being retained during culture. A complete discussion of the design

equations on which counter flow centrifugation, and hence the CCBR is based is given by Sanderson and Bird (1977) [24].

The objective of this dissertation is to characterize high density cell suspension culture in the CCBR and expand the use of the CCBR in novel directions, namely to adherent cell lines such as chondrocytes. The fluid dynamics of the CCBR are characterized in two manuscripts. Chapter II, "A Study of the Coriolis Effect on the Fluid Flow Profile in a Centrifugal Bioreactor," characterizes the flow profile through the CCBR without the presence of cells, and Chapter III, "Characterization of Fluid Flow through a Centrifugal Bioreactor during High Cell Density Culture," describes changes in the fluid flow profile as cells are introduced to the system for long term culture. An analysis of hybridoma cellular growth rate is presented in Chapter IV, "Kinetic Simulation of a Centrifugal Bioreactor for High Population Density Hybridoma Culture," and characterizes the cellular growth kinetics and inhibition due to substrate and metabolite concentrations during high density CCBR culture. Finally, Chapter V, "Use of a Centrifugal Bioreactor for Cartilaginous Tissue Formation from Isolated Chondrocytes," shows the versatility of the CCBR beyond suspension culture, as a cartilage-like tissue is produced from isolated chondrocytes after 3 weeks of culture.

Chapters II and III examine the fluid dynamic of the CCBR during operation with and without cells. The fluid dynamics are of interest as system rotation required for cell immobilization and high density culture give rise to Coriolis forces which effect momentum transport. Various rotating systems including rotating wall bioreactors, cooling passages in turbine blades, and rotating pipes or fluidized beds all present unique fluid flow profiles which are attributed to the Coriolis effect [25-28]. The Coriolis force acts at right angles to the axis of

rotation and the local velocity vector, and is termed a fictitious force as it is a deflecting force doing no work on a material element [29].

Chapter II characterizes the extent to which Coriolis forces affect momentum transport during reactor operation without the presence of cells. It is shown through numerical simulation and experimental observations that for CCBR operating conditions used in cell culture the flow profile is dominated by Coriolis forces. The observed flow profile indicates a preferential flow of fluid along the leading wall of the reactor chamber to its widest point, after which fluid crosses the reactor before flowing out of the chamber. Chapter III then examines how this flow profile is changed by the presence of cells. Again, with the use of numerical simulations and experimental observations it is shown that the flow profile observed in a reactor without cells is completely disrupted during cell culture, and a uniform flow of fluid through the cell bed is observed. The flow profile in the presence of cells is similar to that which would be observed in a traditional fluidized bed, where flow through the bed is uniform to suspend the particles against the gravitational field.

Chapters II and III provide insight into the fluid dynamics of the CCBR indicating that during culture cells are retained in the reactor chamber as a high density fluidized bed of cells. A consequence of maintaining high density cell cultures is that environmental conditions can rapidly change leading to cell growth rate inhibition. Chapter IV provides the results of a kinetic model developed from low density batch cultures which is applicable to the high density CCBR. The model is able to predict glucose, lactate, ammonium ion, and mAb concentrations based on a measured, or expected, cell concentrations and dilution rate. The most valuable use of the developed kinetic model is to predict the magnitude of growth rate inhibition for particular

culture densities and dilution rates, this allows inhibitory conditions to be identified and avoided ensuring maximum growth rate associated mAb production is maintained.

The final objective of this dissertation is to expand the use of the CCBR beyond high density cell suspension culture. Chapter V presents work in which isolated chondrocytes cultured in the CCBR produce a cartilaginous tissue after 3 weeks. There is a need to investigate novel systems for cartilage culture as cartilage degeneration due to trauma, disease, or age induced osteoarthritis affects the majority of individuals around the world at some point in their lives. Novel *in vitro* chondrocyte culture techniques have the possibility to provide further insight into cartilage degeneration and development and must be studied. The CCBR is such a system with the potential to stimulate chondrogenesis through the simultaneous application of multiple mechanical forces.

In vivo cartilage is constantly subjected to mechanical forces including shear, hydrostatic pressure, and compression; which when applied individually have been shown to increase the incorporation of extracellular matrix proteins indicative of healthy cartilage [30-32]. Due to the unique method of cell immobilization the CCBR provides hydrostatic pressure as a result of system rotation, and fluid flow through the reactor chamber provides a shear force on cells and tissues during culture. Few bioreactors are capable of simultaneous application of mechanical forces *in situ* [33-35], making the CCBR a unique model system to study cartilage. Results presented in Chapter V show the cartilage construct developed in the CCBR is similar in GAG and collagen content when compared with pellet culture constructs. The high density chondrocyte constructs subjected to mechanical forces in the CCBR did not undergo further chondrogenesis as was hypothesized. However, optimization of the process and continued

exploitation of the unique properties of the CCBR allow for tissue culture to remain a viable possibility which must be investigated during future research.

References

1. Werner, R. G., Economic aspects of commercial manufacture of biopharmaceuticals. *J Biotechnol* **2004,** 113, (1-3), 171-82.

2. Dalm, M. C.; Cuijten, S. M. R.; van Grunsven, W. M. J.; Tramper, J.; Martens, D. E., Effect of feed and bleed rate on hybridoma cells in an acoustic perfusion bioreactor: part I. Cell density, viability, and cell-cycle distribution. *Biotechnology and Bioengineering* **2004,** 88, (5), 547-57.

3. Golmakany, N.; Rasaee, M. J.; Furouzandeh, M.; Shojaosadati, S. A.; Kashanian, S.; Omidfar, K., Continuous production of monoclonal antibody in a packed-bed bioreactor. *Biotechnolgy and Applied Biochemistry* **2005,** 41, (3), 273-8.

4. Andersen, D. C.; Reilly, D. E., Production technologies for monoclonal antibodies and their fragments. *Current Opinion in Biotechnology* **2004,** 15, (5), 456-62.

5. Mercille, S.; Johnson, M.; Lanthier, S.; Kamen, A. A.; Massie, B., Understanding Factors that Limit the Productivity of Suspension-Based Perfusion Cultures Operated at High Medium Renewal Rates. *Biotechnology and Bioengineering* **2000,** 67, (4), 435-450.

6. Chen, K.; Liu, Q.; Xie, L.; Sharp, P. A.; Wang, D. I. C., Engineering of a mammalian cell line for reduction of lactate formation and high monoclonal antibody production. *Biotechnology and Bioengineering* **2001,** 72, (1), 55-61.

7. Meuwly, F.; Ruffieux, P. A.; Kadouri, A.; von Stockar, U., Packed-bed bioreactors for mammalian cell culture: bioprocess and biomedical applications. *Biotechnol Adv* **2007,** 25, (1), 45-56.

8. Kundu, P. K.; Prasad, N. S.; Electricwala, S. E.; Varma, R.; Datta, D., Getting higher yields of monoclonal antibody in culture. *Indian Journal of Physiology and Pharmacology* **1998,** 42, (2), 155-71.

9. Tang, Y. J.; Ohashi, R.; Hamel, J. F., Perfusion culture of hybridoma cells for hyperproduction of IgG(2a) monoclonal antibody in a wave bioreactor-perfusion culture system. *Biotechnol Prog* **2007,** 23, (1), 255-64.

10. Xie, L.; Wang, D. I. C., High Cell Density and High Monoclonal Antibody Production Through Medium Design and Rational Control in a Bioreactor. *Biotechnology and Bioengineering* **1996,** 51, (6), 725-729.

11. Jan, D. C. H.; Petch, D. A.; Huzel, N.; Butler, M., The Effect of Dissolved Oxygen on the Metabolic Profile of a Murine Hybridoma Grown in Serum-Free Medium in Continuous Culture. *Biotechnology and Bioengineering* **1997,** 54, (2), 153-164.

12. Miller, W. M.; Blanch, H. W.; Wilke, C. R., A kinetic analysis of hybridoma growth and metabolism in batch and continuous suspension culture: Effect of nutrient concentration, dilution rate, and pH. *Biotechnol Bioeng* **1988,** 32, (8), 947-65.

13. Kim, B. J.; Chang, H. N.; Oh, D. J., Application of a cell-once-through perfusion strategy for production of recombinant antibody from rCHO cells in a Centritech Lab II centrifuge system. *Biotechnol Prog* **2007,** 23, (5), 1186-97.

14. Batt, B. C.; Davis, R. H.; Kompala, D. S., Inclined sedimentation for selective retention of viable hybridomas in a continuous suspension bioreactor. *Biotechnology Progress* **1990,** 6, (6), 458-64.

15. Yang, P.; Teo, W.-K.; Ting, Y.-P., Design and performance study of a novel immobilized hollow fiber membrane bioreactor. *Bioresource Technology* **2006,** 97, (1), 39-46.

16. Yang, S.-T.; Luo, J.; Chen, C., A fibrous-bed bioreactor for continuous production of monoclonal antibody by hybridoma. *Advances in Biochemical Engineering/Biotechnology* **2004,** 87, 61-96.

17. Gramer, M. J.; Britton, T. L., Antibody production by a hybridoma cell line at high cell density is limited by two independent mechanisms. *Biotechnology and Bioengineering* **2002,** 79, (3), 277-83.

18. Jackson, L. R.; Trudel, L. J.; Fox, J. G.; Lipman, N. S., Evaluation of hollow fiber bioreactors as an alternative to murine ascites production for small scale monoclonal antibody production. *Journal of Immunological Methods* **1996,** 189, (2), 217-31.

19. Detzel, C. J.; Mason, D. J.; Davis, W. C.; van Wie, B. J., Kinetic Simulation of a Centrifugal Bioreactor for High Population Density Hybridoma Culture. *Biotechnology Progress* **2009,** In Press.

20. Van Wie, B. J.; Brouns, T. M.; Elliott, M. L.; Davis, W. C., A Novel Continuous Centrifugal Bioreactor for High-Density Cultivation of Mammalian and Microbial Cells. *Biotechnology and Bioengineering* **1991,** 38, (10), 1190-1202.

21. Van Wie, B. J.; Hustvedt, E. L., Particle interaction effects on blood cell sedimentation and separations. *Biorheology* **1988,** 25, (4), 651-62.

22. Herman, H. H. Centrifugal Fermentation Processes. US Patent #: 5,622,819, April 22, 1997.

23. Herman, H. H.; Lin, W.; Petrecca, P. J.; Herman, T. M.; Bates, C.; Simmons, R.; Houghton, J., Centrifugal Bioreactors and Their Application in Remediation. In 2001; Vol. 11, pp 15-33.

24. Sanderson, R. J.; Bird, K. E., Cell Separations by Counterflow Centrifugation. *Methods in Cell Biology* **1977,** 15, 1-14.

25. Tekriwal, P., Centrifugal Buoyancy Driven Reverse Flow Near The Leading Wall of a Rotating Cooling Passage. In *ASME Challenges of High Temperature Heat Transfer Equipment*, 1994; Vol. 282.

26. Valentine, D. T.; Jahnke, C. C., Coriolis Effect on Transport Phenomena in Rotating Systems: A Numerical Study. In *Centrifugal Materials Processing, [Proceedings of the Iternational Workshop on Materials Processing at High Gravity]*, Potsdam, NY, June 2-7, 1996, 1997.

27. Hammond, T. G.; Hammond, J. M., Optimized suspension culture: the rotating-wall vessel. *American Journal of Physiology-Renal Physiology* **2001,** 281, (1), F12-F25.

28. Chevray, R.; Chan, Y. N. I.; Hill, F. B., Dynamics of bubbles and entrained particles in the rotating fluidized bed. In 1980; Vol. 26, pp 390-398.

29. Batchelor, G. K., *An Introduction to Fluid Dynamics*. Cambridge University Press: Cambridge, UK, 1967.

30. Saini, S.; Wick, T. M., Concentric cylinder bioreactor for production of tissue engineered cartilage: effect of seeding density and hydrodynamic loading on construct development. *Biotechnol Prog* **2003,** 19, (2), 510-21.

31. Smith, R. L.; Carter, D. R.; Schurman, D. J., Pressure and shear differentially alter human articular chondrocyte metabolism: a review. *Clin Orthop Relat Res* **2004**, (427 Suppl), S89-95.

32. Li, Z.; Yao, S.; Alini, M.; Grad, S., Different response of articular chondrocyte subpopulations to surface motion. *Osteoarthritis Cartilage* **2007,** 15, (9), 1034-41.

33. Schulz, R. M.; Wustneck, N.; van Donkelaar, C. C.; Shelton, J. C.; Bader, A., Development and validation of a novel bioreactor system for load- and perfusion-controlled tissue engineering of chondrocyte-constructs. *Biotechnol Bioeng* **2008,** 101, (4), 714-28.

34. Lagana, K.; Moretti, M.; Dubini, G.; Raimondi, M. T., A new bioreactor for the controlled application of complex mechanical stimuli for cartilage tissue engineering. *Proc Inst Mech Eng [H]* **2008,** 222, (5), 705-15.

35. Wang, P. Y.; Chow, H. H.; Tsai, W. B.; Fang, H. W., Modulation of gene expression of rabbit chondrocytes by dynamic compression in polyurethane scaffolds with collagen gel encapsulation. *J Biomater Appl* **2009,** 23, (4), 347-66.

CHAPTER II

A Study of the Coriolis Effect on the Fluid Flow Profile in a Centrifugal Bioreactor

Christopher J. Detzel, Michael R. Thorson, Bernard J. Van Wie and Cornelius F. Ivory*

Voiland School of Chemical Engineering and Bioengineering, Washington State University

P.O. Box 642710, Pullman, Washington 99164-2710, USA

* Corresponding Author: Tel.: +1 509 335 7716; email: cfivory@wsu.edu

Running Title: Fluid Flow Profile in a Centrifugal Bioreactor

Accepted for publication in *Biotechnology Progress*, January 2009

Abstract

Increasing demand for tissues, proteins, and antibodies derived from cell culture is necessitating the development and implementation of high cell density bioreactors. A system for studying high density culture is the centrifugal bioreactor (CCBR) which retains cells by increasing settling velocities through system rotation, thereby eliminating diffusional limitations associated with mechanical cell retention devices. This paper focuses on the fluid mechanics of the CCBR system by considering Coriolis effects. Such considerations for centrifugal bioprocessing have heretofore been ignored; therefore a simpler analysis of an empty chamber will be performed. Comparisons are made between numerical simulations and bromophenol blue dye injection experiments. For the non-rotating bioreactor with an inlet velocity of 4.3 cm/s, both the numerical and experimental results show the formation of a teardrop shaped plume of dye following streamlines through the reactor. However, as the reactor is rotated the simulation predicts the development of vortices and a flow profile dominated by Coriolis forces resulting in

the majority of flow up the leading wall of the reactor as dye initially enters the chamber, results are confirmed by experimental observations. As the reactor continues to fill with dye, the simulation predicts dye movement up both walls while experimental observations show the reactor fills with dye from the exit to the inlet. Differences between the simulation and experimental observations can be explained by excessive diffusion required for simulation convergence, and a slight density difference between dyed and un-dyed solutions. Implications of the results on practical bioreactor use are also discussed.

Keywords: Coriolis effect; Centrifugal Bioreactor; High Density; Numerical Simulation

1. Introduction

The demand for recombinant proteins, specifically monoclonal antibodies (mAbs), has risen dramatically due to the increased requirement for both therapeutic and diagnostic applications (1-3). Traditional methods of mAb production are incapable of meeting production needs exceeding hundreds of kilograms per year. As such, two approaches to obtain higher mAb yields have been proposed: i) increasing cellular productivity, and ii) increasing volumetric productivity (3). The former involves modification of the growth environment, cellular genome, or other such approach; while increasing volumetric productivity can be achieved through increasing bioreactor cell density.

Traditional cultures of mammalian cells, such as batch and continuous stirred-tank reactors are limited to densities on the order of 10^6 cells/mL, and can reach as high as 10^7 cells/mL if cells are separated from spent medium and returned to the reactor (4-8). Further increases in cellular density necessitate cell immobilization to prevent wash-out as medium

throughput must also be increased. Packed bed bioreactors (PBR) and hollow fiber bioreactors (HFB) both immobilize cells with the use of porous packing or membranes, increasing cellular densities to 10^8 cells/mL while maintaining cell viability (9-12). However, these reactors are commonly plagued by heterogeneous product formation and inactive portions of the biomass due to membrane fouling, mass transport limitations, and non-uniform gradients of inhibitors and nutrients (11, 13, 14).

Another type of bioreactor capable of maintaining cell densities above 10^8 cells/mL is the continuous centrifugal bioreactor (CCBR). The CCBR has been researched by Van Wie *et al.* (1991) and is similar to the Beckman Elutriation System and a centrifugal bioreactor patented by Kinetic Biosystems, Inc., with applications in remediation processes through immobilized bacterial culture (15-17). During operation the CCBR spins in the horizontal plane while medium is supplied to the rotating reactor at the point furthest from the center of rotation, as shown in Fig. 1, through flexible tubing and the use of an anti-twister mechanism (18). Limitations associated with other high density bioreactors are circumvented through the use of non-mechanical cell immobilization. Within the CCBR cells are retained by balancing centrifugal forces with opposing buoyancy and drag forces. Consequently, diffusional limitations are eliminated as medium must flow around each cell to result in a drag force opposite the centrifugal force, thus providing convective transport of nutrients and wastes to and from cells. This results in a uniform environment which can be controlled with dilution rate allowing maintenance of optimal growth conditions for each individual cell during culture.

Of particular interest in this paper is the unique fluid flow profile within the CCBR which results from the Coriolis effect on momentum transport due to reactor rotation. Rotating systems ranging from cooling passages in modern turbine blades to rotating wall bioreactors, rotating

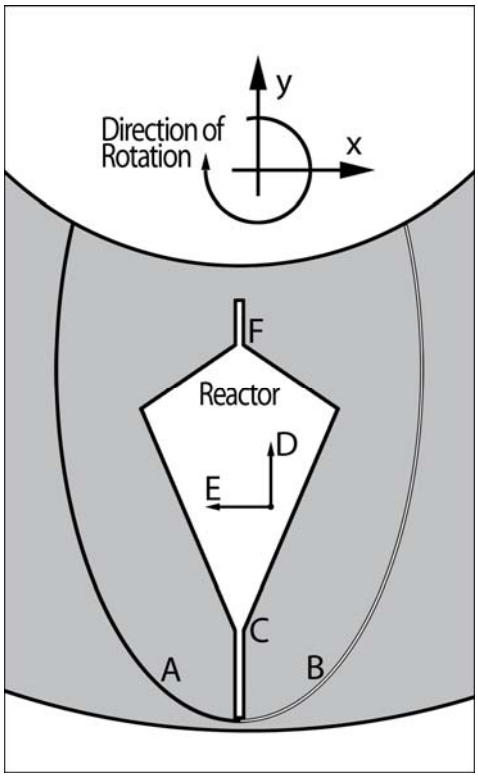

Figure 1. An illustration of the CCBR reactor and rotor (shaded region) showing the unit axis along with the direction of rotation. Inlet tubes feeding the reactor with BPB dyed solution (A) and colorless solution (B) join before the reactor inlet (C). Fluid flows through the reactor radially inward (D) resulting in Coriolis forces with direction to the left (E). The reactor outlet (F) as well as both inlet tubes are bundled and remain untangled during operation through the use of an anti-twister mechanism.

pipes and rotating fluidized beds all have a unique fluid flow profile due to Coriolis forces (19-22). The Coriolis effect is the result of a fictitious force acting at right angles to the axis of rotation and the local velocity vector, the force is termed fictitious as it is a deflecting force which does no work on a material element (23). The change in motion attributed to the Coriolis force is opposite the direction of motion, thus a system rotating anticlockwise will produce a Coriolis force to the right in an attempt to restore a material element to its original position upon the projected path of a circle, completed with the same frequency as that of system rotation (23). This paper will compare experimental observations with numerical simulation results for a CCBR operating at conditions typical of those for cell culture to understand the contribution of Coriolis forces to the CCBR's fluid flow profile. The implications of this modeling effort in the CCBR without cells will be discussed in addition to the framework for future more complex studies including various cell types and population densities.

2. Theory

The phenomenon examined in this paper is the laminar flow profile in the plane normal to the axis of rotation in a conical shaped CCBR. Solid body rotation where motion is referenced to axes rotating along with the bulk fluid gives rise to Coriolis and centrifugal forces, both of which must be assumed to act on the fluid (23). The three dimensional Navier-Stokes equation for incompressible fluid flow in a system rotating about a vertical axis is shown in Eq. 1:

$$\frac{\partial u}{\partial t} + u \cdot \nabla u = -\frac{1}{\rho}\nabla P - 2\Omega \times u + \mu \nabla^2 u \qquad (1)$$

where u is the velocity field vector, ρ is the density, Ω is the angular velocity of the system, μ is

the viscosity of the fluid, and P is the modified pressure accounting for both gravitational and centrifugal forces, as shown in Eq. 2:

$$P \equiv p - \frac{1}{2}\rho\Omega^2 r^2 - \rho g z \qquad (2)$$

where p is the background pressure field, r is the distance from the axis of rotation, and z is distance in the opposite direction to the earth's gravitational field (20, 23, 24). Of particular interest in the application of the CCBR is the Coriolis term, $-2\Omega \times u$, and how this acceleration is translated into a force which drives fluid flow within the CCBR during operation.

Coriolis forces result from a combination of fluid velocity and the angular velocity of the system, resulting in the object following a curved path as viewed from the rotating reference frame. This paper will examine a CCBR void of cells showing how Coriolis forces deflect the flow profile of a stationary system and results in a unique fluid flow profile that will need to be considered when working with high cell density reactor cultures.

3. Materials and Methods

3.1 Solution Preparation

Two liters of pH 7.0 buffer solution were made through combination of 1 L of 100 mM potassium dihydrogen phosphate, 582 mL of 100 mM sodium hydroxide, and 418 mL of deionized water (25). This solution was split in half and Bromophenyl Blue (BPB) was added to one of the solutions to a final concentration of 3 x 10^{-5} M providing a dark contrast solution with which the flow profile within the CCBR chamber could be visualized.

3.2 Visualization of Flow Profile

The equipment used for this research was a COBE® Spectra™ Apheresis System (Gambro BCT Inc., Lakewood, CO) manufactured for use as a blood separation device. The platelet elutriation chamber supplied as part of the Cell Purging tubing set (Gambro BCT Inc., Lakewood, CO) was replaced with a similar smooth-walled chamber cut out of a rectangular piece of acrylic. The acrylic block has two threaded bolt holes on either side of the chamber for attachment to the rotor. During operation fluid supply and removal is through flexible tubing and the use of an anti-twister mechanism previously described by Van Wie *et al.* (15, 18).

Prior to starting reactor rotation, one inlet line was filled with the BPB solution to the point where the two inlet lines converge just before entering the reactor, as shown in Figure 1, while the other inlet line and the entire volume of the reactor were filled with the colorless pH buffered solution. Reactor rotation and fluid flow were started and steady state was reached after about one minute, after which BPB solution was delivered to the reactor at a set inlet flow velocity. Flow profiles were visualized using a variable frequency strobe light and recorded using a Cannon Digital Rebel XT camera (Cannon U.S.A., Inc., Lake Success, NY).

3.3 Simulation Simplification and Setup

The 3D geometry needed for mathematical simulation was created in COMSOL 3.3 by drawing one half of the 2D projection in the x-y plane, Fig. 2 (inset). The 2D figure has corresponding radii and heights to that indicated in Fig. 2. This 2D drawing was then rotated 360 degrees about the reactor midline to create a 3D representation of the conical reactor in COMSOL.

The COMSOL physics used for modeling fluid flow was that of the Incompressible Navier-Stokes approach applied to 3D geometry. Within the subdomain settings of this fluid

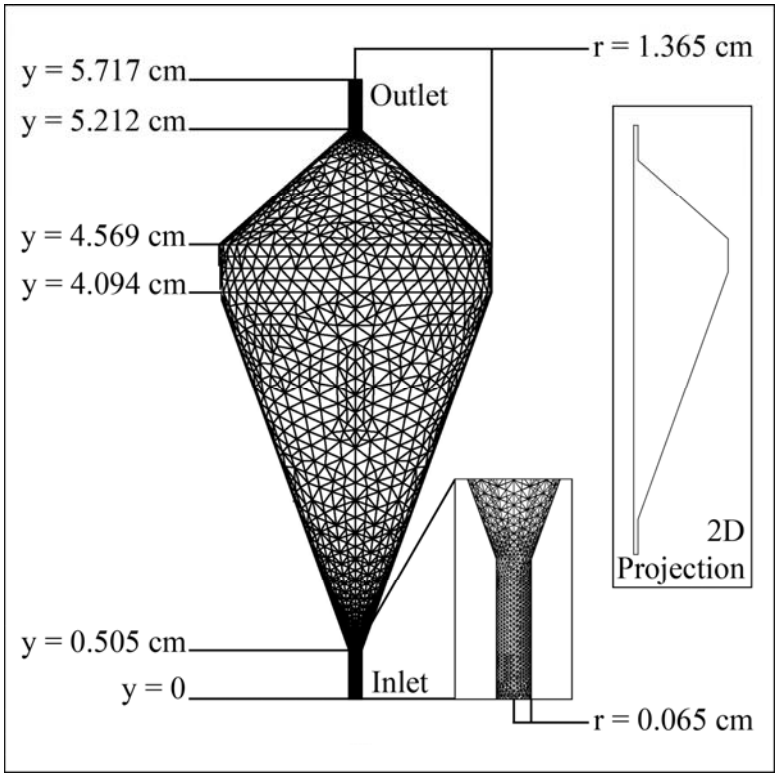

Figure 2. A representation of the centrifugal bioreactor with the computational mesh used to find the Navier-Stokes numerical solution is shown. The total number of nodes and boundary conditions used in numerical simulations are found in Table 1. Radii for the identical inlet and outlet tubes and the widest part of the reactor are indicated, where all other radii vary linearly with height. Corresponding distances from the start of the inlet tube are also indicated. Rotating the 2D projection, inset, creates the 3D reactor for simulation in COMSOL.

Table 1. Boundary conditions and mesh Density for simulations COMSOL v3.3

	Boundary Condition	# of Nodes
Navier-Stokes		86,037
Inlet	y-Velocity 0 – 16 cm/s	
Outlet	Pressure 0 Pa	
All Other Boundaries	No Slip	
Convection & Diffusion		431,402
Inlet	Concentration 0.03 mol/m^3	
Outlet	Convective Flux [a]	
All Other Boundaries	Insulation/Symmetry	

[a] Convective flux boundary conditions assumes $N_i \cdot n = C_i u \cdot n$

flow physics, the density and dynamic viscosity were set to that of water at 25° C assuming these properties were not appreciably changed by the dilute salt solution. The Coriolis forces $F_x = -2\Omega\rho u_y$ and $F_y = 2\Omega\rho u_x$ were added into the sub-domain settings panel as volume forces resulting from the Navier-Stokes Equation for a rotating frame of reference, Eq. 1; density was added to F_x and F_y to coincide with the format of the conservation equation used by COMSOL. All boundary conditions were specified as indicated in Table 1. The inlet boundary condition varied between 0 – 16 cm/s and was specified based on inlet volumetric flow rates and cross-sectional areas used in CCBR practice. A pressure of zero was specified at the outlet boundary which specifies fluid outflow is determined by the influx of material and is particularly appropriate when the outflow may not be normal to the boundary. An example of a mesh configuration used in the Navier-Stokes simulation is shown in Fig. 2 and consists of 86,037 total nodes. The fluid flow simulation was solved for inlet velocities of 0-16 cm/s and RPM in the 0-1200 range. To represent experimental procedures, a transient convection and diffusion mass balance was added to the 3D geometry in COMSOL.

The convection and diffusion portion of the numerical model was coupled to the steady state Navier-Stokes solution and was used to represent the transient flow of dye at steady state through the reactor as was done in experimental procedures. The fluid flow and mass balance simulations were solved independently. First, the Navier-Stokes steady state solution was found, and the resultant fluid flow profile was then coupled to the convection diffusion module by equating the velocity variables of the two modules. The convection and diffusion mass balance was then solved, resulting in mass convection along steady state fluid flow streamlines. Finally, before solving the mass balance an isotropic diffusion coefficient of 5×10^{-10} m^2/s was specified

for BPB as reported by Kakizak *et al.* (26). A constant concentration of BPB was specified at the inlet while a convective flux condition was assumed at the outlet.

The convective flux boundary condition assumes all mass passing through this boundary is due to convection, thereby eliminating transport due to diffusion. A Peclet number is determined by using an outlet velocity of 4.3 cm/s, an outlet diameter of 0.13 cm as the characteristic length, and the diffusion coefficient specified above. The Peclet number value thereby determined is 1×10^5 indicating that mass transport due to convection is much larger than that due to diffusion, which supports the use of the convective flux boundary condition at the outlet. This boundary condition is particularly useful when an outlet concentration is unknown.

As shown in Table 1 the mesh used in the simulation of the convection and diffusional mass balance consists of more nodes (431,402) than that used in the solution of the Navier-Stokes equation because there are fewer independent variables resulting in a less complex system of equations. The transient mass balance has an initial condition of zero BPB throughout the reactor and at time zero a constant concentration of BPB is allowed to enter the reactor and travel along Navier-Stokes solution streamlines. This provided a numerical representation for comparison with experimental observations.

4. Results and Discussion

4.1 Fluid Flow Simulation

Streamlines depicting the steady-state solution of fluid flow through the CCBR at a constant inlet velocity of 4.3 cm/s and various rates of rotation are shown in Fig. 3 and 4. Streamlines depicting the numerical results of the fluid flow are viewed along the z-axis, the axis

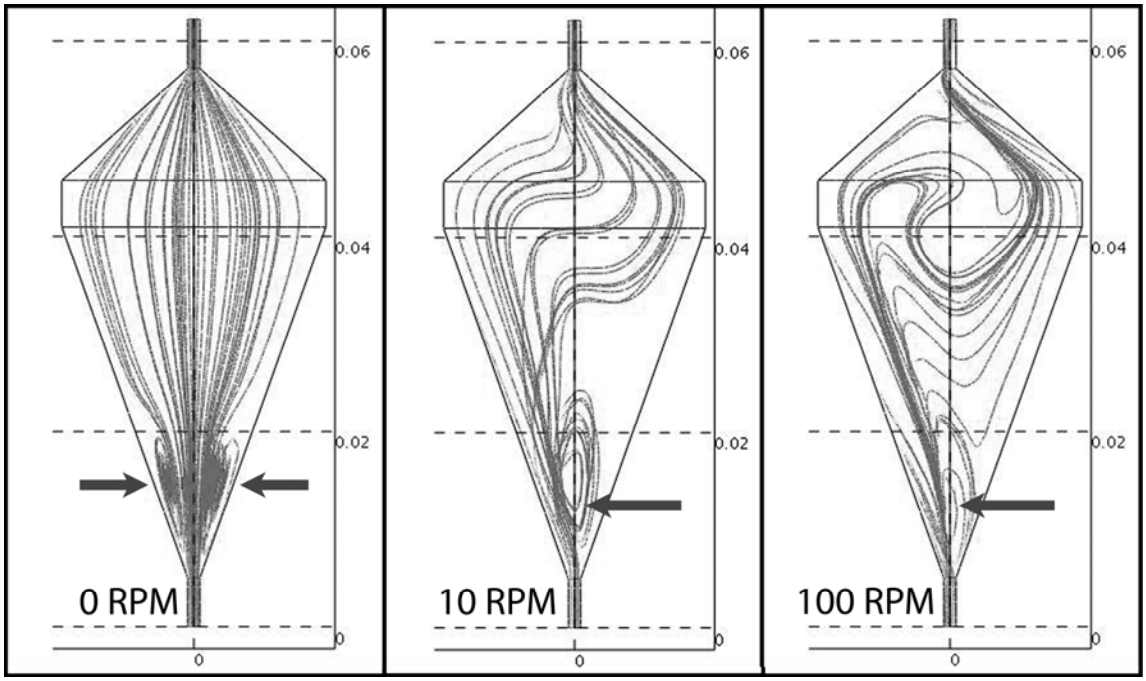

Figure 3. The steady state numerical solutions of the Navier-Stokes flow profile with constant inlet velocity of 4.3 cm/s and increasing system RPM is shown by streamlines depicting the development of a flow profile dominated by Coriolis forces. The size scale is indicated on the right of each figure in terms of meters from the start of the inlet tube of the reactor.

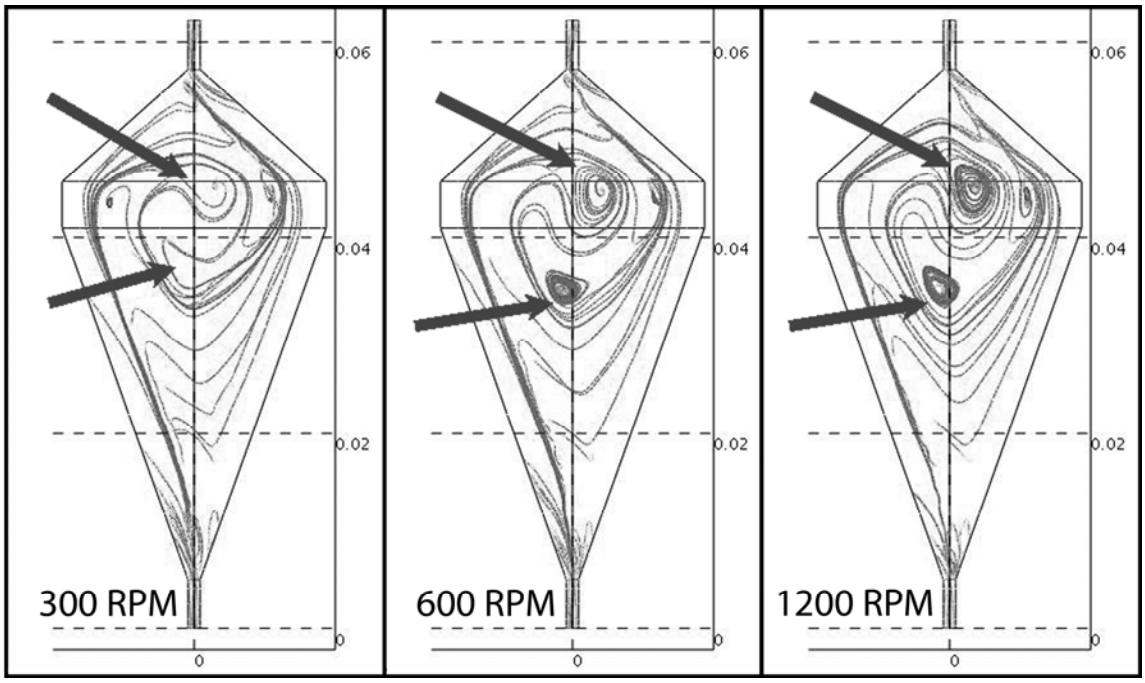

Figure 4. Steady state numerical solutions of the Navier-Stokes flow profile indicating minimal alteration of the overall flow profile as RPM is increased above 100 RPM. The increasing definition and size of vortices results from Coriolis forces causing a material element to complete the projected circle with higher frequency at higher system RPM. Each solution is solved with a constant inlet velocity of 4.3 cm/s.

parallel to that of rotation; all streamlines throughout the 3D geometry are visible although the perspective directly along the z-axis gives the appearance of only a single plane. Shown in Fig. 3 is the effect of Coriolis forces on flow through the reactor as rotor speed is increased. However, once a flow pattern dominated by Coriolis forces is established further increasing the RPM has little effect on the overall flow profile, as shown in Fig. 4.

The importance of Coriolis forces on a fluid flow profile within a system can be estimated through evaluation of the dimensionless Rossby number. The Rossby number is the ratio of the magnitudes of inertial forces to Coriolis forces and is defined as $U/L\Omega$; where U is a representative velocity, L is the unit length over which velocity varies, and Ω is a the angular velocity (23). Coriolis forces are likely to have minimal effect when the Rossby number is much greater than unity, however Coriolis forces will contribute significantly to a system's flow pattern when the Rossby number is much less than one. Taking an inlet velocity of 4.3 cm/s and assuming uniform flow across the reactor cross-section a velocity of 9.4×10^{-3} cm/s will result at the widest point in the reactor which has a diameter of 2.73 cm. Using the diameter as the unit length scale the Rossby number will be 3×10^{-4} and 5×10^{-5} for 100 and 600 RPM, respectively; indicating Coriolis forces will have a significant role in determining the overall fluid flow profile in the CCBR.

As seen in the 0 RPM case, Fig. 3, the resulting profile shows laminar streamlines moving from the inlet to the outlet of the reactor as would be expected for fluid passing through an object with diverging walls. Streamlines show two distinct vortices just past the inlet, shown with arrows in Fig. 3 (0 RPM), which are actually part of a torus-shaped vortex ring around the central axis and the inlet stream. This vortex is the result of a laminar jet of fluid entering the reactor with a velocity of 4.3 cm/s which results in a Reynolds number of 54 within the inlet tube

leading to the reactor. The vortex indicating the presence of the laminar jet is first observed at an inlet velocity of 3.8 cm/s in numerical simulations. Increasing the fluid velocity to 10 cm/s will result in a jet of fluid passing directly through the reactor and a vortex spanning its entire length, Reynolds numbers for each inlet velocity are 48 and 127, respectively.

Shown in the center pane in Fig. 3 is the steady state solution for 10 RPM. At this low RPM the effects of Coriolis forces on the flow profile can be visualized. Deflection of streamlines to the left can be attributed to Coriolis forces by confirming the direction of the force for clockwise rotation and fluid flow toward the axis of rotation, in which case the right-hand rule indicates fluid movement will be deflected to the left. At 10 RPM the streamlines appear to be deflected toward the left wall of the reactor as the walls diverge. At the widest point in the reactor the streamlines predict fluid movement from the left to the right before exiting the reactor. The Rossby number for and inlet velocity of 4.3 cm/s and 10 RPM is 3×10^{-3} when calculated as before. Observing the results at this low RPM indicate Coriolis forces are not yet dominating the flow pattern and inertial forces still contribute to the observed flow profile.

Increasing system rotation to 100 RPM streamlines indicate that immediately after entering the reactor fluid is forced to the left wall, as a result of the increased magnitude of the Coriolis force. Fluid movement in the region of the reactor with the largest cross-section moves in a continuous path from the left wall to the right wall of the reactor along a skewed "N" shaped path before flowing out of the reactor. Finally, although there is minimal flow directly above the inlet as Coriolis forces have caused the majority of flow along the left wall of the reactor, at both 10 and 100 RPM a slowly rotating vortex is predicted in this region as indicated with the arrow.

The development of vortices at the widest cross-section of the reactor becomes apparent when comparing the results of 100 RPM with the higher RPMs shown in Fig. 4. The flow profile remains largely unchanged as RPM increases from 100 to 300; fluid enters the reactor, flows up the leading wall, transverses the reactor to the trailing wall at the widest cross-section, before flowing out of the chamber. This overall flow profile remains largely unchanged as system RPM is increased even further, as shown in Fig. 4. The major change in the flow profile as RPM is increased is the vortices shown with arrows in Fig. 4 become progressively more well defined.

Initially, at low RPM the vortices are not clearly defined, but their development can be seen as RPM is increased from 100 to 600. As suggested by Batchelor (1967) because the Coriolis force is linear in velocity and tends to change the direction of all velocity components at the same rate; an element whose motion is dominated by the Coriolis force moves in a circular path where the projected circle is completed with a frequency of the same order as that of system rotation (23). Therefore, as the system rotation frequency is increased, material elements complete their circular path faster adding definition to the vortices.

A similar situation occurs when system rotation is held constant and inlet velocity is varied. Simulations show that as inlet flow velocity is varied from 1.1 cm/s to 16.4 cm/s, inlet tube Reynolds number varies between 14 and 220, and the resultant flow profile differs very little from that that simulated in Fig. 4 (600 RPM). In the previous discussion decreasing rotation rate from 600 to 10 showed a marked change in the overall flow profile with respect to RPM, and a similar effect would be expected for fluid velocity as both RPM and fluid velocity are linear with respect to Coriolis force magnitude. However, decreasing fluid velocity at a constant rotation rate enhances the importance of Coriolis forces due a reduction of the Rossby

number. Therefore, to increase the importance of inertial forces compared to Coriolis forces the Rossby number must be increased. A Rossby number near unity would diminish the effect of Coriolis forces, however it would require an inlet velocity on the order of 10^5 cm/s, in turn resulting in a turbulent system and invalidate the results presented in this paper. Consequently a change in fluid velocity over the range of possible operating conditions is not expected to have an effect on the observed fluid flow pattern within the CCBR.

4.2 Simulation Convergence

Convergence of the numerical solution was verified in the following ways: According to a theorem by Baker (1983), the error in a finite element solution converges to zero, as the number of elements increases without limit (27). Therefore, a solution obtained using an infinite number of nodes corresponds to the real solution, which can be found by extrapolation from a set of solutions using a large, but finite number of elements. This extrapolation is carried out at a single point in the domain by plotting the velocity against the inverse of the number of elements in several simulations with increasing numbers of elements. Then the y-intercept of this plot is found as the reciprocal of the number of elements goes to zero and is assumed to be the solution for an infinite number of elements corresponding to the real solution. The difference between the projected solution and a given simulation solution is then assumed to be a measure of error at that point, and the error of the entire solution can be estimated by summing the error over multiple points chosen throughout the domain.

The formula for the normalized error of a particular solution with respect to the projected solution is given in Eq. 3,

$$\varepsilon_S = \frac{\sum_{i=1}^{I} \sqrt{\Delta U_i \cdot \Delta U_i}}{\sum_{i=1}^{I} \sqrt{U_{i,P} \cdot U_{i,P}}} = \frac{\sum_{i=1}^{I} \sqrt{\left(u_{i,P} - u_{i,S}\right)^2 + \left(v_{i,P} - v_{i,S}\right)^2 + \left(w_{i,P} - w_{i,S}\right)^2}}{\sum_{i=1}^{I} \sqrt{u_{i,P}^2 + v_{i,P}^2 + w_{i,P}^2}} \qquad (3)$$

where U is the velocity vector and ΔU is the difference between the velocity vector at the projected solution P and a simulation solution S, u v and w are the individual velocity components in the x y and z direction respectively, i represents an individual point, and I is the total number of discrete points within the domain for which the velocity vector is evaluated. The coordinates of the discrete points are independent of the computational mesh.

The projected solution for this system was found at 2,347 individual points using a linear regression to find the y-intercept. The velocity profile for CCBR settings of 600 RPM and 4.3 cm/s was solved using a total of ten different meshes with the number of nodes ranging from 786 to 86,000; where the y-intercept was estimated using the 5 highest mesh densities. Using this method the percent error in the solution was reduced from 38% using 786 nodes to 2.9% when 86,000 nodes were used. Following the same procedure for the non-rotating case and an inlet velocity of 4.3 cm/s yielded a similar result as percent error was reduced from 23% at 786 nodes to 1.6% at 86,000 nodes. The error associated with 44,500 nodes was 3.9% and 1.6% in the rotating and non-rotating case, respectively, and it can be seen that increasing the number of nodes above 44,500 did not substantially alter the numerical solution.

4.3 Experimental Comparisons

Coupling a transient convection and diffusion mass balance to the steady state Navier-Stokes simulation allows direct comparison with the transient dye injection experimental results. This comparison was initially made for the case of the non-rotating system; numerical and experimental results are shown 15 seconds after initial dye injection in Fig. 5A and Fig. 5B,

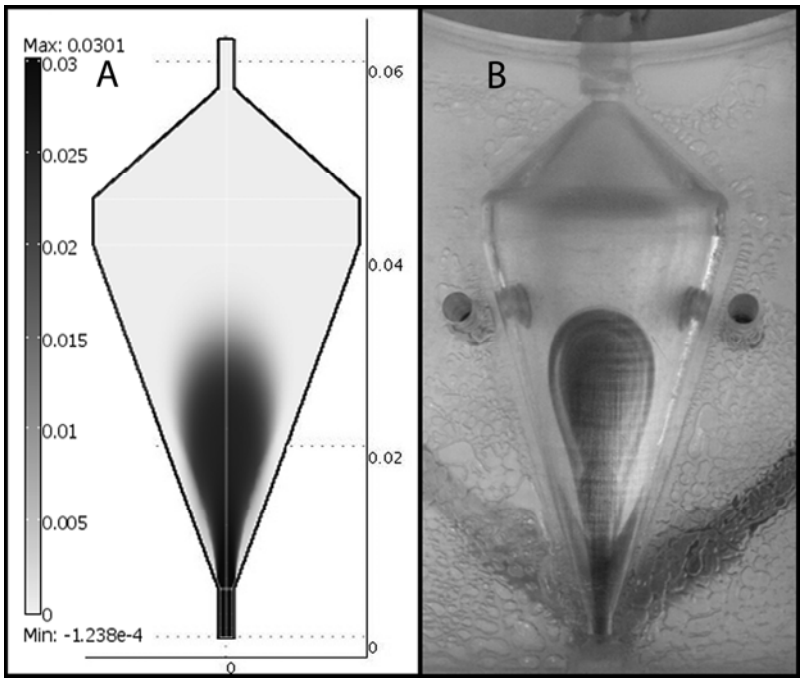

Figure 5. A comparison of the numerical solution (A) and experimental results (B) as dye enters a non-rotating CCBR when viewed from a position parallel to the axis of rotation. Both the numerical and experimental results depict the same profile as dye follows streamlines through the reactor for a system without rotation.

respectively. Numerical results depict concentrations of dye at the middle of the reactor, a single x-y plane at z=0 is shown. Concentrations are reflected as a grayscale gradient from white to black corresponding to low (0 mol/m^3) and high (0.03 mol/m^3) concentrations of BPB dye. The gradient spans -1 x 10^{-4} to 0.0301 mol/m^3 in Fig. 5 which includes non-real negative concentrations and concentrations greater than that of the inlet that result from numerical noise at individual nodes within the global mesh as the simulation attempts to close the mass balance.

In the comparison at 0 RPM it can be seen that the numerical solution, Fig. 5 (A), shows that as dye enters the reactor little dispersions just past the inlet is observed as the dye is entering as a fluid jet, as previously discussed for an inlet velocity of 4.3 cm/s. Both the numerical, Fig. 5 (A) and experimental observations, Fig. 5 (B), indicate a narrow stream of dye entering the reactor before the dye cloud expands radially through momentum transport as the walls of the reactor diverge. However, neither dye injection result shows the presence of the vortex created by the fluid jet. Under current conditions visualization of this vortex would be difficult as the amount of dye entering the vortex would not provide sufficient contrast until it appeared as dispersion due to the nature of the transient dye injection experiment. At later time points (not shown) dye follows steady state streamlines, Fig. 3 (A), expanding radially until reaching the widest cross-section of the reactor then converging on the reactor exit, an observation consistent between both the numerical and experimental results.

During typical hybridoma culture, or other cultures with similarly sized cells, the CCBR operating conditions are set at a rotor speed of 600 RPM and an inlet velocity of 4.3 cm/s. These conditions can provide a cell density near 1 x 10^8 cells/mL; which can be maintained for weeks with adequate nutrient supply (15). Increasing rotor RPM at constant inlet velocity leads to a new equilibrium between centrifugal force and drag force which increases the overall culture

density. However, as previously discussed, the overall flow profile remains largely unchanged within the standard cell culture operating conditions of 300-1200 RPM and 4.3 - 16.4 cm/s. Therefore, a single operating condition of 600 RPM and an inlet velocity 4.3 cm/s will be used for comparison of experimental results with the numerical simulation as the system rotates.

Results at 600 RPM and an inlet fluid velocity of 4.3 cm/s for the numerical solution of the transient dye injection experiment are shown in Fig. 6. The simulated solution at 40 seconds shows dye enters the reactor and flows up the leading wall along streamlines depicted in Fig. 4 (600 RPM). At 70 seconds dye has reached the top of the reactor and follows streamlines around the vortex indicated with the upper arrow in Fig. 4 (600RPM), forcing dye back toward the inlet and the right wall of the reactor. Additionally at this time point dye is observed to the right of the reactor midline, just past the inlet, as diffusion has caused dye to enter streamlines moving toward the right wall of the reactor. At the final time point of 150 seconds, Fig. 6 (150s), the simulation indicates high concentrations of dye throughout the reactor save for the area containing the two vortices indicated with arrows in Fig. 4 (600 RPM). Additionally, dye that has reached the top of the reactor by 70 seconds is not directly entering streamlines exiting the reactor; instead a high concentration front has formed against streamlines moving along the right wall resulting in dye being pulled around the vortices shown in Fig. 4 (600 RPM).

Comparisons of numerical results with experimental observations exhibit similarities and differences. Experimental observations in Fig. 7 (40s) coincide with the simulation at 40 seconds, showing the inlet dye stream moving up the left wall of the reactor. Similarly at 70 seconds experimental results show dye continues to enter the reactor and flow up the left wall as a thin stream. However, rather than follow simulated streamlines around vortices as predicted in the numerical simulation, experimental results show dye completely filling the top portion of the

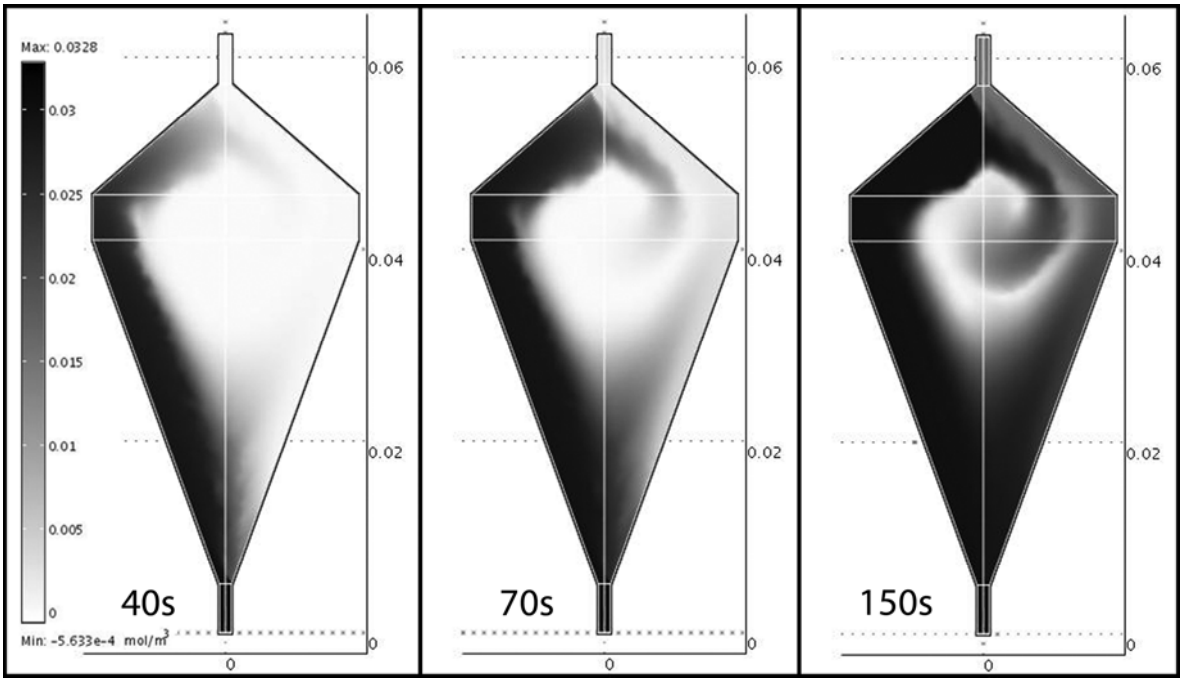

Figure 6. Numerical simulation of the convection and diffusion mass balance at various time points after dye is initially pumped into the reactor with an inlet velocity of 4.3 cm/s and a rotation rate of 600 RPM. The early time point shows dye following streamlines along the left side of the reactor, while later time points show significant diffusion of dye toward the reactor midline which is then pulled along streamlines moving up the right wall of the CCBR.

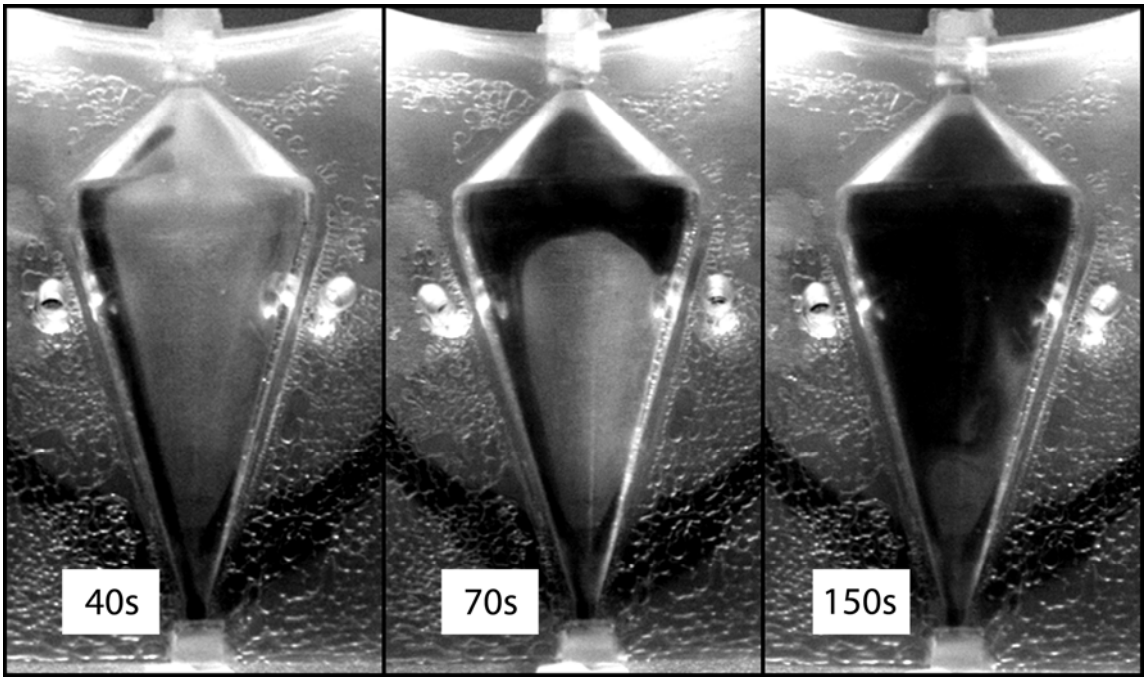

Figure 7. Experimental results as dye is pumped with a constant inlet velocity of 4.3 cm/s into a reactor rotating at 600 RPM. As predicted by the simulation, dye initially moves up the left side of the reactor due to the Coriolis forces and then begins to fill from the top (exit) to the bottom (inlet) of the reactor.

reactor which continues until the entire reactor is dyed, as seen at 150 seconds, Fig. 7 (150s). At 150 seconds the majority of the reactor is colored indicating high concentrations of BPB throughout except for a small area along the right wall near the inlet. This small un-dyed area near the inlet does not persist and is just the last portion of the reactor to be dyed during experiments, making it unlikely dye is excluded from this region as the result of a vortex not seen in the simulation.

The most notable difference between the simulation and experimental observations is that the simulation predicts diffusion of dye away from the stream moving up the left wall of the reactor. In the simulation this diffusion results in dye moving up both walls, where as experimentally a sharp interface between the dyed and undyed fluid along the left wall is observed throughout the experiment. The sharp interface implies minimal diffusion during experimentation and that diffusion is over predicted in the simulation. As stated earlier the diffusion coefficient for BPB is small, 5 x 10^{-10} m^2/s, however, COMSOL was unable to find a solution without the use of artificial diffusion in the transient mass balance portion of the simulation. Isotropic artificial diffusion which increases diffusion near steep gradients, which are shown experimentally as the sharp dyed interfaces, was then used in the simulation making convergence possible.

COMSOL defines isotropic artificial diffusion, D_{art}, as

$$D_{art} = \delta_{ID} h |\beta| \tag{4}$$

where δ_{ID} is the isotropic diffusion tuning parameter, h is the local mesh size, and β is the magnitude of the convective velocity which can be found using the sum of the squares of the x, y, and z velocity components. The general transient mass balance on the species is then changed

from its general form in Eq. 5 to include the artificial diffusion term as shown in Eq. 6

$$\frac{\partial c}{\partial t} + \nabla \cdot \left(-D\nabla c\right) = R - u \cdot \nabla c \tag{5}$$

$$\frac{\partial c}{\partial t} + \nabla \cdot \left(-\left(D + D_{art}\right)\nabla c\right) = R - u \cdot \nabla c \tag{6}$$

where D is the original diffusion within the system, c is concentration, R is a generation term, and u is the velocity vector. From Eq. 4 it can be seen that the amount of added artificial diffusion will not be globally uniform, but instead is locally dependant on the mesh size and convective velocity at a particular node in the system. As a result, COMSOL adds artificial diffusion only when needed to reach a solution. Using a tuning parameter of 0.1, the lowest value resulting in a simulation solution, the maximum artificial diffusion is on the order of 10^{-7} m^2/sec which is needed primarily along the left wall of the reactor immediately past the inlet. Throughout the remainder of the reactor a minimum artificial diffusion of at least 10^{-8} m^2/sec is needed. In either case the diffusion in the system is increased by multiple orders of magnitude over that of BPB alone. Thus increased diffusion due to artificial diffusion is likely leading to the presence of BPB along the right wall of the reactor which is not seen experimentally.

When comparing numerical and experimental results of dye movement through the reactor an important consideration is that simulation results show a single x-y plane at z=0 (middle of the reactor) and experimental observations are viewed along the z axis through the thickness of the reactor. Although only similar viewpoints can be shown results should be comparable according to the Taylor-Proudman theorem. For very small values of the Rossby number, the Taylor-Proudman theorem specifies that the derivatives of velocity in the axial direction become small, and thus particle velocity becomes 2D in the plane perpendicular to the

axis of rotation (23, 28, 29). Therefore, all x-y planes independent of position along the z-axis should have the same concentration profile. Numerical results support the Taylor-Proudman theorem and upon viewing multiple planes along the z-axis the same concentration profile is observed, data not shown. Therefore, the full thickness view of the reactor in experimental results is likely not contributing to discrepancies with the numerical simulation results.

Discrepancies observed between the numerical solution and experimental observations are likely attributed to the following reasons. First, diffusion of dye within the mass balance simulation is several orders of magnitude larger than the actual diffusion of BPB due to artificial diffusion required for simulation convergence. Diffusion of dye across the reactor midline is seen in the simulation initially at 40 seconds and is far more apparent at later time points which results in dye flowing up the right wall of the reactor, whereas experimental observations show no diffusion of dye away from the inlet stream. It may be possible to eliminate artificial diffusion by increasing the number of mesh nodes within the 3D representation of the CCBR. However, this is not possible at the current time due to simulation complexity and current computer hardware limitations, as the number of nodes which can be solved in a particular simulation is limited by the amount of physical memory (16GB).

Second, it has been observed during experimentation that addition of BPB to the buffered salt solution reduced density when compared with the original solution. This was confirmed through visualization of dye moving through the reactor with the inlet and outlet rotated 90 degrees into the plane of Earth's gravity. If density remained constant with the addition of BPB the same results shown in Fig. 5 are expected. However, when the reactor is oriented with the inlet below the outlet, dye quickly rises as a thin stream; and if the orientation is reversed, inlet is above the outlet, dye fills the reactor as a single front across the entire cross section. These two

observations lead to the conclusion that the solution containing BPB is less dense than the original buffer solution. The solution density difference may begin to explain why the reactor fills with dye from the exit to the inlet moving as a sharp front during experiments with system rotation as the less dense dyed solution is retained in the region with the lowest gravitational force. Despite these differences agreement between the numerical and experimental observations has been shown for the transient movement of dye through the reactor, particularly at initial time points before density and diffusion can affect results.

4.4 Implications in CCBR Bioprocessing

The importance of this work lies first in its implications for fluid mechanics of flow through rotating vessels. During operation with system rotation one might assume flow to be only slightly effected by system rotation. However, experimental observations indicate a radical change in the fluid flow profile over that observed without any rotation and this flow profile remains largely unchanged at all possible operation conditions for high cell density culture. With the use of simulation software such as the COMSOL package used in this work rapid assessment of a wide range of operating conditions is possible enhancing the understanding of system fluid dynamics and how the rotating and non-rotating systems differ.

This work also has CCBR bioprocessing implications for priming and flushing operations to change system concentrations of different nutrients or metabolites. The rate at which these operations can be accomplished is impacted by the amount of time it takes for the reactor to reach a steady state concentration coinciding with a new inlet concentration. One typically uses a residence time analysis to determine the required time for reactor concentrations to reach a new steady state. If we were to consider complete replacement of the CCBR contents in a plug flow system it would take one time constant or about 240 sec for the system to reach a new steady

state at an inlet velocity of 4.3 cm/s. However, it is believed that a mixed flow is more likely as modeling and experimental results clearly indicate fluid enters the reactor and flows up the left wall, then cross the chamber before exiting which clearly is not plug flow behavior. Preliminary experiments to investigate mixing within the CCBR (data not shown) indicate a behavior similar to that of a CSTR where it will take three time constants to displace 95% of the reactor contents.

Second, this work has implications as to how the fluid flow profile impacts cell culture conditions and how the flow profile presented here will be affected by different cell culture parameters such as cell size and population density. For very small cells, such as bacteria, it is possible they will be entrained in fluid and either pass directly through the reactor along predicted streamlines or be trapped in vortices where cells are less likely to receive ample fresh medium needed for growth. Disrupting the CCBR flow profile that results because of the Coriolis effect with the use of a mesh or by other mechanical means may become necessary to retain small diameter cells for long term high density culture.

How larger mammalian cells are retained in the CCBR and their effect on the flow profile is of interest from a bioprocessing standpoint. Preliminary research has shown that a dense culture of mammalian cells is retained in the lower half of the reactor furthest from the center of rotation, while a fluid head space fills the remainder of the reactor. One of two hypotheses is likely to explain how high density cultures of cells are retained in the CCBR. First, if the fluid flow profile shown in Fig. 4 (600) does not change a circular flow pattern of cells may develop. Cells would be pulled up the left wall in the stream containing most of the fluid flow to the widest point where they begin to move across the reactor. As cells move toward the right wall the direction of the drag force is no longer opposite the centrifugal force and cells would begin to settle toward the inlet along the right wall of the reactor. After settling to near the inlet the cells

would once again be pulled up the left wall creating a constant circulation of cells during culture. The second hypothesis would be that larger cells disrupt the simulated flow profile resulting in a more uniformly dispersed flow profile throughout the cell bed rather than the scenario where entrant fluid flows solely along the left wall. However, it is entirely possible that a more elaborate flow profile, similar to that shown in this manuscript, may be maintained in the fluid head space above the cells. Therefore, a future simulation study will be conducted in which cell sedimentation analysis for dense suspensions is added to the Coriolis force analysis presented here and compared with experimental cell cultures at varying operating conditions.

5. Concluding Remarks

The effect of Coriolis forces on the fluid flow profile within a rotating bioreactor has been studied through mathematical simulation and dye injection experiments. Numerical simulations at an inlet flow rate of 4.3 cm/s and various RPMs in a 12.5 mL CCBR chamber show the development of a fluid flow profile dominated by Coriolis forces as RPMs are increased from 0 to 100. Rotation speeds above 100 RPM result in a flow pattern largely unchanged with the exception of vortices becoming more defined. Additionally, it has been shown though a discussion of the Rossby number and numerical simulations that the inlet fluid velocity has little effect on the fluid flow profile at a particular RPM.

Coupling of the steady-state Navier-Stokes solution with a mass balance provides a method for direct comparison with transient dye injection experiments. Comparisons between the numerical and experimental results, particularly at early time points, show agreement in the how dye enters the reactor and flows up the leading wall due to Coriolis forces. Discrepancies arise at later time points when the dye has almost completely filled the reactor and can be

attributed to experimental fluid density differences and excessive diffusion within the numerical simulation.

The diffusion of BPB is dominated by artificial diffusion in the simulation as it increases the diffusion coefficient of BPB by several orders of magnitude which is required for solution convergence. The use of artificial diffusion results in simulation prediction of dye movement up both walls of the reactor as dye diffuses into streamlines moving along the right wall; this is opposed to experimental observations where diffusion of dye from the inlet stream along the left wall is never observed. Similarly, a slight difference in density between dyed and undyed solutions contributes to differences in the final concentration profiles of dye within the reactor. Experimentally, the reactor is filled with dye as a sharp front moves from the outlet to the inlet, likely due to a difference in solution density which is exaggerated in the presence of centrifugal acceleration; while the simulation predicts a low concentration of dye will be maintained within vortices over time.

In conclusion, these results show that the overall flow profile of an empty CCBR chamber is dominated by Coriolis forces over the range of operation typically used in high density culture. The mixing that occurs in the system has obvious implications for priming or flushing the reactor as the system behaves similar to a well stirred vessel requiring three time constants or more for adjustment of reactor nutrient concentrations during operation. Further investigation will be done on how the fluid flow profile described in this paper is affected by the presence of cells being cultured in the reactor. It is hypothesized that smaller microbial cultures will be affected more by Coriolis forces as they are carried along streamlines, possibly becoming trapped in vortices. For larger cells, it is expected that studies will reveal that larger sedimentation rates will serve to deflect streamlines affected by Coriolis forces leading to a more

uniform flow around each cell resulting in a stable homogeneous fluidized bed of cells. In either case understanding how cells affect the surprising fluid flow pattern presented in this paper will provide valuable insight for predicting operating conditions capable of retaining a variety of different cells.

Acknowledgements

The authors would like to acknowledge support from the Biotechnology Training Grant, NIH 5T32-GM008336-16 for graduate student support and the Washington State Voiland School of Chemical Engineering and Bioengineering for graduate student support and supplies. Equipment in the form of the COBE Spectra Apheresis System and supplies in the form of Cell Purging tubing sets and corporate technical research staff consultation are a result of a donation by Gambro BCT Inc., Lakewood, CO. Mr. R. Hutchinson of the Washington State University College of Engineering and Architecture Machine Shop was helpful in design and fabrication of the CCBR chambers that were used in these experiments.

References

1. Landry, Y.; Gies, J. P., Drugs and their molecular targets: an updated overview. *Fundam Clin Pharmacol* **2008,** 22, (1), 1-18.

2. Migliore, C.; Giordano, S., Molecular cancer therapy: Can our expectation be MET? *Eur J Cancer* **2008**.

3. Kundu, P. K.; Prasad, N. S.; Electricwala, S. E.; Varma, R.; Datta, D., Getting higher yields of monoclonal antibody in culture. *Indian Journal of Physiology and Pharmacology* **1998,** 42, (2), 155-71.

4. Batt, B. C.; Davis, R. H.; Kompala, D. S., Inclined sedimentation for selective retention of viable hybridomas in a continuous suspension bioreactor. *Biotechnology Progress* **1990,** 6, (6), 458-64.

5. Jan, D. C. H.; Petch, D. A.; Huzel, N.; Butler, M., The Effect of Dissolved Oxygen on the Metabolic Profile of a Murine Hybridoma Grown in Serum-Free Medium in Continuous Culture. *Biotechnology and Bioengineering* **1997,** 54, (2), 153-164.

6. Kim, B. J.; Chang, H. N.; Oh, D. J., Application of a cell-once-through perfusion strategy for production of recombinant antibody from rCHO cells in a Centritech Lab II centrifuge system. *Biotechnol Prog* **2007,** 23, (5), 1186-97.

7. Miller, W. M.; Blanch, H. W.; Wilke, C. R., A kinetic analysis of hybridoma growth and metabolism in batch and continuous suspension culture: effect of nutrient concentration, dilution rate, and pH. Reprinted from Biotechnology and Bioengineering, Vol. 32, Pp 947-965 (1988). *Biotechnology and Bioengineering* **2000,** 67, (6), 853-71.

8. Xie, L.; Wang, D. I. C., High Cell Density and High Monoclonal Antibody Production Through Medium Design and Rational Control in a Bioreactor. *Biotechnology and Bioengineering* **1996,** 51, (6), 725-729.

9. Golmakany, N.; Rasaee, M. J.; Furouzandeh, M.; Shojaosadati, S. A.; Kashanian, S.; Omidfar, K., Continuous production of monoclonal antibody in a packed-bed bioreactor. *Biotechnolgy and Applied Biochemistry* **2005,** 41, (3), 273-8.

10. Gramer, M. J.; Poeschl, D. M., Screening tool for hollow-fiber bioreactor process development. *Biotechnology Progress* **1998,** 14, (2), 203-9.

11. Jackson, L. R.; Trudel, L. J.; Fox, J. G.; Lipman, N. S., Evaluation of hollow fiber bioreactors as an alternative to murine ascites production for small scale monoclonal antibody production. *Journal of Immunological Methods* **1996,** 189, (2), 217-31.

12. Yang, S.-T.; Luo, J.; Chen, C., A fibrous-bed bioreactor for continuous production of monoclonal antibody by hybridoma. *Advances in Biochemical Engineering/Biotechnology* **2004,** 87, 61-96.

13. Hay, P. D.; Veitch, A. R.; Gaylor, J. D., Oxygen transfer in a convection-enhanced hollow fiber bioartificial liver. *Artificial Organs* **2001,** 25, (2), 119-30.

14. Yang, P.; Teo, W.-K.; Ting, Y.-P., Design and performance study of a novel immobilized hollow fiber membrane bioreactor. *Bioresource Technology* **2006,** 97, (1), 39-46.

15. Van Wie, B. J.; Brouns, T. M.; Elliott, M. L.; Davis, W. C., A Novel Continuous Centrifugal Bioreactor for High-Density Cultivation of Mammalian and Microbial-Cells. *Biotechnology and Bioengineering* **1991,** 38, (10), 1190-1202.

16. Herman, H. H.; Lin, W.; Petrecca, P. J.; Herman, T. M.; Bates, C.; Simmons, R.; Houghton, J., Centrifugal Bioreactors and Their Application in Remediation. In 2001; Vol. 11, pp 15-33.

17. Herman, H. H. Centrifugal Fermentation Processes. US Patent #: 5,622,819, April 22, 1997.

18. Van Wie, B. J.; Elliott, M. L.; Lee, J. M., Development and Characterization of a Continuous Centrifugal Bio-Reactor. *Biotechnology and Bioengineering Symp.* **1986,** 17, 335-344.

19. Tekriwal, P., Centrifugal Buoyancy Driven Reverse Flow Near The Leading Wall of a Rotating Cooling Passage. In *ASME Challenges of High Temperature Heat Transfer Equipment*, 1994; Vol. 282.

20. Valentine, D. T.; Jahnke, C. C., Coriolis Effect on Transport Phenomena in Rotating Systems: A Numerical Study. In *Centrifugal Materials Processing, [Proceedings of the Iternational Workshop on Materials Processing at High Gravity]*, Potsdam, NY, June 2-7, 1996, 1997.

21. Hammond, T. G.; Hammond, J. M., Optimized suspension culture: the rotating-wall vessel. *American Journal of Physiology-Renal Physiology* **2001,** 281, (1), F12-F25.

22. Chevray, R.; Chan, Y. N. I.; Hill, F. B., Dynamics of bubbles and entrained particles in the rotating fluidized bed. In 1980; Vol. 26, pp 390-398.

23. Batchelor, G. K., *An Introduction to Fluid Dynamics*. Cambridge University Press: Cambridge, UK, 1967.

24. van de Konijnenberg, J. A.; Nielsen, A. H.; Rasmussen, J. J.; Stenum, B., Shear-flow instability in a rotating fluid. *Journal of Fluid Mechanics* **1999,** 387, 177-204.

25. Robinson, R. A.; Stokes, R. H., *Electrolyte Solutions*. 2 ed.; Butterworth & Co. Ltd.: London, 1959.

26. Kakizaki, H.; Aonuma, C.; Nakatani, K., Mass transfer of weak acid in nanometer-sized pores of octadecylsilyl-silica gel. *Journal of Colloid and Interface Science* **2007,** 307, (1), 166-171.

27. Baker, A. J., *Finite Element Computational Fluid Dynamics*. Hemisphere Publishing Corporation: New York, 1983.

28. Baroud, C. N.; Plapp, B. B.; Swinney, H. L.; She, Z. S., Scaling in three-dimensional and quasi-two-dimensional rotating turbulent flows. *Physics of Fluids* **2003,** 15, (8), 2091-2104.

29. Greenspan, H. P., *The Theory of Rotating Fluids*. Cambridge University Press: Cambridge, UK, 1968.

CHAPTER III

Fluid Flow through a High Cell Density Fluidized Bed during Centrifugal Bioreactor Culture

Christopher J. Detzel, Bernard J Van Wie, and Cornelius F. Ivory*

Voiland School of Chemical Engineering and Bioengineering, Washington State University

P.O. Box 642710, Pullman, Washington 99164-2710, USA

* Corresponding Author: Tel.: +1 509 335 7716; email: cfivory@wsu.edu

Running Title: Flow Profile in a High Cell Density Centrifugal Bioreactor

Submitted to *Biotechnology Progress*, April 2009

Abstract

An increasing demand for products such as tissues, proteins, and antibodies from mammalian cell suspension cultures is driving interest in increasing production through high cell density bioreactors. The centrifugal bioreactor (CCBR) retains cells by balancing settling forces with surface drag forces due to medium throughput and is capable of maintaining cell densities above 10^8 cells/mL. This paper builds on a previous study where the fluid mechanics of an empty CCBR were investigated and showed fluid flow is non-uniform and dominated by Coriolis forces, raising concerns about nutrient and cell distribution. In this paper we demonstrate that the previously reported Coriolis forces are still present in the CCBR, but masked by the presence of cells. Experimental dye injection observations during culture of 15 μm hybridoma cells show a continual uniform darkening of the cell bed, indicating the region of the reactor containing cells is well mixed. These observations are reflected in simulation results of CCBR culture with

mammalian cells ranging in size from 10 – 20 μm. Experimental observations and simulation results both show an increase in cell density when centrifugal force is doubled at a constant inlet velocity; the cell volume fraction within the cell bed is increased from 0.16 to 0.26 when RPM is increased from 650 to 920 at a constant inlet flow rate of 6.5 cm/s during experimentation. Results presented in this paper indicate cells maintained in the CCBR behave similar to a high density fluidized bed of cells providing a homogenous environment to ensure optimal growth conditions.

Keywords: centrifugal bioreactor, coriolis force, fluidized bed, high density, mammalian cell

1. Introduction

The increased demand for complex post-translationally modified proteins for therapeutic and diagnostic purposes has necessitated the use of mammalian hosts [1-4]. Industrial methods used for bacterial culture are incapable of meeting production needs exceeding hundreds of kilograms per year when the use of mammalian hosts is necessitated. Slower cellular growth and protein production rates by mammalian cells limit protein production when compared to bacterial cultures. Consequently, two approaches to increase productivity in mammalian cultures are being investigated: increasing specific cellular productivity and increasing volumetric productivity [3, 5]. The former may be accomplished through modification of the growth environment or cellular genome, whereas volumetric productivity is a direct reflection of maximum bioreactor culture cell density.

The batch culture of hybridoma cells using continuous stirred-tank reactors is limited in density, on the order of 10^6 cells/mL, due to cell wash-out at medium flow rates required to

sustain optimal growth conditions [6-9]. However, density can be increased another order of magnitude to 10^7 cells/mL if viable cells are separated from spent medium and recycled to the reactor [10], or if a filter device on the reactor effluent is used to prevent cell escape, as is the case with a wave bioreactor-perfusion culture system [5]. Furthermore, any additional increases in bioreactor cell density require the use of a cell immobilization technique.

Mechanical cell immobilization occurs in packed bed bioreactors (PBRs) and hollow fiber bioreactors (HFBs) with the use of porous packing or membranes, respectively. As a result, cellular densities can reach maximums of 10^8 cells/mL while cell viability is maintained [11-15]. The limitations of these bioreactors lie in heterogeneous product formation due to inactive portions of the biomass caused by membrane fouling, mass transport limitations, and non-uniform nutrient and inhibitor gradients [13, 16, 17].

Another bioreactor capable of exceeding cell densities of 10^8 cells/mL is the continuous centrifugal bioreactor (CCBR). The CCBR, used in the present manuscript, has been described previously [18], and is similar to systems studied by Van Wie *et al.* for yeast and hybridoma culture [19] and by Kinetic Biosystems Inc. for use in wastewater remediation [20, 21]. Unique to the CCBR is the method of cell immobilization. In contrast to mechanical immobilization used in PBRs and HFBs, the CCBR immobilizes cells with the use of centrifugal force balanced by opposing buoyant and drag forces during steady-state operation. As medium flows through the reactor chamber at flow rates necessary to sustain high density cultures a drag force is imposed on cells which is balanced with centrifugal force resulting from system rotation. Consequently, nutrient and waste transport is by convection, eliminating mass transfer limitations associated with other high density bioreactors.

Previous work has shown the fluid flow profile in the CCBR without the presence of cells is dominated by Coriolis forces [18]. Obviously, Coriolis forces are still present during operation with or without cells, but to what extent is the previously reported flow profile changed by the presence of cells. If the flow profile is unchanged, and the majority of fluid flows up the leading wall of the reactor it is likely a circulation of cells along previously reported streamlines will result. Alternatively, cells may completely disrupt the non-uniform flow profile creating a uniform flow through the cell bed, emulating particles suspended in a fluidized bed.

This paper will examine the fluid flow profile in the CCBR during high density hybridoma cell culture using both numerical simulations and experimental observations. The implications of the resultant flow profile on the culture of various cell types and use of the simulation will be discussed.

2. Theory

The mixture model for laminar flow in COMSOL v3.5 is a macroscopic two-phase flow model which was used to simulate the movement of fluid and cells through the CCBR. The mixture model relies on the following assumptions: the density of each individual phase is constant for both fluid and cells, both phases share the same pressure field, and the relative velocity between the two phases is determined by assuming a balance between pressure, gravity and viscous drag. The equations defining the system in COMSOL for the momentum of the mixture (Eq. 1), the mixture continuity equation (Eq. 2), and the dispersed phase (cells) transport equation (Eq. 3) as follows:

$$\rho \frac{\partial \boldsymbol{u}}{\partial t} + \rho(\boldsymbol{u} \cdot \nabla)\boldsymbol{u} = -\nabla p - \nabla \cdot \left(\Phi_d \rho_d \left(1 - \frac{\Phi_d \rho_d}{\rho}\right) \boldsymbol{u}_{slip} \boldsymbol{u}_{slip}\right) + \nabla \cdot \tau + \rho \boldsymbol{g} + \boldsymbol{F}$$

Eq. 1

$$(\rho_c - \rho_d)\left[\nabla \cdot \left(\Phi_d \left(1 - \frac{\Phi_d \rho_d}{\rho}\right) \boldsymbol{u}_{slip}\right) + \frac{m_{dc}}{\rho_d}\right] + \rho_c(\nabla \cdot \boldsymbol{u}) = 0 \qquad \text{Eq. 2}$$

$$\frac{\partial \Phi_d}{\partial t} + \nabla \cdot \left(\Phi_d \mathbf{u} + \Phi_d \left(1 - \frac{\Phi_d \rho_d}{\rho}\right) \mathbf{u}_{slip}\right) = -\frac{m_{dc}}{\rho_d} \qquad \text{Eq. 3}$$

where **u** denotes mixture velocity, ρ is mixture density with subscripts d and c corresponding to the individual phase densities where d denotes the dispersed phase (cells) and c denotes the continuous phase (fluid), p represents pressure, Φ_d is the volume fraction of the dispersed phase, $\mathbf{u}_{slip}$ denotes the relative velocity between the two phases, τ represents the viscous stresses tensor, and **F** is any additional volume force i.e., Coriolis forces in the CCBR system. Finally, m_{dc} is the mass transfer rate from the dispersed phase to the continuous phase, which is zero in this instance.

COMSOL's mixture model calculates mixture properties as weighted averages of the continuous and dispersed phase properties. The mixture velocity is a mass fraction weighted average of the individual velocities, whereas the mixture density is a volume fraction weighted average of the two individual phase densities. Another important parameter to be calculated is the slip velocity which corresponds to the relative velocity between the two phases. The Hadamard-Rybczynski model for solid particles, Eq. 4, is specified in COMSOL and derived from a balance on the viscous drag, pressure, and gravity forces acting on the dispersed phase.

$$\frac{3}{4}\frac{C_d}{d_d}\rho_c \mathbf{u}_{slip}^2 = -\frac{(\rho - \rho_d)}{\rho}\nabla p \qquad \text{Eq. 4}$$

where d_d is the particle diameter, C_d is the drag coefficient which for this simulation is taken to be the drag from creeping flow around a sphere, 24/Re. Thus, the slip velocity simplifies to that shown in Eq. 5 in which η_c is the continuous phase viscosity.

$$\mathbf{u}_{slip} = -\frac{(\rho - \rho_d) d_d^2}{18 \rho \eta_c} \nabla p \qquad \text{Eq. 5}$$

Lastly, the mixture viscosity must be estimated. The simulation package must account for the increased viscosity and therefore increased viscous drag due to particle-particle interactions at high particle concentrations. The mixture viscosity is estimated using a Krieger type model shown in Eq. 6.

$$\eta = \eta_c \left(1 - \frac{\Phi_d}{\Phi_{max}}\right)^{-2.5\Phi_{max}} \qquad (6)$$

where η mixture viscosity, and Φ_{max} is the maximum packing concentration attainable in the dispersed phase. For randomly packed rigid spheres the maximum solids concentration is typically about 65% [22]. However, due to the deformable nature of a cell membrane, a maximum packing concentration of 0.75 was chosen, as it was found that variations in this parameter from 0.75 to 0.90 did not affect simulation results.

3. Materials and Methods

3.1 Cell Line and Culture

The cell line used in this research was mouse hybridoma MM1A [23]. The MM1A cell line secretes an IgG1 monoclonal anti-body specific to the epsilon chain of the CD3 T-cell receptor complex. High glucose Dulbecco's Modified Eagle Medium (DMEM) supplemented with 10% Calf Bovine Serum (CBS) (Hyclone, Logan, UT) was used for all cell culture. DMEM

was also supplemented with 2 mM L-Glutamine, 100 units/mL penicillin, 100 mg/mL streptomycin, 10 mM HEPES Buffer, and 3 x 10^{-5} M 2-mercapto-ethanol. All medium ingredients were purchased from Invitrogen (Carlsbad, CA) unless otherwise indicated. Cell counts and viability assays for all cultures were performed using a Trypan Blue Exclusion Assay with a Hemocytometer.

Prior to inoculating the CCBR, 5 x 10^8 total cells were cultured using multiple 100 and 150 mm Petri dishes. During this batch culture process, medium and cells from confluent Petri dishes were collected, centrifuged, and counted to determine total cell number and viability. The counted cells were then split into multiple dishes and this process was repeated every 1-2 days until the cell count reached 5 x 10^8 total cells which were then harvested and suspended in 15 mL of culture medium to be used for CCBR inoculation.

3.2 Solution Preparation

Phosphate Buffered Saline (PBS), pH 7.3, was used as the base salt buffer solution in these experiments. The use of PBS allowed cells to remain viable over multiple experiments. A dark blue contrasting solution to the colorless PBS was prepared by the addition of Bromophenol Blue (BPB) to 0.03 mM in PBS, allowing visualization studies of the flow profile to be performed.

3.3 Flow Profile Visualization

The equipment used for this research was a COBE® Spectra™ Apheresis System (Gambro BCT Inc., Lakewood, CO) manufactured for use as a blood separation device. The bioreactor chamber supplied as part of the Cell Purging tubing set (Gambro BCT Inc., Lakewood, CO) was replaced with a similar smooth-walled chamber cut out of a rectangular

piece of acrylic. The acrylic block had two threaded bolt holes on either side of the chamber for rotor attachment.

Prior to reactor inoculation all fluid lines and the reactor chamber must be filled with fluid. Dyed PBS fills the lines from its reservoir to the mixing point tee directly before the reactor inlet using a pump C in Fig. 1, while colorless PBS fills all remaining lines and the reactor chamber with use of pump B. The cell suspension containing 5×10^8 total cells is initially introduced to the system without rotation and evenly dispersed throughout the recycle line, after which volumetric flow rate and rotation rate are specified. Immediately after initiation of system rotation the three valves shown in Fig. 1 are set such that all fluid leaving the reactor is recycled for 10-15 minutes using the colorless liquid pump B. It is necessary to operate at full recycle initially so the fluidized cell bed has time to establish itself and ensure all cells are retained within the reactor. After the cell bed is established fluid exiting the reactor can be sent directly to waste without cell loss.

To visualize the flow profile the colorless fluid pump B was simultaneously stopped as the BPB dyed solution, pump C, was started at the same flow rate. The flow of dye through the reactor was illuminated using a variable speed strobe light and recorded using a Nikon D-60 Digital SLR camera (Nikon Inc., Melville, NY).

3.4 Simulation Simplification and Setup

The 3D geometry needed for the mathematical simulation was created in COMSOL 3.5 by drawing one half of the 2D projection in the x-y plane and rotating this drawing 360 degrees as has been previously described [18]. The COMSOL physics used for this modeling is the Mixture Model for Laminar Flow of multiphase momentum transport which has been outlined in detail in the Theory section. Constants which must be specified in this model include the density

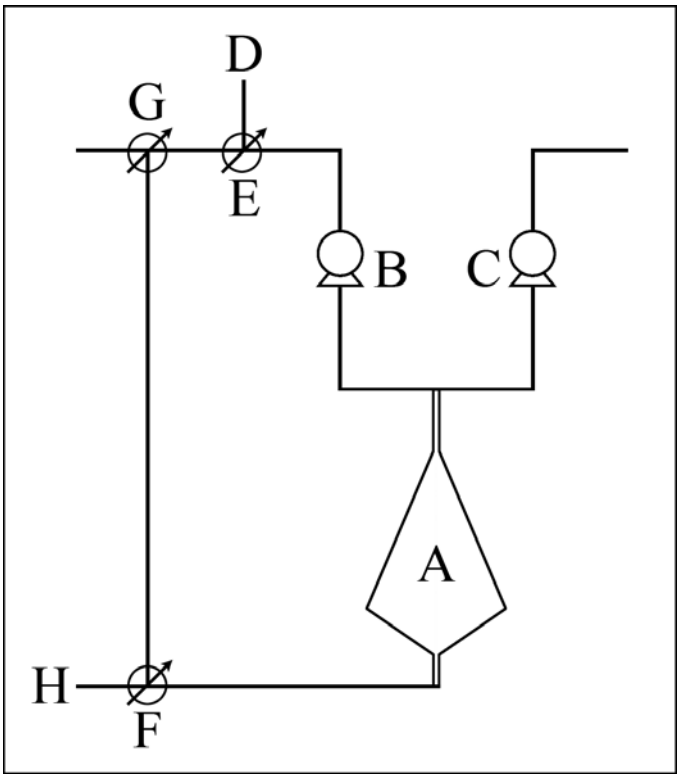

Figure 1. Process flow diagram of the system used to visualize movement of fluid throughout the CCBR (A). Pumps were used to move either undyed PBS (B) or BPB dyed PBS (C) from a reservoir to the reactor. Inoculation line (D) and valve (E) were used to introduce cells into the system, while valves (F) and (G) were used to recycle reactor effluent or direct the effluent directly to waste (H).

and viscosity of the continuous phase which are 992 kg/m^3 and 6.123 x 10^{-4} Pa·s, respectively, assuming negligible difference between such values for liquid water and PBS at 37 °C. Additionally, hybridoma cell density, diameter, and maximum packing volume fraction were specified for the dispersed phase as 1075 kg/m^3 [24], 15 μm [25], and 0.75, respectively.

Additional volume forces acting on the system must also be specified, these include the Coriolis forces and centrifugal force. Solving the Navier-Stokes Equation in a rotating frame of reference necessitates the inclusion of body forces $F_x = -2\Omega\rho u_y$ and $F_y = 2\Omega\rho u_x$ where F_x and F_y are the Coriolis forces in the x and y directions, Ω is the angular velocity, ρ is the mixture density and u_x and u_y are the individual components of velocity in their respective directions. Due to the design of the reactor, the centrifugal force is not constant throughout the reactor chamber and decreases linearly from the inlet to the outlet. Centrifugal force $F_C = \Omega^2(D - y)$ is incorporated as a gravity term where F_C is the centrifugal force, D is a constant 13.14 cm representing distance from the center of rotation to the reactor inlet, and y is the positive distance from the reactor inlet to any point in the reactor.

Model set-up is completed by defining boundary conditions throughout the system for both the continuous and dispersed phases. The boundary condition at the outlet for the continuous phase was defined as a pressure of zero such that fluid outflow is determined by the specified influx of material, a condition which is particularly useful when fluid flow leaving the system may not be normal to the boundary. The boundary condition for the dispersed phase at the reactor exit was defined as the dispersed phase outlet allowing solids to cross the boundary. Therefore, to maintain a steady-state concentration of cells throughout the simulation the flux across the outlet boundary is defined using an integration coupling boundary variable, which is

then specified as the inlet flux boundary condition for the dispersed phase. The continuous phase boundary condition at the inlet consists of a specified fluid velocity.

All other boundaries in the system were defined as no slip wall conditions for the continuous phase and Insulation/Symmetry for the dispersed phase prohibiting cells or fluid from crossing solid boundaries. All simulations were solved with a mesh similar to that described previously in the manuscript discussing flow through the CCBR without cells [18], however for the current simulation 100,722 nodes are evenly distributed throughout the system as opposed to 86,037 nodes for the simulation without cells.

4. Results and Discussion

4.1 Formation of the Fluidized Bed of Cells

The development of a fluidized bed of cells can be observed in the experimental CCBR as rotation is increased from 0 to 650 RPM as follows: initially, through continual pumping at an inlet fluid velocity of 6.5 cm/s without system rotation the 5×10^8 total cells inoculated into the system become evenly dispersed throughout the recycle loop and reactor chamber. Immediately after rotation begins an evenly dispersed low density cell suspension is seen throughout the reactor chamber, shown in Figure 2 (A). As the system rotation increases to a steady-state value of, 650 RPM, the settling velocity of the cells is enhanced and the initial formation of a fluidized bed of cells can be observed in Fig. 2 (B) as an opaque white color. The top third of the reactor in Fig. 2 (B) still contains some cells which have not yet settled into the fluidized bed as evidenced by the diffuse opaque region above the cell bed. However, after operation at 650 RPM for 10 minutes all cells in the recycle loop have circulated to the reactor and a steady-state

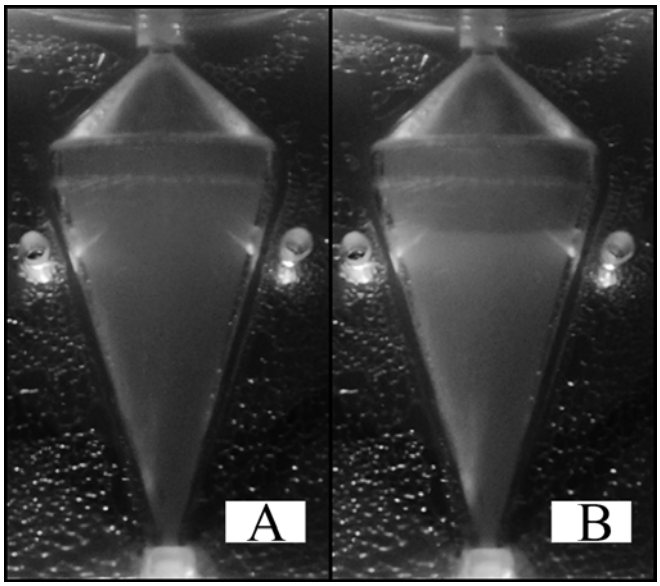

Figure 2. The progressive development of a fluidized bed of cells beginning with 5 x 10^8 cells/mL evenly distributed throughout the reactor chamber and recycle loop (A). Cells begin to settle into the opaque cell bed in the lower half of the chamber (B) due to the balanced centrifugal and drag forces from CCBR operation at 650 RPM and an inlet velocity of 6.5 cm/s. At steady-state the region above the cell bed will become clear as all cells will be retained in a well defined fluidized bed of cells.

cell bed separated from the rest of the reactor by a sharp interface between the clear fluid and cell bed is observed, Fig. 3 (A).

During steady-state operation the centrifugal force is balanced against opposing drag and buoyant forces which results in an equilibrium cell bed volume less than the total volume of the reactor chamber, 11.4 mL. If the equilibrium balance of these forces is disrupted by changes in either system RPM or inlet fluid velocity the cell bed volume will change, as is shown in Fig. 3 when centrifugal force is doubled while inlet velocity remains constant at 6.5 cm/s. At 650 RPM, Fig. 3 (A), the top of the cell bed is 3.54 cm above the reactor inlet resulting in a cell bed volume of 5.5 mL; an average value of the cell bed height is estimated from the observation of still images recorded over multiple experiments. Doubling the centrifugal force by increasing RPM to 920, Fig. 3 (B), decreases the cell bed height and volume to 2.96 cm and 3.4 mL, respectively. Assuming a cell diameter of 15 μm and all 5×10^8 cells are evenly dispersed throughout the cell bed, at 650 RPM a density of 9.1×10^7 cells/mL and a cell volume fraction of 0.16 results. At a RPM of 920 cell density increases to 1.5×10^8 cells/mL and the cell volume fraction increases to 0.26. The same type of results are observed for variations in inlet fluid velocity at constant RPM; however, fluid velocity and cell density are inversely proportional.

4.2 Experimental Visualization Results

Prior work has shown that, without cells, fluid moves through the CCBR along streamlines following a circuitous path from the reactor inlet to the outlet during steady-state operation [18]. As fluid enters the reactor void of cells it flows along the leading edge of the rotating reactor, at the widest cross-section fluid flow transverses the reactor to the opposite wall in an “Z” shaped pattern before exiting the chamber [18]. This flow pattern is dominated by

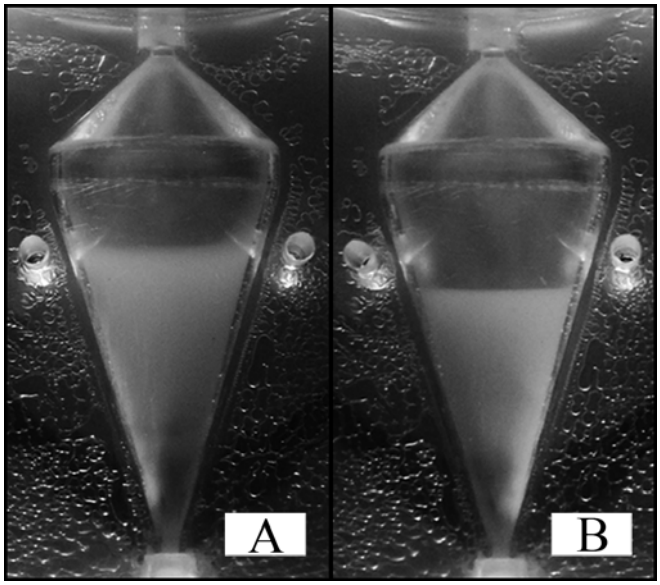

Figure 3. Steady-state operation of the CCBR at a constant inlet velocity of 6.5 cm/s at a RPM of 650 (A) and 920 (B). The centrifugal and drag forces are at a balanced equilibrium (A) resulting in a cell bed volume of 5.5 mL and a cell density of 9.1×10^7 cells/mL. Increasing the RPM to 920 (B) doubles the centrifugal force, requiring a new equilibrium between the centrifugal and drag forces to be reached. As a result the cell bed volume is decreased to 3.4 mL and density is increased to 1.5×10^8 cells/mL.

Coriolis forces, and analysis of the Rossby number shows their impact is no less important when cells are maintained in the CCBR.

An indication the effect Coriolis forces will have on a system can be estimated through evaluation of the Rossby number, defined as $U/L\Omega$; where U is the fluid velocity representative of the system, L is a unit length, and Ω is the angular velocity [26]. The Rossby number is a ratio of the inertial forces to Coriolis forces; a value much less than one indicates Coriolis forces contribute significantly to momentum transport, while the opposite is true for Rossby numbers much greater than unity. At the widest cross-section of the reactor, 2.73 cm, a velocity of 1.4×10^{-2} cm/s results assuming uniform flow at an inlet flow rate of 5.4 mL/min. Using this velocity and diameter the Rossby number is 7×10^{-5} at 650 RPM, assuming no cells are present. Inclusion of cells in this analysis only minimally increases fluid velocity at a cell volume fraction of 0.16, consequently increasing the Rossby number to 9×10^{-5}, clearly indicating the significant role of Coriolis forces in momentum transport during cell culture in the CCBR.

For the previously reported flow profile to remain unchanged during cell culture, the cells would have to circulate along previously reported streamlines. Cells would have to be carried up the leading wall of the reactor along streamlines to the widest cross-section where they would begin to move across the reactor to the opposite wall. As cells traverse the reactor flow is no longer opposite the centrifugal force and cells would begin to settle toward the inlet where they would once again become entrained in the incoming fluid flowing along the leading wall of the reactor, thus creating a constant circulation of cells. However, this scenario seems unlikely as Fig. 3 shows the cell bed volume decreases as RPM is increased. Previous work showed no effect on the fluid flow profile when RPM is increased from 650 to 920 [18]. Therefore, if cells

were circulating along streamlines which remain unchanged at normal cell culture operating conditions the cell bed volume could not be dependent on RPM as is shown in Fig. 3; consequently it is unlikely that cell retention is due to circulation along previously reported streamlines.

It is more likely that cells disrupt the flow profile in the CCBR resulting in a uniform flow of medium which suspends cells against the centrifugal force, much in the same manner as particles are suspended in a traditional fluidized bed. Bed expansion at fluid velocities greater than the minimum fluidization velocity is a distinct characteristic of fluidized beds and is observed in the CCBR. Compression of the cell bed as RPM is increased, as shown in Fig. 3, is analogous to what happens as fluid velocity is decreased in a traditional fluidized bed. The dependence of bed volume on reactor settings supports the characterization of cells retained in the CCBR as behaving like a fluidized bed of cells which are suspended against the centrifugal force by a uniform flow through the cell bed.

Observations of selected time points during dye injection experiments shown in Fig. 4 also suggest a uniform flow of fluid through the cell bed. Before any dye has been injected, Fig. 4 (A), the cell bed again appears as the opaque region in the bottom portion of the reactor. The darker shaded region near the inlet, indicated with an arrow in Fig. 4 (A), is not carryover dye from a previous experiment present at time zero, but instead is a small population of dead cells retained in the cell bed. The cell membranes of dead cells become permeable to the BPB dye, and have been permanently dyed during previous experiments which results in this observed shaded region. The dead cells are retained near the inlet as the volume of a cell decreases upon death ultimately resulting in an increase in cell density and thus their retention closer to the inlet. Additionally, it may appear as if the population of dead cells is preferentially retained along a

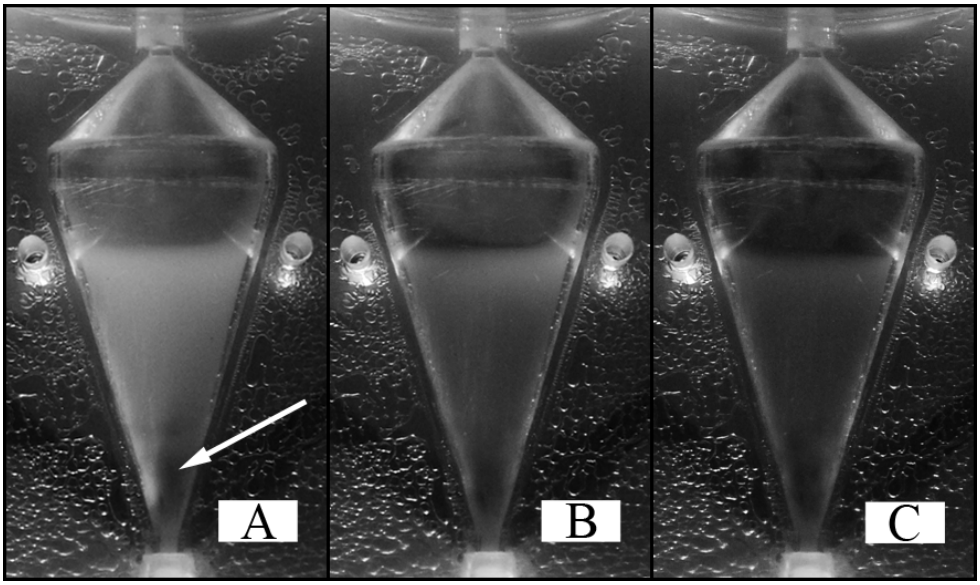

Figure 4. Before any dye injection (A) the steady-state result at 650 RPM and an inlet velocity of 6.5 cm/s shows a sharp interface between the opaque cell bed and the cell free clear fluid above. The darkened region indicated with the arrow (A) is not the presence of a dye gradient, but is a population of dead cells dyed with BPB. The cell bed continually darkens as BPB is supplied to the system, observed at 40 seconds (B) and 80 seconds (C) after dye injection begins. Uniform darkening of the cell bed indicates cells are retained in a region which is well mixed.

right side of the reactor in Fig. 4 (A) when in fact is not observed during experimentation, but is a result of the strobe light reflecting off the reactor giving the impression of a lighter shaded region.

As dye begins to enter the reactor the cell bed continuously darkens uniformly as shown at 40 seconds, Fig. 4 (B), and 80 seconds, Fig. 4 (C). At 40 seconds dye can be seen directly on top of the cell bed and along the left wall, while the entire region above the cell bed appears dyed at 80 seconds. The continual uniform darkening of the entire cell bed and the absence of any observable gradient of dye suggest the cell bed is well mixed which results in even distribution of dye throughout. These observations provide strong evidence and support the premise that a well mixed region of cells disrupts any stable non-uniform flow profile that was observed in the absence of cells, and more importantly flow around each cell provides the necessary drag force resulting in their suspension against the increased settling force.

4.3 Macroscopic Rayleigh-Taylor Instabilities

An unexpected observation from this work is the putative formation of Rayleigh-Taylor (RT) instabilities at the top interface of the cell bed, as shown in Fig. 5. In general, macroscopic RT instabilities result from the perturbation of an unstable system in which surface tension may be neglected, an interface separates two fluids of differing densities, and the more dense fluid is non-uniformly accelerated into a less dense fluid [27-30]. This phenomenon has been extensively studied primarily due to its implications in stellar and planetary interiors as well as other applications including geophysical fluid dynamics.

Necessary in the formation of RT instabilities is the presence of a sharp interface separating two fluids of differing densities. In this case the interface at the top of the cell bed serves this purpose. As previously reported the addition of BPB to a dilute salt solution resulted

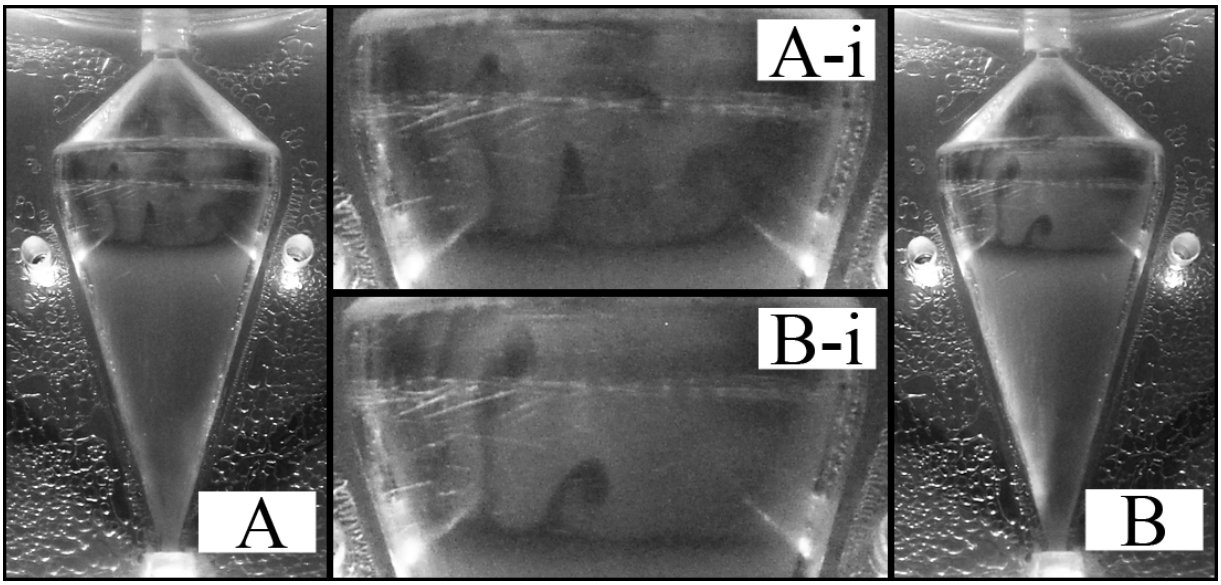

Figure 5. Observed at the interface separating the top of the cell bed from the PBS above is the presence of Rayleigh-Taylor (RT) instabilities. RT instabilities result from the non-uniform acceleration of a more dense fluid into a less dense fluid, when the two fluids are separated by a sharp interface. Previous results have shown the addition of BPB to a dilute salt solution decreases solution density. Therefore, the observed RT instabilities are an artifact of the dye injection procedure used to visualize the flow profile and would not be present during cell culture with a homogeneous culture medium.

in a small decrease in fluid density which is exaggerated during high gravity operation of the CCBR [18]. Consequently, the BPB colored PBS is less dense than the original colorless PBS. As BPB dyed solution is supplied to the reactor it becomes evenly dispersed throughout the well-mixed cell bed, and eventually accumulates as a thin layer on the interface at the top of the cell bed as can be observed in Fig. 5. The enhanced gravity in the CCBR accelerates the more dense colorless PBS into the less dense layer of BPB dyed PBS leading to the formation of RT fingers extending from the upper cell bed interface toward the outlet as shown in Fig. 5.

4.4 Numerical Simulation

It has previously been shown that the fluid flow profile observed experimentally without the presence of cells can be numerically simulated in COMSOL showing a similar flow pattern dominated by Coriolis forces [18]. Experimental results discussed throughout this manuscript have indicated the fluid flow profile dramatically changes in the presence of cells. The ability of a numerical simulation to mimic these results provides a tool to further understand the fluid dynamics of the CCBR.

To complete a simulation of the fluid dynamics in the CCBR during cell culture a steady-state simulation was solved using a transient approach in COMSOL; a transient simulation was able to mimic steady-state when simulation solutions no longer changed with time. First, an initial cell volume fraction of 0.07 was specified throughout the reactor chamber corresponding to 5×10^8 total cells. Then rotor speed and inlet fluid velocity were ramped up individually from zero to steady state values of 650 and 6.5 cm/s over 10 simulation seconds beginning 5 and 8 seconds into the simulation, respectively. After 50 seconds the simulation cell volume fraction no longer changed and a steady-state solution was assumed to have been reached for a specified set of operating conditions.

Numerical and experimental steady-state results show similar cell volume fractions throughout the reactor. Results are shown in Fig. 6 at both 650 and 920 RPM, where all results have a constant inlet fluid velocity of 6.5 cm/s. The simulated results indicate cell volume fraction along the reactor midline. At both RPMs no cells are indicated in the inlet tube leading to the reactor, but cell volume fraction rapidly increases directly after the end of the inlet tube to 0.15 and 0.22 for 650 and 920 RPM, respectively. These densities are maintained for 2.5 cm at 650 RPM and 2.0 cm at 920 RPM after which the cell volume fraction gradually decreases back to zero. The experimental cell volume fractions in Fig. 6 calculated from recorded still images are comparable to simulation results and correspond to 0.16 and 0.26 at 650 and 920 RPM, respectively.

The absence of a sharp interface at the top of the cell bed is a notable difference between simulation and experimental results. Contributing to the gradient in cell volume fraction observed at the interface is the necessary inclusion of artificial diffusion for COMSOL to reach a converged solution. The concept of artificial diffusion required for both the momentum and dispersed phase transport equations is the same as that which has been previously described [18]. Briefly, artificial diffusion within COMSOL stabilizes an equation set by adding a term to the physical diffusion constant of a particular equation. The addition of artificial diffusion is locally dependant on the mesh size and convective velocity, resulting in the non-uniform incorporation of artificial diffusion only when necessary for solution convergence, typically near steep gradients or sharp interfaces. Anisotropic streamline diffusion stabilizes the momentum and dispersed phase transport equations through its addition only in the directions of flow (direction of the streamline), while isotropic artificial diffusion adds necessary additional stabilization to the dispersed phase transport equation through a general increase of the overall magnitude of

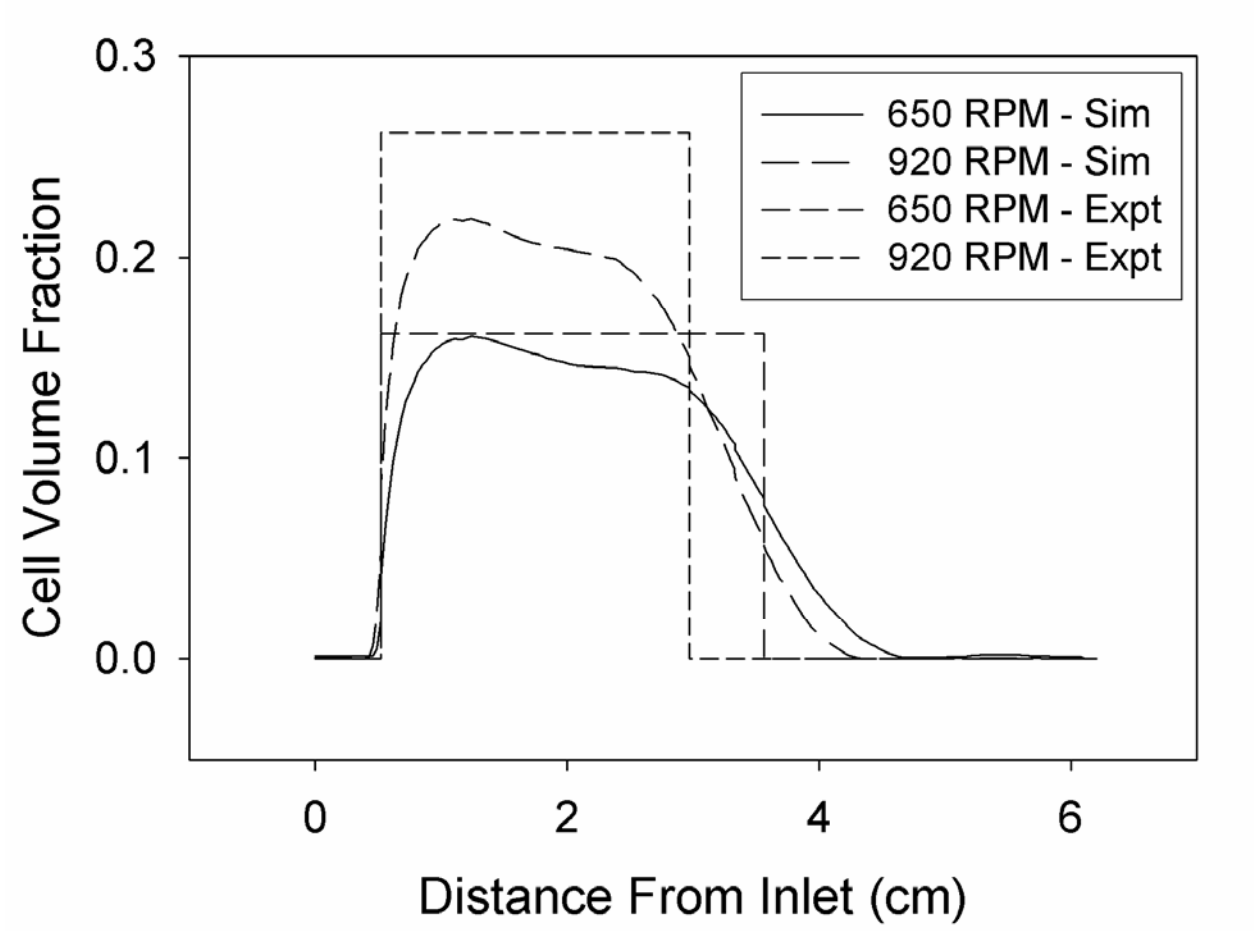

Figure 6. Cell volume fractions at various RPM and a constant inlet velocity of 6.5 cm/s are shown. Experimental cell volume fractions of 0.16 and 0.26 at 650 and 920 RPM were determined assuming a cell bed of uniform density and a volume calculated from still photographs. Simulation results along the reactor centerline indicate similar maximum cell volume fractions of 0.15 and 0.22 for RPMs of 650 and 920, respectively. The diffuse interface at the top of the cell bed in numerical results can be attributed to artificial diffusion, while a constant maximum cell volume fraction is not predicted in simulations due to the accumulation of cells along the right wall of the reactor.

diffusion. The term added when using anisotropic diffusion is shown in Eq. 7 while the term for isotropic diffusion is shown in Eq. 8.

$$c_{art,aniso} = \frac{\delta h \beta_i \beta_j}{\|\beta\|} \quad \text{Eq. 7}$$

$$c_{art,iso} = \delta h \|\beta\| \quad \text{Eq. 8}$$

The tuning parameter, δ, is set as 0.25 in all cases, but isotropic diffusion requires an additional tuning parameter input, the scale factor which is set to 0.01 in this simulation. The mesh element size is defined as h, and β is the convective velocity vector while β_i and β_j are individual components of the convective velocity tensor ensuring artificial diffusion is only added in the direction of flow. Due to computer memory limitations, further increases in mesh density which would theoretically eliminate artificial diffusion and allow the simulation of a sharp interface are not possible at this time.

The inability of the simulation to produce a sharp interface negates the possibility of simulating the presence of RT instabilities, as a sharp interface is necessary for their formation. However, the inability to simulate RT instabilities is of little significance to the overall validity of the simulation because the instabilities are an artifact of the differing density solutions used to visualize flow through the cell bed. During typical cell culture, medium with a homogeneous density will be supplied to the reactor eliminating the possibility of RT instability formation.

The second obvious difference between simulation and experimental results is that the simulation, Fig. 6, does not predict a constant cell volume fraction throughout the cell bed. Two peaks in cell volume fraction are observed along the reactor midline for a single RPM, where a region of increased concentration is closest to the reactor inlet. The region of increased cell concentration is in actuality localized to the right wall of the reactor near the inlet which is

revealed in Fig. 7. The x-y plane at z=0 corresponds to the gray shaded region in Fig. 7 (A), and the cell volume fraction along each horizontal line at different distances from the inlet is shown in Fig. 7 (B). A region of increased cell concentration along the right wall is shown by cell volume fraction increasing across a reactor cross-section and reaching a maximum at the reactor wall, this trend is observed at distance less than 2.00 cm from the inlet. However, at distances greater than 2.00 cm a constant cell volume fraction across a reactor cross-section is predicted, Fig. 7 (B).

It seems likely cells would concentrate in this region along the right wall of the reactor near the inlet based on the fluid flow profile observed in the CCBR without cells, which showed little flow in this region. Although the results presented in this manuscript have indicated a radically different flow profile in the presence of cells, Coriolis forces are no less important and still play a significant role in the fluid mechanics of the system. This is shown by a small increase in cell concentration along the right-side wall of the reactor, Fig. 7 (B), due to Coriolis forces causing preferential flow along the opposite wall, similar to that observed without cells.

According to the Taylor-Proudman theorem the results shown in Fig. 7 for a single plane perpendicular to the axis of rotation can be assumed to correspond to all other planes along the axis of rotation. The Taylor-Proudman theorem states that for very small values of the Rossby number the derivatives of velocity in the axial direction become small, and thus particle velocity becomes 2D in the plane perpendicular to the axis of rotation [18, 26, 31, 32]. Thus, cell volume fractions taken parallel to the axis of rotation will be constant at any point throughout the reactor. The only deviation being small increases at reactor walls, ± 0.03 differences in cell volume fraction, due to the no-slip boundary condition for the continuous phase, for which numerical data are not shown.

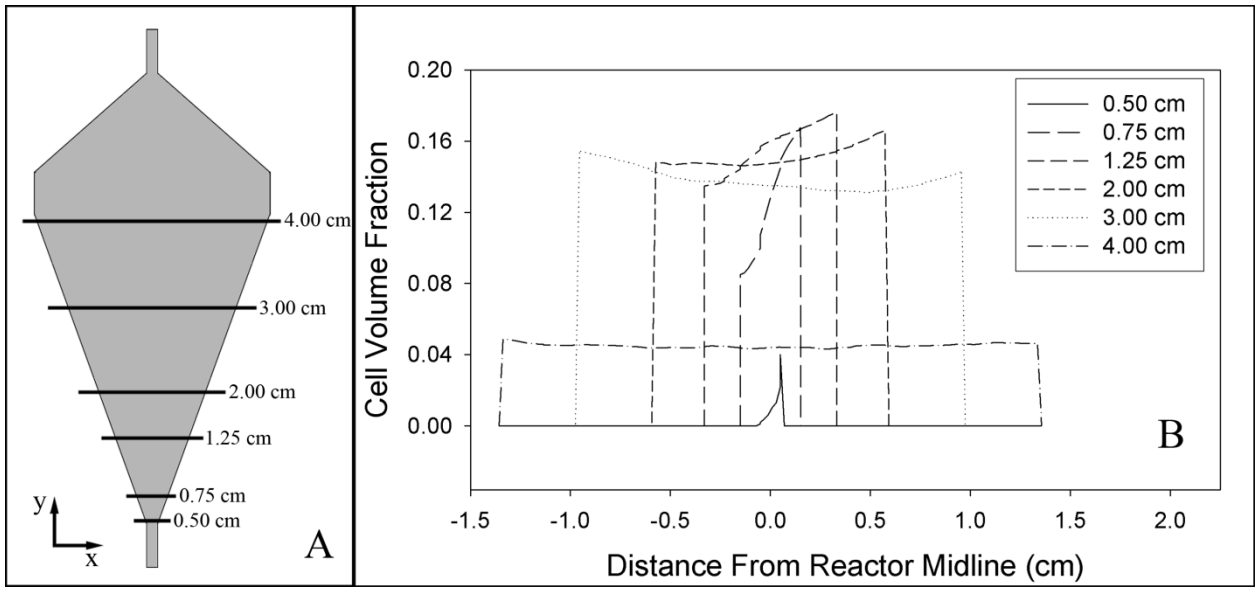

Figure 7. An increasing density of cells across a reactor cross-section reaching a maximum at the right reactor wall indicates a region of increased cell concentration. The gray shaded area in panel (A) corresponds to the x-y plane at z=0 and the volume fraction along each horizontal line is shown in panel (B). Accumulation of cells along the right-side wall of the reactor suggests a preferential flow along the opposite wall. The left wall of the reactor is the same wall along which the majority of fluid flow is observed during CCBR operation in the absence of cells.

4.5 Implications for CCBR Bioprocessing

The most obvious implications this work has for bioprocessing is in understanding how different cell types are retained and distributed throughout the CCBR during long term culture. The numerical simulation has closely approximated cell volume fraction and bed height throughout the CCBR for 15 μm diameter cells, at different operating conditions. CCBR cell culture hinges on balancing the opposing centrifugal and drag forces, both of which are highly dependent on cell size. Therefore, different size cell types will behave differently in the CCBR, and understanding the effect of cell size is critical to successful long term cell culture.

Different applications of the CCBR other than high density hybridoma culture require various cells types to be retained in the reactor. For instance some cells, white blood cells or bacteria, have much smaller diameters of 10 μm or 2 μm, respectively [21]. Larger mammalian cells or particles on the order of 20 μm could also possibly be cultured in the CCBR. Simulation results along the centerline of the CCBR at constant operating conditions of 650 RPM and 6.5 cm/s for various cell sizes are shown in Fig. 8. As cell size is decreased from 20 μm the simulation predicts the maximum cell volume fraction will decrease while dispersion throughout the reactor chamber increases and becomes more uniform, ultimately limiting cell retention.

An analysis of the effect of cell size on centrifugal, drag and buoyant forces provides insight in to the results shown in Fig. 8. For example, decreased cell size results in decreased drag, buoyancy, and centrifugal forces; however, from Fig. 8 it is clear the reduction in these two forces is not at the same rate. If all forces changed at the same rate the cell volume faction and bed height would remain constant as cell diameter changed. These forces decreasing at different rates are to be expected as drag force depends on cross-sectional area (d^2) while the buoyancy

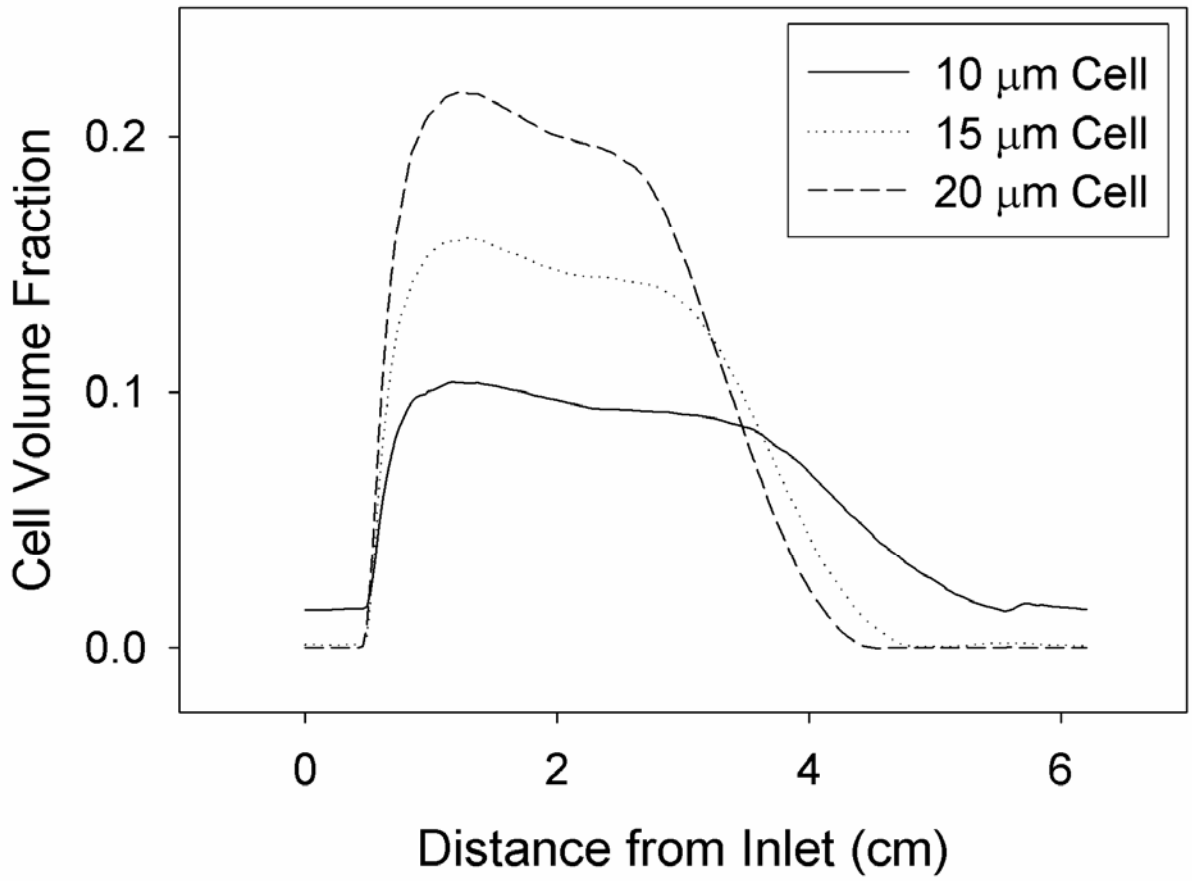

Figure 8. At constant reactor settings of 650 RPM and an inlet velocity of 6.5 cm/s the effect of cell size on cell volume fraction distribution throughout the reactor is shown for 5 x 10^8 total cells. As the diameter of a cell is decreased from 20 μm to 10 μm the maximum cell volume fraction decreases from 0.22 to 0.10 while cells become more dispersed throughout the entire reactor making cell retention difficult. These effects are due to the fact that as cell size is decreased the magnitude of the settling force decreases faster than the drag force indicating reactor settings must be carefully tuned for each cell type and desired culture density.

and gravitational forces are volume dependent (d^3). To illustrate this point, decreasing diameter from 15 μm to 10 μm results in a reduction in the magnitude of the drag force by about 55%, whereas the settling force which accounts for both the centrifugal and buoyant force is reduced 70%. This analysis clearly shows each individual cell culture will require a unique set of operating conditions which can be estimated using this simulation and then fine tuned experimentally to reach desired densities and cell retention producing efficient long term cultures.

5. Concluding Remarks

The inclusion of cells, or other similar particulates, in the fluid dynamic analysis of the CCBR has significant consequences on the observed fluid flow profile. Without cells, flow through the CCBR is dominated by Coriolis forces, where upon entering the reactor chamber fluid is forced to flow along the leading wall of the reactor. This characteristic flow profile remains unchanged at all typical cell culture operating conditions. However, results presented in this manuscript show the flow profile is radically changed in the presence of cells, ultimately allowing for the possibility of cells to be retained in the CCBR during culture.

Both experimental observations and numerical results show cell volume fraction is highly dependent on reactor settings, specifically RPM and inlet velocity. Experimental results have shown that doubling the centrifugal force while inlet velocity remains unchanged can increase the cell volume fraction from 0.16 at 650 RPM to 0.26 at 920 RPM. The simulation predicts similar behavior with small deviations in the maximum cell volume fraction at each RPM, 0.15 and 0.22 for 650 and 920 RPM, respectively.

Furthermore, dye injection experiments show a continually darkening cell bed without the presence of any observable dye gradients, indicating the region of the reactor containing cells is well mixed throughout. Therefore, a uniform flow of fluid through the cell bed results in the suspension of cells against the enhanced settling force of the CCBR. These results and those showing that the cell bed volume is coupled to operating conditions lead to the conclusion that the cell bed behaves similarly to a well mixed fluidized bed of cells, ultimately disrupting the previously reported flow profile.

Finally, analyses throughout this manuscript were performed using a general hybridoma cell size of 15 μm. However, the versatility of the CCBR lies in that both the centrifugal and drag force are individually tunable allowing various cells types with different cell sizes to be cultured. An analysis of cell size typical of mammalian cells, and volume fraction distribution for a uniform set of reactor conditions has shown that as cell size decreases the maximum cell volume fraction also decreases, while at the same time cell retention is diminished due to an increasingly even dispersion of cells throughout the entire reactor chamber.

An understanding that mammalian cells retained in the reactor behave as a well mixed fluidized bed whose porosity is dependent not only on reactor settings but also cell size greatly increases the understanding of CCBR fluid dynamics. The ability to generally determine necessary reactor settings using numerical simulations is a valuable tool ensuring the successful long term culture of various cell types, increasing the number of foreseeable applications of CCBR culture.

Acknowledgements

The authors would like to acknowledge the Biotechnology Training Grant (NIH 5T32-GM008336-16) and the Gene & Linda Voiland School of Chemical Engineering and Bioengineering for graduate student support and supplies. Equipment in the form of the COBE© Spectra Apheresis System and Cell Purging tubing sets in addition to corporate technical research staff consultation are a result of a donation by Gambro BCT Inc., Lakewood, CO. Mr. R. Hutchinson of the Washington State University College of Engineering and Architecture Machine Shop was instrumental in design and fabrication of the CCBR chambers used in these experiments.

References

1. Landry, Y.; Gies, J. P., Drugs and their molecular targets: an updated overview. *Fundam Clin Pharmacol* **2008,** 22, (1), 1-18.

2. Migliore, C.; Giordano, S., Molecular cancer therapy: Can our expectation be MET? *Eur J Cancer* **2008**.

3. Kundu, P. K.; Prasad, N. S.; Electricwala, S. E.; Varma, R.; Datta, D., Getting higher yields of monoclonal antibody in culture. *Indian Journal of Physiology and Pharmacology* **1998,** 42, (2), 155-71.

4. Werner, R. G., Economic aspects of commercial manufacture of biopharmaceuticals. *J Biotechnol* **2004,** 113, (1-3), 171-82.

5. Tang, Y. J.; Ohashi, R.; Hamel, J. F., Perfusion culture of hybridoma cells for hyperproduction of IgG(2a) monoclonal antibody in a wave bioreactor-perfusion culture system. *Biotechnol Prog* **2007,** 23, (1), 255-64.

6. Jan, D. C. H.; Petch, D. A.; Huzel, N.; Butler, M., The Effect of Dissolved Oxygen on the Metabolic Profile of a Murine Hybridoma Grown in Serum-Free Medium in Continuous Culture. *Biotechnology and Bioengineering* **1997,** 54, (2), 153-164.

7. Kim, B. J.; Chang, H. N.; Oh, D. J., Application of a cell-once-through perfusion strategy for production of recombinant antibody from rCHO cells in a Centritech Lab II centrifuge system. *Biotechnol Prog* **2007,** 23, (5), 1186-97.

8. Miller, W. M.; Blanch, H. W.; Wilke, C. R., A kinetic analysis of hybridoma growth and metabolism in batch and continuous suspension culture: effect of nutrient concentration, dilution rate, and pH. Reprinted from Biotechnology and Bioengineering, Vol. 32, Pp 947-965 (1988). *Biotechnology and Bioengineering* **2000,** 67, (6), 853-71.

9. Xie, L.; Wang, D. I. C., High Cell Density and High Monoclonal Antibody Production Through Medium Design and Rational Control in a Bioreactor. *Biotechnology and Bioengineering* **1996,** 51, (6), 725-729.

10. Batt, B. C.; Davis, R. H.; Kompala, D. S., Inclined sedimentation for selective retention of viable hybridomas in a continuous suspension bioreactor. *Biotechnology Progress* **1990,** 6, (6), 458-64.

11. Golmakany, N.; Rasaee, M. J.; Furouzandeh, M.; Shojaosadati, S. A.; Kashanian, S.; Omidfar, K., Continuous production of monoclonal antibody in a packed-bed bioreactor. *Biotechnolgy and Applied Biochemistry* **2005,** 41, (3), 273-8.

12. Gramer, M. J.; Poeschl, D. M., Screening tool for hollow-fiber bioreactor process development. *Biotechnology Progress* **1998,** 14, (2), 203-9.

13. Jackson, L. R.; Trudel, L. J.; Fox, J. G.; Lipman, N. S., Evaluation of hollow fiber bioreactors as an alternative to murine ascites production for small scale monoclonal antibody production. *Journal of Immunological Methods* **1996,** 189, (2), 217-31.

14. Yang, S.-T.; Luo, J.; Chen, C., A fibrous-bed bioreactor for continuous production of monoclonal antibody by hybridoma. *Advances in Biochemical Engineering/Biotechnology* **2004,** 87, 61-96.

15. Nilsang, S.; Nehru, V.; Plieva, F. M.; Nandakumar, K. S.; Rakshit, S. K.; Holmdahl, R.; Mattiasson, B.; Kumar, A., Three-dimensional culture for monoclonal antibody production by hybridoma cells immobilized in macroporous gel particles. *Biotechnol Prog* **2008,** 24, (5), 1122-31.

16. Yang, P.; Teo, W.-K.; Ting, Y.-P., Design and performance study of a novel immobilized hollow fiber membrane bioreactor. *Bioresource Technology* **2006,** 97, (1), 39-46.

17. Hay, P. D.; Veitch, A. R.; Gaylor, J. D., Oxygen transfer in a convection-enhanced hollow fiber bioartificial liver. *Artificial Organs* **2001,** 25, (2), 119-30.

18. Detzel, C. J.; Thorson, M. R.; Van Wie, B. J.; Ivory, C. F., A Study of the Coriolis Effect on the Fluid Flow Profile in a Centrifugal Bioreactor. *Biotechnology Progress* **2009,** In Press.

19. Van Wie, B. J.; Brouns, T. M.; Elliott, M. L.; Davis, W. C., A Novel Continuous Centrifugal Bioreactor for High-Density Cultivation of Mammalian and Microbial-Cells. *Biotechnology and Bioengineering* **1991,** 38, (10), 1190-1202.

20. Herman, H. H. Centrifugal Fermentation Processes. US Patent #: 5,622,819, April 22, 1997.

21. Herman, H. H.; Lin, W.; Petrecca, P. J.; Herman, T. M.; Bates, C.; Simmons, R.; Houghton, J., Centrifugal Bioreactors and Their Application in Remediation. In 2001; Vol. 11, pp 15-33.

22. Jaeger, H. M.; Nagel, S. R., Physics of the Granular State. *Science* **1992,** 255, (5051), 1523-1531.

23. Davis, W. C.; MacHugh, N. D.; Park, Y. H.; Hamilton, M. J.; Wyatt, C. R., Identification of a monoclonal antibody reactive with the bovine orthologue of CD3 (BoCD3). *Vet Immunol Immunopathol* **1993,** 39, (1-3), 85-91.

24. Graham, J., *Biological Centrifugation*. BIOS Scientific Publishers Ltd: Oxford, UK, 2001; p 91-93.

25. deZengotita, V. M.; Schmelzer, A. E.; Miller, W. M., Characterization of hybridoma cell responses to elevated pCO(2) and osmolality: intracellular pH, cell size, apoptosis, and metabolism. *Biotechnol Bioeng* **2002,** 77, (4), 369-80.

26. Batchelor, G. K., *An Introduction to Fluid Dynamics*. Cambridge University Press: Cambridge, UK, 1967.

27. Chen, X. M.; Fried, E., Rayleigh-Taylor problem for a liquid-liquid phase interface. *Journal of Fluid Mechanics* **2006,** 560, 395-414.

28. El-Dib, Y. O., Nonlinear hydromagnetic Rayleigh-Taylor instability for strong viscous fluids in porous media. *Journal of Magnetism and Magnetic Materials* **2003,** 260, (1-2), 1-18.

29. Malkin, A. Y., Surface Instabilities. *Colloid Journal* **2008,** 70, (6), 673-689.

30. McFadden, G. B.; Coriell, S. R.; Gurski, K. F.; Cotrell, D. L., Convective instabilities in two liquid layers. *Journal of Research of the National Institute of Standards and Technology* **2007,** 112, (5), 271-281.

31. Greenspan, H. P., *The Theory of Rotating Fluids*. Cambridge University Press: Cambridge, UK, 1968.

32. Baroud, C. N.; Plapp, B. B.; Swinney, H. L.; She, Z. S., Scaling in three-dimensional and quasi-two-dimensional rotating turbulent flows. *Physics of Fluids* **2003,** 15, (8), 2091-2104.

CHAPTER IV

Kinetic Simulation of a Centrifugal Bioreactor for High Population Density Hybridoma Culture

Christopher J. Detzel[a], Derek J. Mason[a], William C. Davis[b], and Bernard J. Van Wie[a,*]

[a] Voiland School of Chemical Engineering and Bioengineering, Washington State University

P.O. Box 642710, Pullman, Washington 99164-2710, USA

[b] Department of Veterinary Microbiology and Pathology, Washington State University

P.O. Box 647010, Pullman, WA 99164-7010

[*] Corresponding Author: Tel: 509-335-4103; Fax: 509-335-4806; email: bvanwie@che.wsu.edu

Running Title: Centrifugal Bioreactor Simulation for Mammalian Cell Culture

Accepted for Publication in *Biotechnology Progress*, March 2009

Abstract

Demand for increasingly complex post-translationally modified proteins, such as monoclonal antibodies (mAbs), necessitates the use of mammalian hosts for production. The focus of this paper is a continuous centrifugal bioreactor (CCBR) capable of increasing volumetric productivity for mAb production through high density hybridoma culture, exceeding 10^8 cells/mL. At these extreme densities environmental conditions such as substrate and inhibitor concentrations rapidly change, dramatically affecting growth rate. The development of a kinetic model predicting glucose, mAb, lactate, and ammonium concentrations based on dilution rate and cell density is shown in this paper. Additionally, it is found that pH affects both growth rate and viability, and a range of 6.9 to 7.4 is needed to maintain growth rate above 90% of the

maximum. Modeling shows that operating an 11.4 mL CCBR inoculated with 2.0 x 10^7 cells/mL at a dilution rate of 1.3 h^{-1}, results in a predicted growth rate 82% of the maximum value. At the same dilution rate increasing density to 6.0 x 10^7 cells/mL decreases the predicted growth rate to 60% of the maximum; however, by increasing dilution rate to 6.1 h^{-1} the growth rate can be increased to 86% of the maximum. Using the kinetic model developed in this research the concentration of glucose, mAb, lactate, and ammonium are all predicted within 13% of experimental results. This model and an understanding of how RPM impacts cell retention serve as valuable tools for maintaining high density CCBR cultures, ensuring maximum growth associated mAb production rates.

Keywords: High Population Density Bioreactor; Hybridoma; Kinetic Simulation; pH; Inhibition

1. Introduction

Increasing demand for recombinant proteins, particularly monoclonal antibodies (mAbs), for therapeutic and diagnostic needs has fueled research on novel bioreactors capable of increasing production without sacrificing quality [1-3]. Proteins requiring post-translational modifications such as glycosylation, phosphorylation, and folding demand the use of mammalian hosts, while production requirements exceeding grams per patient per year necessitate increased production capabilities [4-7]. Consequently, bioreactor systems including fed-batch and various perfusion systems designed to increase volumetric productivity may be used to meet these production needs [1, 8, 9].

Many different techniques exist for protein production by mammalian cells, each with varying advantages and limitations. Batch cultures of hybridoma cells are used for *in vitro*

production of mAbs, but low cell densities on the order of 10^6 cells/mL, and decreased viabilities limit productivity [10-12]. Continuous feed stirred tank reactor (CSTR) cultures can be used to maintain high viabilities but process densities are further limited to 2-3 x 10^6 cells/mL because of wash-out as cells are entrained in passing medium. Thus, cell retention devices must be employed to maintain high viability cultures as densities and medium flow rates proportionally increase. Densities can be increased as high as 20 x 10^6 cells/mL in CSTR culture if cells are separated from spent medium and returned to the culture through techniques such as centrifugation, membrane separation, or a vertical sedimentation column [13, 14].

Cell immobilization can also be employed to prevent wash-out and is accomplished using hollow fiber bioreactors (HFBs) and packed bed bioreactors (PBRs). Both HFBs and PBRs are capable of supporting cell densities up to 10^8 cells/mL while maintaining high cell viability [2, 7, 15-17]. Though volumetric productivity is dramatically increased over batch or continuous suspension cultures, membrane fouling, diffusional limitations, and non-uniform gradients commonly plague HFBs and PBRs leading to heterogeneous product formation and inactive portions of the biomass [16-20].

In addition to these high density bioreactors a continuous centrifugal bioreactor (CCBR) has been developed; capable of sustaining highly viable cultures at densities above 10^8 cells/mL [21, 22]. The CCBR is similar to the Beckman Elutriation System and a system patented by Kinetic Biosystems, Inc. that is seeing practical application for use in waste stream remediation by flowing through an immobilized culture of bacterial cells [23, 24]. The typical problems associated with HFBs and PBRs are not observed within the CCBR due to the unique method of cell immobilization through the balance of centrifugal forces with opposing drag and buoyant forces. To maintain a homogeneous fluidized bed of cells fluid must flow around individual

cells such that drag forces can suspend each cell against the centrifugal field, consequently providing convective transport of nutrients and wastes to and from cells. However, needed for the CCBR are models that adequately predict nutrient and metabolite concentrations within the reactor ensuring maximal growth rate is maintained for the duration of the culture. Kinetic modeling provides a tool to estimate growth rate dependence on the concentration of substrates such as glucose or glutamine, and metabolites including lactate and ammonia, each of which are directly affected by dilution rate and cell concentration. Increasing lactate and ammonium ion concentrations not only impact growth rate but also result in lower medium pH , which further contributes to growth rate depression [12, 25-29].

In this paper we present a kinetic growth model derived from low density batch studies and verify that the developed model accurately predicts the CCBR culture environment. We have chosen glucose as the substrate, as well as the metabolites ammonium and lactate as the primary parameters of interest and demonstrate their role in growth rate inhibition. We go on to demonstrate model reliability for the extremely dense culture environment within the CCBR, and discuss the utility of this model for understanding high density cultures and their rapidly changing growth environment. Furthermore, we have performed studies that tie culture medium pH to growth rate inhibition and reduced viability; emphasizing the need to maintain pH at an optimal value. This paper will demonstrate how the CCBR is an excellent analytical tool for studying high population density systems, though industrial development shows its potential as a process production system [23, 24].

2. Theory

2.1 Kinetic Modeling

For this work a generalized model proposed by Han and Levenspeil [30] was specified and applied to the CCBR culture. This model was chosen as it simultaneously accounts for multiple product and substrate inhibition to determine cellular growth rate. Ammonium and lactate were chosen as inhibitory parameters given that they are both recognized as major byproducts of metabolism which inhibit growth, while glucose is a major energy source required by cells. Additionally, each model parameter can be sensed with either enzyme or ion selective electrodes making online detection easily available for process control to further optimize the CCBR.

Concentrations of cells, glucose (substrate), mAb, ammonium ion and lactate are represented by C_{Cell}, C_G, C_{mAb}, C_A, and C_L respectively, the observed growth rate is determined with Eq. 1 while μ_{max} is the maximum specific growth rate. Critical inhibitor concentrations where the observed growth rate is equal to zero are represented by C_{A_max} and C_{L_max}, respectively. The Monod constant, C_M, is defined as the concentration of the limiting substrate resulting in half of the maximum growth rate, while *n*, *m*, *p*, and *q* are orders of inhibition and vary depending on the type of observed inhibition, D is dilution rate, and C_{Cell_out} represents the concentration of cells leaving the reactor when it has filled to capacity. Additionally, cell growth rate is coupled to concentrations of glucose, mAb, ammonium, and lactate through yield coefficients represented by Y_{GC}, Y_{mAbC}, Y_{AC}, and Y_{LC} in Eq. 2-5 where C_{i0} is the feed concentration of any of the aforementioned species.

Dilution rate is defined as F/V, the inverse of mean residence time, where F is the flow rate of fresh medium into the reactor and V is the reactor volume (11.4 mL); since volume

remains constant, dilution rate changes are analogous to changing the amount of fresh medium fed to the CCBR. Therefore, a fresh feed flow rate of 1 mL/min results in a dilution rate of 0.09 min^{-1} and a residence time of 11.4 min. Consequently, the effect of changing dilution rate is apparent almost immediately when compared to the time scale of an entire culture. The Runge-Kutta method was used to approximate the numerical solution for this set of equations where initial conditions correspond to concentrations of each species in fresh culture medium, e.g., 400 mg/dL for glucose whereas all other species have an initial condition of zero concentration.

$$\frac{\partial C_{Cell}}{\partial t} = \mu_{\max} \cdot \frac{\left(1 - \frac{C_L}{C_{L\_\max}}\right)^n \cdot \left(1 - \frac{C_A}{C_{A\_\max}}\right)^m \cdot C_G \cdot C_{Cell}}{C_G + C_M \cdot \left(1 - \frac{C_L}{C_{L\_\max}}\right)^q \cdot \left(1 - \frac{C_A}{C_{A\_\max}}\right)^p} - \left(D \cdot C_{Cell\_out}\right) \tag{1}$$

$$\frac{\partial C_G}{\partial t} = D\left(C_{G0} - C_G\right) - Y_{GC} \cdot \left(\frac{\partial C_{Cell}}{\partial t}\right) \tag{2}$$

$$\frac{\partial C_{mAb}}{\partial t} = D\left(C_{mAb0} - C_{mAb}\right) + Y_{mAbC} \cdot \left(\frac{\partial C_{Cell}}{\partial t}\right) \tag{3}$$

$$\frac{\partial C_A}{\partial t} = D\left(C_{A0} - C_A\right) + Y_{AC} \cdot \left(\frac{\partial C_{Cell}}{\partial t}\right) \tag{4}$$

$$\frac{\partial C_L}{\partial t} = D\left(C_{L0} - C_L\right) + Y_{LC} \cdot \left(\frac{\partial C_{Cell}}{\partial t}\right) \tag{5}$$

2.2 Centrifugal Bioreactor

The CCBR retains cells within the reactor through increasing settling velocities, as a result of centrifugal force, which offset opposing buoyant and drag forces associated with high medium throughput required to sustain dense long term cell cultures [21, 22]. Each of the

aforementioned forces and their relative directions within the bioreactor are shown in Figure 1. The settling force on a cell is due to the difference between the buoyancy of the particle in the suspending medium and the gravitational force, enhanced due to centrifugation. The settling force at any point within the reactor is described by Eq. 6; where F_s is the force of sedimentation, R is the radius of the particle or cell, ρ_p and ρ_f represent the density of the particle and suspending fluid respectively, ω is the angular velocity and r is the distance from the center of rotation to the point of interest.

$$F_s = \frac{4}{3}\pi R^3 \left(\rho_p - \rho_f\right)\omega^2 r \tag{6}$$

Counteracting the settling force in the bioreactor is a drag force imposed on any particle contained within a moving stream. Determination of the Reynolds number for the particle (Re_p) in a fluidized bed shows that at the reactor inlet and outlet, regions with highest superficial velocity, the Re_p is at a maximum of 0.36, less than the requirement of unity for flow to be considered laminar. The equation for the drag on a particle in a laminar stream, Stokes Drag, is shown in Eq. 7; where F_d is the drag force on the particle, μ_f is the viscosity of the fluid, R is the radius of the particle, and V_0 is the velocity of the stream.

$$F_d = 6\pi\mu_f R V_0 \tag{7}$$

Briefly, the reactor chamber is designed such that centrifugal and drag forces diminish proportionally as the distance from the center of rotation is decreased. This is achieved through the conical shape of the bioreactor and results in retention of cells within the chamber at a homogeneous density. Rigorous evaluation and development of the design equations for a counter-flow centrifugation system are presented by Sanderson and Bird [31]. In addition to the

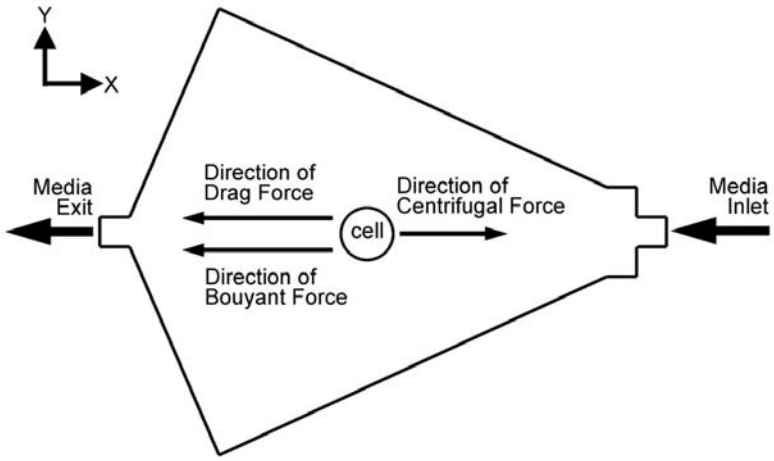

Figure 1. Indicates the forces acting on individual cells within the CCBR and their relative direction of action on that cell. Cell immobilization in this manner prevents wash-out allowing for increased perfusion of medium throughout the fluidized bed of cells, maintaining both high density and viability during culture.

settling and drag forces present in the CCBR the Coriolis force which results from the system rotation can affect the fluid dynamics within the CCBR system. Operation of the CCBR without the presence of cells results in a fluid flow profile significantly impacted by Coriolis forces [32], however this flow pattern is disrupted when cells are present (data not yet published). Consequently, Coriolis forces have little impact on the distribution of nutrients throughout the CCBR chamber and thus have an insignificant influence on growth kinetics.

For the work examined in this paper the forces on a particle are summed, and hindered settling or particle interaction effects as a function of bed porosity, ε, to the 2.7 power are included [33]. To account for the density difference between a single particle and the suspending fluid a term ($\rho_p - \rho_{susp}$) replaces the typical ($\rho_p - \rho_f$) term, however, ($\rho_p - \rho_{susp}$) equals ($\rho_p - \rho_f$) x ε. Then the velocity of the particle relative to the container is set to zero by setting the fluid velocity equal to the absolute value of the particle settling velocity. One then solves for velocity of a particle to arrive at Eq. 8.

$$v = \frac{2}{9} R^2 (\rho_p - \rho_f) \omega^2 r \frac{\varepsilon^{4.7}}{\mu_f} \tag{8}$$

In this paper values of the fluid velocity are taken at the centroid of the volume of the cone containing cells and the porosity is assumed to be uniform throughout this volume. Calculations of inlet fluid velocities or porosity using Eq. 8 for comparison with experimental values are sensitive to cell diameter, cell density, and particularly sensitive to the exact reactor volume fraction containing cells. Consequently, comparison of predicted porosity and fluid velocity with experimental conditions results in poor agreement without precise knowledge of this volume. However, predictions of the effect of changing CCBR angular velocity, RPM, on

porosity can be reliably made if the superficial velocity, v, remains constant. This results in a simple relationship between porosity, ε, and angular velocity as indicated in Eq. 9.

$$\varepsilon_2 = \varepsilon_1 \cdot \left(\frac{\omega_1}{\omega_2} \right)^{\frac{2}{4.7}} \tag{9}$$

3. Materials and Methods

3.1 Cell Culture

The cell line used for this research was the mouse hybridoma MM1A [34]. This cell line secretes an IgG1 monoclonal anti-body specific to the epsilon chain of the CD3 T-cell receptor complex. Medium used in all cultures was Dulbecco's Modified Eagle Medium (DMEM) which was supplemented to achieve the following final concentrations; 10% Calf Bovine Serum (CBS) (Hyclone, Logan, UT), an additional 2 mM L-Glutamine for an initial concentration of 6 mM, 100 units/mL penicillin, 100 μg/mL streptomycin, 10 mM HEPES Buffer, and 3 x 10^{-5} M 2-mercapto-ethanol. High glucose DMEM was used for all experiments except batch cultures for determining kinetic constants, in which case glucose free DMEM was supplemented to varying concentrations of glucose. All medium ingredients other than CBS were purchased from Invitrogen (Carlsbad, CA). Cell counts and viability assays for all cultures were performed using a Trypan Blue Exclusion Assay and a Hemocytometer.

3.2 Batch Culture

Initial rate experiments were conducted to determine kinetic model parameters according to the approach outlined by Glacken *et al.* [35]. The approach results in pseudo-steady state relationships as the measurements are taken over a short time at low cell concentrations to ensure

cell growth rate is solely a function of known constant concentrations of inhibitor and or substrate.

Initial rate experiments were carried out in 12-well tissue culture plates containing 4 mL of medium. Varying concentrations of filter sterilized glucose (Sigma, St. Louis, MO), ammonium chloride (J.T. Baker, Phillipsburg, PA), or sodium lactate (Sigma, St. Louis, MO) were added to glucose free DMEM in individual wells. Each well was inoculated with 2.0×10^5 total cells from a larger stock being maintained in exponential growth phase. Cells were counted every 14 hours to determine growth rate at each concentration. The lowest concentration of each inhibitor resulting in a growth rate of zero was used as the maximum concentrations in the kinetic model, while orders of inhibition were determined from Lineweaver-Burke plots [30].

Batch culture was also used to determine the effect of pH on growth rate and viability. The pH of the culture medium in a 12-well plate was changed with the addition of 1 M hydrochloric acid (Sigma, St. Louis, MO) or 1 M sodium hydroxide (Sigma, St. Louis, MO). Cells were seeded at a lower concentration of 5×10^4 total cells per well as it was found that more consistent results were obtained using a single count at the end of 48 hours for calculating the growth rate. Counting cells every 14 hours as described above for the nutrient and metabolite studies led to periods of irregular pH as the medium equilibrated between normal laboratory atmosphere and the increased CO_2 incubator atmosphere. Following the 48 hour culture period pH was immediately measured ensuring the value reflected equilibrium with incubator CO_2 concentrations. Finally cells were counted to assess viability and growth rate as a function of pH.

Yield coefficients for glucose, ammonium ion, lactate, and mAb were determined using a 25 mL batch culture with an initial concentration of 2×10^5 cells/mL. Concentrations of cells

and every species of interest were determined every 14 hours. By plotting species concentration versus cell concentration the yield coefficient is determined from the linear region of the resultant curve.

3.3 Bioreactor Culture

The centrifugal apparatus used for this research study is a COBE® Spectra™ Apheresis System (Gambro BCT Inc., Lakewood, CO) manufactured for use as a blood separation device. The bioreactor chamber itself consists of a single conical chamber (11.4 mL) which is part of the Cell Purging tubing set (Gambro BCT Inc.) made for attachment to the COBE® Spectra™. Cell Purging tubing sets are supplied sterile from the manufacturer, and intended for single use applications. To conserve cost, tubing sets in our laboratory are used for multiple individual experiments and sanitized by pumping 70% ethanol through the entire system for at least 24 hours between experiments. Prior to reactor start-up tubing sets were modified to reflect the flow profile shown in Figure 2, where medium is routed to and from the reactor through tubes using an anti-twister mechanism similar to that shown by Van Wie *et al.* [22].

After sanitization the tubes and reactor were emptied of ethanol, then rinsed and filled with sterile DMEM. All air was removed from the system prior to start-up as the presence of bubbles results in a disruption of the cell bed during reactor operation, and ultimately loss of CCBR culture. Reactor experiments were begun by spinning the Spectra™ rotor at a given RPM, e.g. 650 RPM, corresponding to 60 G's at the reactor inlet and 35 G's at the reactor exit. Next the feed pump, which combines flow from the fresh feed and recycle streams, was adjusted to supply 5.2 mL/min of medium to the reactor, corresponding to a fluid speed of 0.37 cm/s at the reactor entrance, 0.035 cm/s at the cell bed center of mass, and 0.016 cm/s at the reactor's

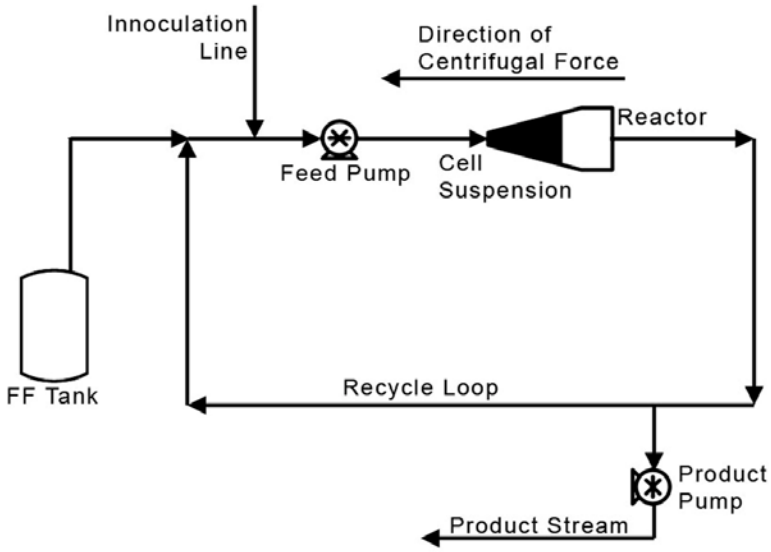

Figure 2. Process flow diagram for CCBR used in the culture of hybridoma cells. The 11.4 mL reactor was inoculated with 175-250 million cells which were subsequently cultured for 14-28 days. A 1L feed tank (FF tank) provides fresh DMEM and spent medium is removed by the product pump. Because the CCBR behaves as a continuously stirred tank reactor, a sample taken of the product stream is representative of concentrations of substrates and metabolites in the reactor.

widest point. Typically 2.0 - 2.5 x 10^8 total MM1A cells, being maintained in the exponential growth phase in a batch culture process, were supplied to the system through a valve connected to the inoculation line. Initially the product pump was set to 0.25 mL/min; this automatically sets the fresh feed to the same flow rate based on a mass balance and in this case corresponds to a dilution rate of 1.3 h^{-1}. Product flow rate was increased as needed to maintain adequate nutrient supply and pH.

Sampling the reactor to assess cell viability and density was accomplished by stopping the centrifugal rotor and allowing the feed pump to remain running at an increased rate of 16.5 mL/min for 20 min. This operation resulted in the even distribution of cells throughout the recycle loop resulting in a single continuously stirred tank reactor (CSTR) with at total volume of 31.5 mL. This process was repeated at least once per day and most often twice per day to assess cell density and viability while medium collected from the product stream was stored for later determination of glucose, ammonium, lactate and MAb concentrations.

3.4 MAb Quantification

MAb concentration was determined using the Mouse IgG LL NANORID Kit (The Binding Site Limited, Birmingham, UK). Briefly, the NANORID Kit quantifies MAb concentration by diffusion through an agarose gel containing a mono-specific antibody. Samples are added to a cylindrical well and over time allowed to reach equilibrium between complex formation and breakdown with the mAb contained in the gel; consequently, ring diameter is proportional to sample concentration. Ring diameter was determined with a Transidyne General Calibrating Viewer (Transidyne General Corporation distributed by Kellestad Laboratories Inc., Chaska, MN).

3.5 Glucose, Ammonium Ion, and Lactate Quantification

Glucose was quantified using Glucose Color Reagent (Raichem, San Diego, CA). The method contained within the package insert was adapted for use with a 96-well plate. Briefly, 150 µl of color reagent was added to each well followed by 10 µl of either standard or sample diluted 1:10 which was added to specific wells. The reaction was allowed to go to completion by incubating for 10 min at 37°C. Then the plate was read at a 500 nm wavelength using a Spectra Rainbow plate reader (SLT Instruments, Austria). Sample concentration was determined from a standard curve.

Ammonium ion was quantified using Ammonia Reagent (Raichem, San Diego, CA). The method contained within the package insert was again adapted for use with a 96-well plate. Briefly, 110 µl of Reagent 1, containing 2-Oxoglutarate and reduced nicotinamide adenine dinucleotide phosphate (NADPH) is added to 20 µl of sample. After an initial absorbance measurement at 340 nm using a Victor3 plate reader (Perkin Elmer, Waltham, MA), 5 µl of Reagent 2 containing glutamate dehydrogenase is added to the mixture catalyzing the formation of L-glutamate and $NADP^+$. The amount of NADPH oxidized is equal, on a molar basis, to the amount of ammonium ion contained in the sample. A second absorbance reading at 340 nm is made following 5 minutes of incubation at room temperature. The absorbance from Reading 2 is subtracted from the absorbance from Reading 1 and the resultant change in absorbance was used for concentration determination using a standard curve.

Lactate was quantified using a lactate reagent from Sigma Diagnostics (Sigma Diagnostics, St. Louis, MO). The procedure was again adapted for use in a 96-well plate; specifically, 10 µL of either standard or sample diluted 1:10 was added to appropriate wells, and

then 100 μL of reagent, containing lactate oxidase which reacts with lactic acid and catalyzes the oxidative condensation of chromogen precursors to produce a colored dye was added to each well. Concentration was determined from a standard curve after reading the plate at 540 nm with the Spectra Rainbow plate reader.

4. Results and Discussion

4.1 Impact of pH

Decreased culture pH will occur when the buffering capacity of the medium is overcome; this can happen due to accumulation of lactic acid, as most of the glucose during mammalian cell culture is metabolized to lactate [15, 26, 36], or the formation of carbonic acid through the release of CO_2 during cellular respiration [15]. The individual impact of extracellular pH on growth rate and viability was studied in low density batch cultures (inoculation density of 1.25 x 10^4 cells/mL) to ensure buildup of metabolites did not further effect pH or cellular growth rate. Results are shown in Figure 3. Due to error associated with the pH measurement the average of the growth rate and viability for replicate experiments is reported for measurements within 0.05 pH units. Results reveal that viability and growth rates are both reduced as cultures deviate from an optimal pH of 7.2. Figure 3 indicates for maintenance of 80% of the maximum growth rate pH must be maintained between 6.8 and 7.6, and for 90% of the maximum growth rate to be observed pH must be maintained between 6.9 and 7.4.

4.2 Model Parameters

As outlined in the Methods section initial rate batch culture experiments were conducted to determine the growth model constants in Eq. 1-5, the values for which appear in Table 1. The

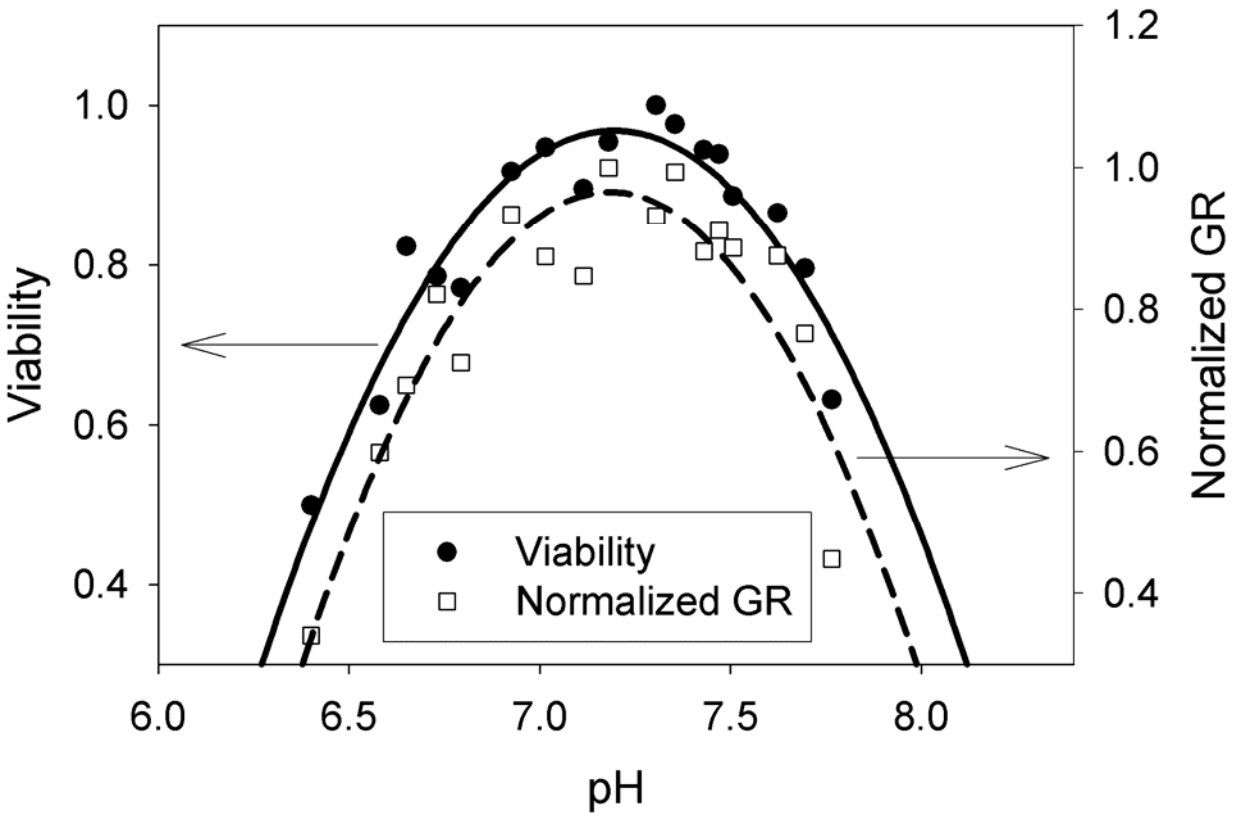

Figure 3. Cell growth rate and viability dependence on medium pH. As pH deviates from the optimum of 7.2 both growth rate and viability are affected to an increased degree. To maintain viability and growth rate above 90% pH must be maintained within a range of 6.9 to 7.4 throughout a culture.

Model Parameter	**Value**
μ_{max}	0.065 h^{-1}
C_{L_max}	929 mg/dL
C_{A_max}	5.78 mM
C_M	16 mg/dL
n (lactate)	0.22
m (ammonium ion)	0.52
p (ammonium ion)	-1.16
q (lactate)	0.55
Y_{GC}	15.0 x 10^{-5} (mg/dL)/(cell/mL)
Y_{mAbC}	5.6 x 10^{-5} (μg/mL)/(cell/mL)
Y_{AC}	0.13 x 10^{-5} (mM)/(cell/mL)
Y_{LC}	17.1 x 10^{-5} (mg/dL)/(cell/mL)

Table 1. Values of the constants for the proposed kinetic model in Eq. 1-5.

initial rate approach for determining constants was used as it most resembles the conditions within the CCBR. Using the initial rate approach cells are subjected to a constant concentration of substrate or inhibitor and the growth rate response for the condition is observed, much the same during CCBR operation. At steady state in the CCBR, when the reactor is full of cells, the growth rate and rate at which cells are removed from the system by the product stream are equal; consequently a constant cellular concentration is maintained, resulting in constant concentrations of substrate and inhibitors at a single dilution rate.

In this paper steady state is modeled by setting both the cellular growth rate and rate at which cells leave the system in Eq. 1 equal to zero. Although this is not physically correct, conceptually it serves the same purpose as setting the rate at which cells are leaving the reactor equal the cellular growth rate, because both result in zero change in CCBR cell concentration. Additionally, because the concentration of cells is unchanged with respect to time during steady state Eq. 2-5 will also equal zero, resulting in constant concentrations of all modeled parameters.

Types of cellular growth rate inhibition and orders of inhibition were determined through construction of Lineweaver-Burk plots, $1/\mu$ vs. $1/C_{Glucose}$ for both ammonium ion and lactate [30]. The Lineweaver-Burk plot for lactate suggests uncompetitive inhibition as varying inhibitor concentrations provide lines with the same slope and as inhibitor concentrations increase y-intercept values also increase. A similar double reciprocal plot for ammonium ion shows that as inhibitor concentrations are increased the resultant slopes also increase. However, because of the lack of intersection at a single point and because the resultant orders of inhibition m and p are greater and less than zero, respectively, ammonium exhibits a general type of inhibition as proposed by Han and Levenspiel [30].

Glucose was chosen as the lone substrate in this model although it is well known that both glucose and glutamine are necessary substrates providing the major energy and carbon sources for mammalian cell growth. A multiple substrate model can be developed from one of three forms; the interactive or multiplicative form, additive form, or non-interactive form to predict growth rate dependence from both glucose and glutamine [37]. However, development of such a model would require twice as many fitted parameters and it is best if a simpler model can be selected that will adequately predict cell growth. Additionally, it will be shown that glutamine does not reach inhibitory levels due to spontaneous degradation or metabolic depletion, based on observed CCBR ammonium ion concentrations and literature values of the ratio of consumed glutamine to ammonia production. Therefore, glutamine can be omitted as a modeled parameter eliminating the need for a multiple substrate model for practical system simulation.

4.3 Combined Impact of pH and Predicted Inhibition

The impact of pH along with substrate and metabolite concentrations on growth rate is further illustrated for a CCBR seeded with 2.5 x 10^8 cells (2.2 x 10^7 cells/mL for the 11.4 mL CCBR) and operated at a constant dilution rate of 1.3 h^{-1} and 650 RPM. As shown in Figure 4 there is an initial lag phase of 45 h after which exponential growth is observed until cells fill the reactor at a density of 5.8 x 10^7 cells/mL. At this point pH drops to a minimum of 6.75 where Figure 3 shows growth rates will be limited to 77% of the maximum value from pH alone.

Normalizing Eq. 1 to the maximum specific growth rate of 0.065 h^{-1} will provide a fraction of the maximum specific growth rate which will be observed at a particular cell concentration and dilution rate. Doing so results in a model predicted growth rate which is 61% of the maximum. Individual contributions for each metabolite ion can be determined by

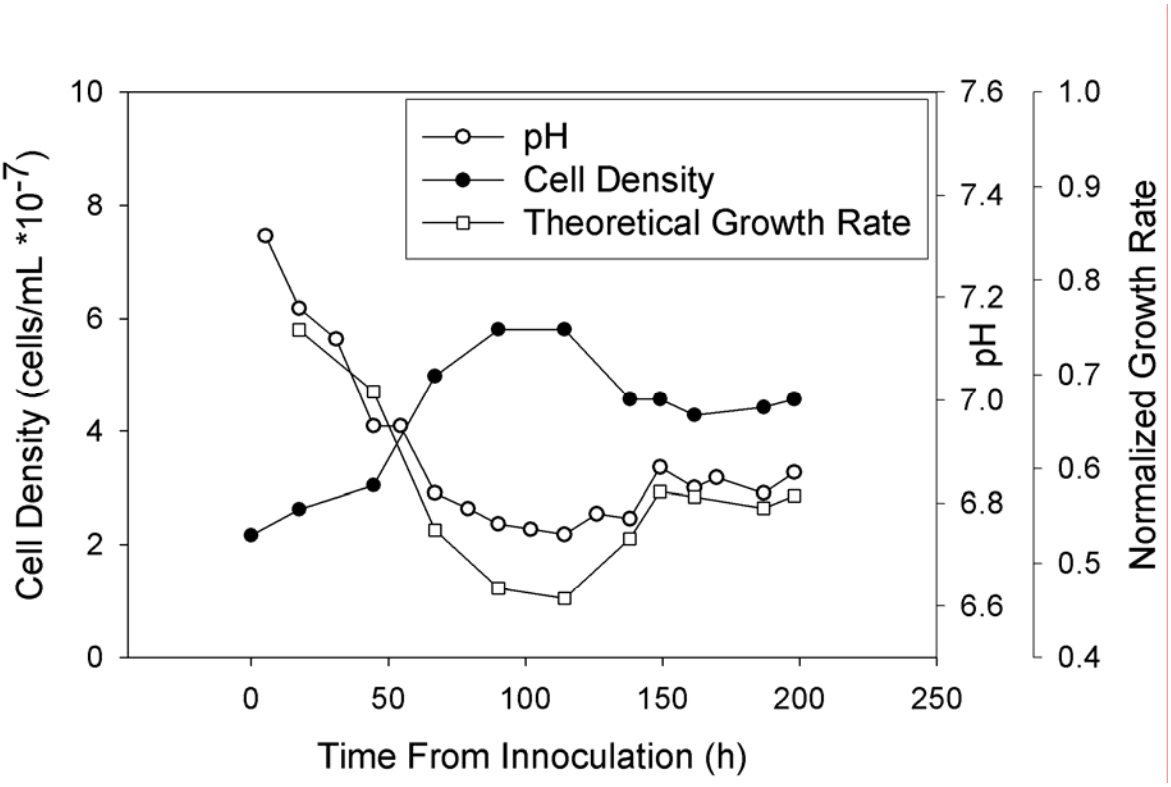

Figure 4. Impact of pH on CCBR culture at a constant 1.3 h^{-1} dilution rate. As cell population increases to 5.8 x 10^7 cells/mL inhibition increases as substrate concentration and pH both decrease while inhibitory metabolites increase resulting in an overall growth rate predicted to be 47% of the maximum. Theoretical growth rate is calculated based on a combined term including a fit to the pH growth rate curve and contributions from lactate, ammonium and glucose inhibition factors. The significant inhibition results in a decrease in cell number and a subsequent slight increase in overall inhibition to 60% of the maximum growth rate at a culture density of 4.6 x 10^7 cells/mL.

evaluating the single exponential term in the numerator containing the inhibitor of interest; in the same fashion substrate inhibition can be determined if C_G is divided by the denominator of Eq. 1. Individual contributions of lactate, ammonium, and substrate are 0.92, 0.77, and 0.86, respectively, where a value of 1 would indicate no inhibition. Therefore, the combined inhibition from pH, metabolite accumulation, and substrate depletion results in a predicted growth rate that is 47% of the maximum ultimately contributing to a decline in CCBR culture density to 4.6 x 10^7 cells/mL. The lower concentration of cells results in decreased glucose consumption and metabolite production and an observed rises in pH to 6.85, consequently the overall inhibition is reduced and a growth rate which is nearly 60% of the maximum results.

Inhibiting pH levels can be eliminated through increasing dilution rate to provide adequate buffering capacity. Additionally, increasing dilution rates minimize inhibition through lowering lactate and ammonium ion concentrations while raising substrate levels. When pH, substrate and inhibitor concentrations are regulated by stepwise increases in dilution rate from an initial value of 1.3 h^{-1} up to 5.2 h^{-1}, as shown in Figure 5, cells experience a lag phase followed by an exponential growth phase until cells fill the reactor at a steady state concentration of 8.5 x 10^7 cells/mL. During the initial steady state, from 52 to 143 h when the dilution rate varies between 3.5 and 4.4 h^{-1}, the collective set of inhibition terms in Eq. 1 predict a growth rate multiplier between 0.72 and 0.78 for the maximum growth rate. Lactate concentrations provide little inhibition with a term value between 0.94-0.96, glucose has slightly lower values between 0.91-0.93, and the ammonium term has the largest predicted impact between 0.84 and 0.88. The pH inhibition is minimal as pH was maintained between 6.90 and 7.35 with an average pH of 7.12 corresponding to an inhibition multiplier of 0.96 for the maximum growth rate.

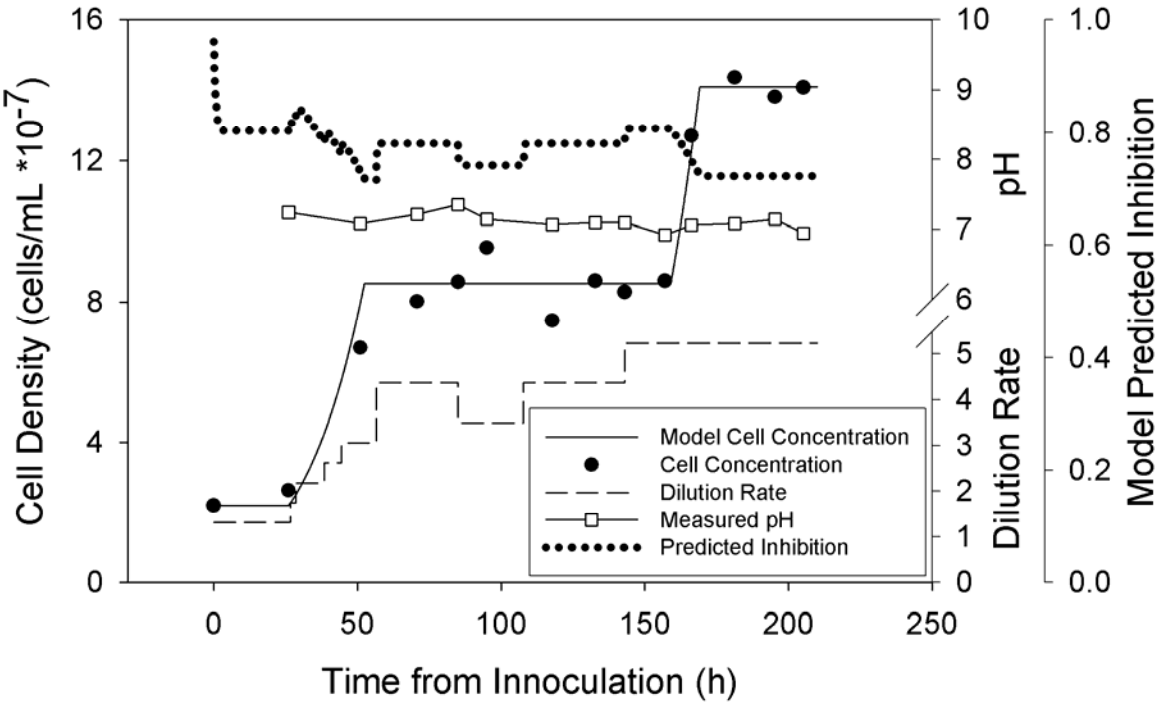

Figure 5. The impact of dilution rate and CCBR RPM on inhibition and cell culture density. To diminish inhibition effects dilution rate can be used to increase substrate concentration while decreasing lactate, and ammonium ion levels, as well as maintain pH buffering capacity. A steady state concentration of 8.5 x 10^7 cells/mL is maintained with a dilution rate between 3.5 and 4.4 h^{-1} corresponding to an overall normalized model-predicted growth rate between 0.72 and 0.78. Limited inhibition ensures that as centrifugal force is increased a second steady state at increased cell concentration will result.

Collectively the overall inhibition during the initial steady state results in a growth rate between 69-75% of the maximum.

If the centrifugal force is increased without a subsequent increase in drag force (i.e. at constant inlet flow rate) a higher population density can be maintained within the reactor. To illustrate this point, Figure 5 shows results for an RPM increase from 650 RPM at 143 h to a final RPM of 1200 at 181 h, which corresponds to a total increase in centrifugal force by a factor of 3.4. The RPM was increased through a series of steps as follows; 750 RPM at 143h, 850 RPM at 166 h and finally 1200 RPM at 181 h. An initial increase in RPM from 650 to 750 will increase the centrifugal force by a factor of 1.3 and using Eq. 9 result in a 38% increase in cell number. The second increase at 166 h to 850 RPM increases the centrifugal force by a factor of 1.7, corresponding to a predicted 70% increase in cell density to 1.4×10^8 cells/mL which is the density determined experimentally at 1200 RPM. Based on Eq. 9 cell density should have reached 2×10^8 cells/mL at 1200 RPM. Predictions of cell density using Eq. 9 are within 30% of experimentally determined values reinforcing the need for extremely accurate cell bed volume determinations and a better understanding of all the fluid dynamics affecting cell density before more accurate predictions can be made.

During the final steady state the ammonium ion multiplier is 0.84, while lactate and glucose multipliers are 0.94, 0.91, respectively; a pH multiplier of 0.95 is due to an average pH of 7.06 from 170-210 h. Consequently, an overall growth rate which is 68% of the maximum would likely necessitate an increase in dilution rate to maintain the culture for weeks or months. To maintain a growth rate which is 90% of the maximum and ensure the culture is sustained the

dilution rate would have to increase to 22 h^{-1} – an explanation and thorough analysis of this will be provided in the model utility section to follow.

As has been consistently shown through predictions with the kinetic model the ammonium ion term has the largest deleterious impact on cellular growth rate for the MM1A cell line. Work by Hassell *et al.* [26] and Doyle and Butler [25] shows the effect of ammonium ion on cellular growth rate supporting it's significant impact on MM1A growth rate. First of all, the work shows growth rate sensitivity to ammonium ion is cell line dependant. Secondly, it is the small quantity of dissolved NH_3 instead of the measured NH_4^+ concentration that has the greatest effect on growth rate. This is supported by the fact that IC_{50} values of ammonium chloride increase as the ratio of NH_3/NH_4^+ is decreased with decreasing pH [25, 26]. Because the pK_a of ammonium ion is 9.25, at the optimal pH for cell growth of 7.2, 99% of dissolved ammonia will be the less toxic protonated species, making the ammonium ion phenomenon more important at pHs above the optimal value for cell growth.

4.4 Model Efficacy

Figure 6 is used to illustrate the accuracy of the model in predicting actual concentrations for a CCBR experiment seeded with 1.6 x 10^7 cells/mL, and run for 261 h at 700 RPM with a constant inlet flow rate of 5.2 mL/min with an initial dilution rate of 1.3 h^{-1}. During operation pH was checked every 12 hours and as pH declined toward 7.0 dilution rate was adjusted by incremental increases of ~1 h^{-1} ensuring pH remained between 7.0 and 7.2 with an average of 7.1 over the entire culture. According to Figure 3 the pH range for this experiment corresponds to conditions with little inhibition from pH and observed growth rates greater than 96% of the maximum specific growth rate.

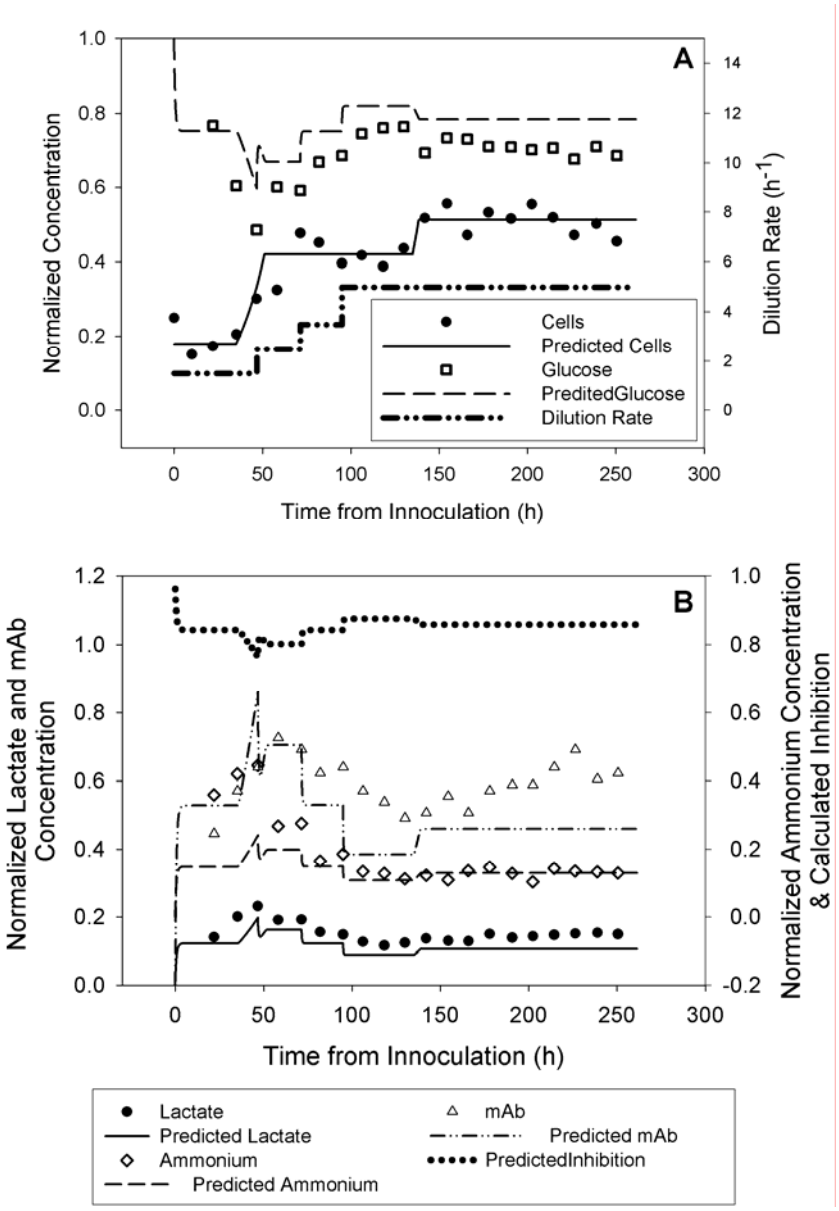

Figure 6. Comparison of model predicted and actual concentration data collected every 12 h during 261 h CCBR run. Comparison of model predicted values and actual normalized measured concentrations show all relative standard deviations are below 13%: (A) Cell concentrations were normalized to 1 x 10^9 total cells; glucose to 400 mg/dL; (B) Concentrations of lactate were normalized to 929 mg/dL; ammonium ion to 5.7 mM; and mAb to 70 μg/mL. The calculated inhibition value consists of all terms multiplying μ_{max} in Eq. 1.

Three dilution rate increases are observed following the lag phase as the initial dilution rate of 1.3 h^{-1} is increased to 5.0 h^{-1} over a 48 h period. Consequently, simultaneous step changes in monitored species concentrations are seen depending on whether species are being consumed or produced in the CCBR. Results shown in Figures 6A and 6B indicate that following an initial 35 h lag phase exponential growth is observed resulting in a density of 3.7 x 10^7 cells/mL that remains relatively constant over the period covering 55-135 h. At the beginning of this period the overall inhibition multiplier is 0.80 and through a series of dilution rate increases is raised to 0.88 at 95 h.

Although there was no apparent change in process conditions a new steady state with a density to 4.5 x 10^7 cells/mL is observed at 140 h. The increase in cell concentration can be explained by considering that the new less inhibitory conditions provides an environment more supportive of cell growth. After a lag phase of about 45 h from the last dilution rate change, which is similar in duration to the lag phase experienced at the start of culture, an increased cellular growth rate now exceeding the rate of removal from the reactor results, allowing the reactor cone to fill to a slightly larger extent. Of significance is the comparison of CCBR species concentrations to model predicted values derived from Eq. 2-5, shown in Figure 6. Both modeled and actual concentrations are normalized before finding relative standard deviations; cells are normalized to 1.0 x 10^9 total cells, mAb and glucose to 70 μg/mL and 400 mg/dL respectively, while ammonium and lactate are normalized to maximum inhibitor concentrations of 5.8 mM and 930 mg/dL, respectively. As shown in Figure 6, we see excellent agreement over the entire 260 h run. Relative standard deviations between model predicted and experimentally determined concentrations for the various species are 8.1% for glucose, 13% for mAb, 9.3% for

ammonium ion, 3.8% for lactate, and 7.2% for the cell concentration (when considering the model is set to a steady population density at a given RPM).

Although glutamine is not predicted with this model it can be shown it does not contribute significantly to growth rate inhibition based on literature values of kinetic parameters and measured ammonium ion concentrations. It has been shown for various hybridoma cell lines that ammonia is produced at a ratio of 0.4 - 0.8 mols per mol of glutamine consumed [10, 36, 38, 39]. Medium used in the experiments for this paper is supplemented with glutamine prior to culture, resulting in an initial concentration of 6 mM. If one uses the lower limit yield coefficient of 0.4 mols ammonia per mol glutamine consumed, the largest theoretical amount of glutamine consumed will result. Using the average ammonium ion concentration over the final 100 h of experimental culture in Figure 6, 0.75 mM, a minimum glutamine concentration of 4.1 mM will result. Additionally, Acosta et al. reported a Monod constant for glutamine of 0.08 mM [38]. Therefore, for glutamine depletion to result in a 10% reduction in growth rate concentrations would have to fall below 0.72 mM, which is significantly lower than the worst case scenario calculated above. Therefore, we conclude that inhibition due to glutamine is insignificant in the current study.

In addition to cellular metabolism glutamine is spontaneously degraded to ammonia and pyrrolidone carboxylic acid and the rate of degradation is both medium type and pH dependant [40]. Over the course of 400 h Ozturk and Palsson [40] found up to 40% of medium glutamine could decompose, and not accounting for this decomposition raised the yield coefficient of mols of ammonia produced per mol of glutamine consumed from the actual value of 0.52 to an apparent value of 0.68. Not accounting for glutamine decomposition can produce up to a 300% error when determining cellular consumption of glutamine and production rates of ammonia

[40]. However, because growth rate inhibition depends on total ammonia concentration, knowing whether ammonia is produced by cells or as a result of decomposition is of little importance for calculating total growth rate inhibition, as in this paper. Furthermore, the low concentration of ammonium ion measured in the culture medium indicates that at worst only 30% of the initial glutamine is consumed. According to the kinetic considerations already stated, the initial concentration would have to be reduced by nearly 90% before significant inhibition due to glutamine depletion is observed.

4.5 Implications for Centrifugal Bioreactor Scale-Up

Using this kinetic model to optimize the conditions within the CCBR will result in a maximum cellular growth rate. Although, the volume of the CCBR is small, 11.4 mL, the productivity of the system in terms of mAb production rate can be quite significant. Using the rate of mAb production in the final 100 h of Figure 6, 40 μg/mL, and the dilution rate of 4.3 h^{-1} it is possible to produce 48 mg/day of mAb. To increase productivity it is possible to increase reactor volume; for example tubing sets are available from Gambro which use a 40 mL reactor. Furthermore, our lab has made modifications to the CCBR rotor allowing two reactor chambers to be cultured simultaneously. The rotor could easily be modified to hold 4 reactors and if each were of the 40 mL type the total system volume would be increased 15-fold over the current apparatus discussed in this paper, thus making it possible to produce over 600 mg/day of mAb. Production could easily be increased beyond this to over a gram per day if culture population density is increased through changes in rotor RPM.

Traditional scale-up of the CCBR process where reactor size is increased to meet production needs would likely result in complications such as extreme amounts of power required for system rotation in addition to mechanical instability during the rotation of large

reactor volumes. Traditional scale-up also limits the applicability of small volume kinetic analysis due to the increased mechanical stresses on cells from mixing requirements and nutrient gradients within the bioreactor which lead to non-uniform growth rates. However, it appears more likely that CCBR scale-up would include many small volume reactors operating in parallel, similar to that which has been done commercially by Kinetic Biosystems, Inc. for use in waste water processing [23, 24]. As each small volume reactor in a scaled-up process would provide the same uniform environment the kinetic analysis developed in this manuscript would directly apply, providing accurate environmental predictions during cell culture.

Bioreactor process optimization is not solely achieved through increasing cellular growth rates at various densities, as in this study, but through jointly maximizing cellular productivity and density. Cellular protein productivity is often not directly related to growth rate; commonly protein production rates increase when cells are stressed or in a growth arrested state [12, 17, 41-43]. Unfortunately, increased protein productivity observed during these conditions is countered by apoptosis which results from culture stresses that may include nutrient limitation, metabolite accumulation, and mechanical stresses [44-47], thereby limiting the overall productivity of the bioreactor. Apoptosis, or programmed cell death, is a physiological process characterized by the suicidal response of a cell to a non-lethal physiological or environmental stimulus [41, 44].

Within the current study the method of cellular death, be it necrosis or apoptosis, was not differentiated as understanding the collective impact of process conditions on cellular growth rate during CCBR operation was the primary objective. However, as has been presented in this manuscript manipulation of the dilution rate influences inhibition of both substrate and metabolite concentrations. Identification of substrate and metabolite concentrations which result in apoptosis versus necrosis and the relation to protein productivity is of interest for future

studies to further optimize the system. Additionally, due to the unique cell immobilization method within the CCBR mechanical stresses and their possible role in activation of apoptosis pathways should be studied to further understand cell culture optimization for the CCBR technology.

4.6 Model Utility

Given our model can accurately predicts cell, glucose, mAb, lactate and ammonium ion concentrations, we can learn valuable information about what is required to maintain optimal growth conditions at extreme culture densities. This can be done for a variety of cell concentrations achievable through increases in CCBR RPM up a maximum density of 3×10^8 cells/mL.

To assess the impact of dilution rate we can rearrange the model in Eq. 1 for the normalized growth rate μ/μ_{max} to determine the fraction of maximum growth rate that will be achieved for various cell densities as presented in Figure 7. For maintaining higher population densities Figure 7 clearly shows the necessity of increasing dilution rate which has the impact of reducing the concentration of toxic metabolites and increasing the concentration of substrate. For example, to maintain a cell concentration of 1×10^7 cells/mL above 90% of the maximum growth rate requires a dilution rate of 1.66 h^{-1} whereas μ will be a mere 31% of the maximum value at the same dilution rate when the population density increases to 2×10^8 cells/mL. This type of analysis provides a valuable tool for finding the most effective dilution rate to maintain optimum growth rate conditions.

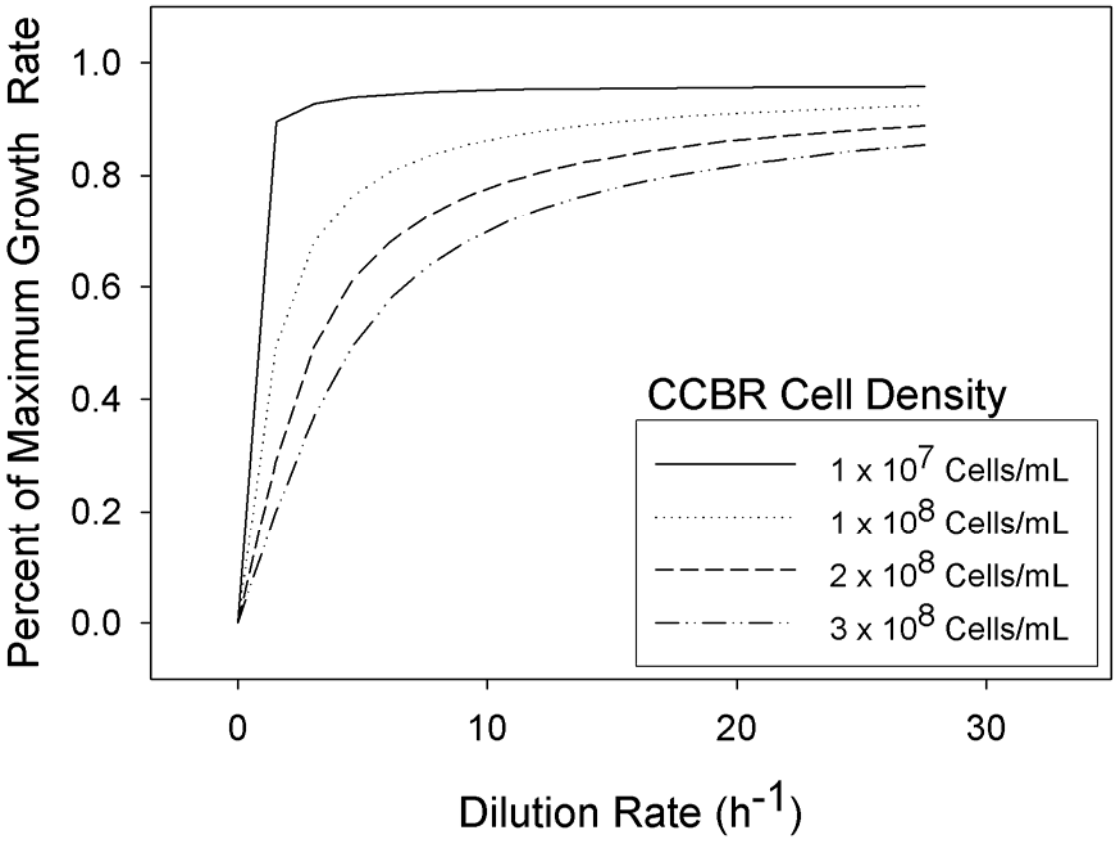

Figure 7. Maximum growth rate as a function of varying dilution rates and cell concentration maintained within the CCBR. As the cell population density is increased the dilution rate must also be increased to prevent inhibition due to lactate and ammonium ion accumulation as well as glucose depletion.

In order to maintain a density of 2 x 10^8 cells/mL at 90% of the maximum growth rate our model indicates a dilution rate of 33 h^{-1} and a corresponding fresh feed flow rate of 6.3 mL/min would be required. Because the required fresh feed flow rate is higher than the 5.2 mL/min inlet feed rate we've used thus far the inlet feed rate would need to increase in order to accommodate the necessary dilution rate. From this discussion it is apparent that to maintain the desired density within the reactor while increasing inlet feed rate the RPM would also have to be increased to ensure cells are retained within the reactor.

5. Conclusions

The CCBR system used for this work immobilizes cells allowing continuous high density mammalian cell culture for protein production. High density culture increases volumetric protein productivity, but lends itself to rapid changes in environmental conditions leading to growth rate inhibition through substrate depletion, metabolite accumulation, or suboptimal culture pH. A kinetic model describing mAb concentrations and the dependence of cellular growth rate on glucose, ammonium ion, and lactate concentrations has been developed using low density small volume batch studies. Additional batch studies show an optimum pH of 7.2 for the MM1A hybridoma; furthermore, viabilities and growth rates are maintained within 90% of maximum values when pH values are between 6.9 and 7.4.

An example is presented for a culture operated at an initial population density of 1.6 x 10^7 cell/mL and dilution rate of 1.3 h^{-1} at which growth rate is predicted to be 96% of the theoretical maximum. As biomass increases to 4.5 x 10^7 cells/mL an unchanged dilution rate reduces the predicted growth rate to 67% of the maximum through accumulation of ammonium ion and lactate in addition to glucose depletion, the individual contributions of each to overall inhibition are 0.81, 0.93, and 0.89, respectively. However, kinetic modeling predicts, and

experimental results confirm, that by increasing the dilution rate from 1.3 to 5.2 h^{-1} growth rate inhibition in the CCBR will be significantly reduced.

Furthermore, due to the unique cellular immobilization technique of the CCBR every cell is individually bathed in culture medium, which enhances the likelihood each cell is subjected to the same steady-state environmental conditions. Consequently, the proposed kinetic model may be extended to predict dilution rate requirements for much higher density cultures of 2 x 10^8 cells/mL and above. Finally, the design of the CCBR which provides continuous medium provision and removal of toxic metabolites is an ideal system for the study of high density culture, providing a tool to identify characteristics inherent to any reactor designed to enhance productivity through increased cell density.

Acknowledgements

The authors acknowledge the Biotechnology Training Grant (NIH 5T32-GM008336-16) and the Gene & Linda Voiland School of Chemical Engineering and Bioengineering for graduate student support and supplies. Equipment in the form of the COBE© Spectra Apheresis System and Cell Purging tubing sets in addition to corporate technical research staff consultation are a result of a donation by Gambro BCT Inc., Lakewood, CO. Mr. R. Hutchinson of the Washington State University College of Engineering and Architecture Machine Shop was instrumental in design and fabrication of the CCBR chambers used in these experiments.

References

1. Dalm, M. C.; Cuijten, S. M. R.; van Grunsven, W. M. J.; Tramper, J.; Martens, D. E., Effect of feed and bleed rate on hybridoma cells in an acoustic perfusion bioreactor: part I. Cell density, viability, and cell-cycle distribution. *Biotechnology and Bioengineering* **2004,** 88, (5), 547-57.

2. Golmakany, N.; Rasaee, M. J.; Furouzandeh, M.; Shojaosadati, S. A.; Kashanian, S.; Omidfar, K., Continuous production of monoclonal antibody in a packed-bed bioreactor. *Biotechnolgy and Applied Biochemistry* **2005,** 41, (3), 273-8.

3. Mercille, S.; Johnson, M.; Lanthier, S.; Kamen, A. A.; Massie, B., Understanding Factors that Limit the Productivity of Suspension-Based Perfusion Cultures Operated at High Medium Renewal Rates. *Biotechnology and Bioengineering* **2000,** 67, (4), 435-450.

4. Andersen, D. C.; Reilly, D. E., Production technologies for monoclonal antibodies and their fragments. *Current Opinion in Biotechnology* **2004,** 15, (5), 456-62.

5. Chen, K.; Liu, Q.; Xie, L.; Sharp, P. A.; Wang, D. I. C., Engineering of a mammalian cell line for reduction of lactate formation and high monoclonal antibody production. *Biotechnology and Bioengineering* **2001,** 72, (1), 55-61.

6. Simon, L.; Karim, M. N., Identification and control of dissolved oxygen in hybridoma cell culture in a shear sensitive environment. *Biotechnology Progress* **2001,** 17, (4), 634-42.

7. Meuwly, F.; Ruffieux, P. A.; Kadouri, A.; von Stockar, U., Packed-bed bioreactors for mammalian cell culture: bioprocess and biomedical applications. *Biotechnol Adv* **2007,** 25, (1), 45-56.

8. Goldman, M. H.; James, D. C.; Rendall, M.; Ison, A. P.; Hoare, M.; Bull, A. T., Monitoring recombinant human interferon-gamma N-glycosylation during perfused fluidized-bed and stirred-tank batch culture of CHO cells. *Biotechnology and Bioengineering* **1998,** 60, (5), 596-607.

9. Kundu, P. K.; Prasad, N. S.; Electricwala, S. E.; Varma, R.; Datta, D., Getting higher yields of monoclonal antibody in culture. *Indian Journal of Physiology and Pharmacology* **1998,** 42, (2), 155-71.

10. Xie, L.; Wang, D. I. C., High Cell Density and High Monoclonal Antibody Production Through Medium Design and Rational Control in a Bioreactor. *Biotechnology and Bioengineering* **1996,** 51, (6), 725-729.

11. Jan, D. C. H.; Petch, D. A.; Huzel, N.; Butler, M., The Effect of Dissolved Oxygen on the Metabolic Profile of a Murine Hybridoma Grown in Serum-Free Medium in Continuous Culture. *Biotechnology and Bioengineering* **1997,** 54, (2), 153-164.

12. Miller, W. M.; Blanch, H. W.; Wilke, C. R., A kinetic analysis of hybridoma growth and metabolism in batch and continuous suspension culture: Effect of nutrient concentration, dilution rate, and pH. *Biotechnol Bioeng* **1988,** 32, (8), 947-65.

13. Batt, B. C.; Davis, R. H.; Kompala, D. S., Inclined sedimentation for selective retention of viable hybridomas in a continuous suspension bioreactor. *Biotechnology Progress* **1990,** 6, (6), 458-64.

14. Kim, B. J.; Chang, H. N.; Oh, D. J., Application of a cell-once-through perfusion strategy for production of recombinant antibody from rCHO cells in a Centritech Lab II centrifuge system. *Biotechnol Prog* **2007,** 23, (5), 1186-97.

15. Gramer, M. J.; Britton, T. L., Antibody production by a hybridoma cell line at high cell density is limited by two independent mechanisms. *Biotechnology and Bioengineering* **2002,** 79, (3), 277-83.

16. Jackson, L. R.; Trudel, L. J.; Fox, J. G.; Lipman, N. S., Evaluation of hollow fiber bioreactors as an alternative to murine ascites production for small scale monoclonal antibody production. *Journal of Immunological Methods* **1996,** 189, (2), 217-31.

17. Yang, S.-T.; Luo, J.; Chen, C., A fibrous-bed bioreactor for continuous production of monoclonal antibody by hybridoma. *Advances in Biochemical Engineering/Biotechnology* **2004,** 87, 61-96.

18. Gramer, M. J.; Poeschl, D. M., Screening tool for hollow-fiber bioreactor process development. *Biotechnology Progress* **1998,** 14, (2), 203-9.

19. Hay, P. D.; Veitch, A. R.; Gaylor, J. D., Oxygen transfer in a convection-enhanced hollow fiber bioartificial liver. *Artificial Organs* **2001,** 25, (2), 119-30.

20. Yang, P.; Teo, W.-K.; Ting, Y.-P., Design and performance study of a novel immobilized hollow fiber membrane bioreactor. *Bioresource Technology* **2006,** 97, (1), 39-46.

21. Van Wie, B. J.; Brouns, T. M.; Elliott, M. L.; Davis, W. C., A Novel Continuous Centrifugal Bioreactor for High-Density Cultivation of Mammalian and Microbial Cells. *Biotechnology and Bioengineering* **1991,** 38, (10), 1190-1202.

22. Van Wie, B. J.; Elliot, M. L.; Lee, J. M., Development and Characterization of a Continuous Centrifugal Bio-Reactor. *Biotechnology and Bioengineering Symp.* **1986,** 17, 335-344.

23. Herman, H. H. Centrifugal Fermentation Processes. US Patent #: 5,622,819, April 22, 1997.

24. Herman, H. H.; Lin, W.; Petrecca, P. J.; Herman, T. M.; Bates, C.; Simmons, R.; Houghton, J., Centrifugal Bioreactors and Their Application in Remediation. *Remediation* **2001,** 11, (4), 15-33.

25. Doyle, C.; Butler, M., The effect of pH on the toxicity of ammonia to a murine hybridoma. *Journal of Biotechnology* **1990,** 15, (1-2), 91-100.

26. Hassell, T.; Gleave, S.; Butler, M., Growth inhibition in animal cell culture. The effect of lactate and ammonia. *Applied Biochemistry and Biotechnology* **1991,** 30, (1), 29-41.

27. Muthing, J.; Kemminer, S. E.; Conradt, H. S.; Sagi, D.; Nimtz, M.; Karst, U.; Peter-Katalinic, J., Effects of buffering conditions and culture pH on production rates and glycosylation of clinical phase I anti-melanoma mouse IgG3 monoclonal antibody R24. *Biotechnol Bioeng* **2003,** 83, (3), 321-34.

28. Osman, J. J.; Birch, J.; Varley, J., The response of GS-NS0 myeloma cells to pH shifts and pH perturbations. *Biotechnol Bioeng* **2001,** 75, (1), 63-73.

29. Ozturk, S. S.; Palsson, B. O., Growth, metabolic, and antibody production kinetics of hybridoma cell culture: 2. Effects of serum concentration, dissolved oxygen concentration, and medium pH in a batch reactor. *Biotechnology Progress* **1991,** 7, (6), 481-94.

30. Han, K.; Levenspiel, O., Extended Monod Kinetics for Substrate, Product, and Cell Inhibition. *Biotechnology and Bioengineering* **1988,** 32, 430-437.

31. Sanderson, R. J.; Bird, K. E., Cell Separations by Counterflow Centrifugation. *Methods in Cell Biology* **1977,** 15, 1-14.

32. Detzel, C. J.; Thorson, M. R.; Van Wie, B. J.; Ivory, C. F., A Study of the Coriolis Effect on the Fluid Flow Profile in a Centrifugal Bioreactor. *Biotechnology Progress* **2009,** In Press.

33. Van Wie, B. J.; Hustvedt, E. L., Particle interaction effects on blood cell sedimentation and separations. *Biorheology* **1988,** 25, (4), 651-62.

34. Davis, W. C.; MacHugh, N. D.; Park, Y. H.; Hamilton, M. J.; Wyatt, C. R., Identification of a monoclonal antibody reactive with the bovine orthologue of CD3 (BoCD3). *Vet Immunol Immunopathol* **1993,** 39, (1-3), 85-91.

35. Glacken, M. W.; E., A.; Sinskey, A. J., Mathematical descriptions of hybridoma culture kinetics: I. Initial Metabolic Rates. *Biotechnology and Bioengineering* **1988,** 32, 491-506.

36. Fitzpatrick, L.; Jenkins, H. A.; Butler, M., Glucose and glutamine metabolism of a murine B-lymphocyte hybridoma grown in batch culture. *Appl Biochem Biotechnol* **1993,** 43, (2), 93-116.

37. Beyenal, H.; Chen, S. N.; Lewandowski, Z., The double substrate growth kinetics of Pseudomonas aeruginosa. *Enzyme and Microbial Technology* **2003,** 32, (1), 92-98.

38. Acosta, M. L.; Sanchez, A.; Garcia, F.; Contreras, A.; Molina, E., Analysis of kinetic, stoichiometry and regulation of glucose and glutamine metabolism in hybridoma batch cultures using logistic equations. *Cytotechnology* **2007,** 54, (3), 189-200.

39. Martinelle, K.; Doverskog, M.; Jacobsson, U.; Chapman, B. E.; Kuchel, P. W.; Haggstrom, L., Elevated glutamate dehydrogenase flux in glucose-deprived hybridoma and myeloma cells: Evidence from H-1/N-15 NMR. *Biotechnology and Bioengineering* **1998,** 60, (4), 508-517.

40. Ozturk, S. S.; Palsson, B. O., Chemical Decomposition of Glutamine in Cell-Culture Media - Effect of Media Type, Ph, and Serum Concentration. *Biotechnology Progress* **1990,** 6, (2), 121-128.

41. Arden, N.; Betenbaugh, M. J., Regulating apoptosis in mammalian cell cultures. *Cytotechnology* **2006,** 50, (1-3), 77-92.

42. Martens, D. E.; de Gooijer, C. D.; van der Velden-de Groot, C. A.; Beuvery, E. C.; Tramper, J., Effect of dilution rate on growth, productivity, cell cycle and size, and shear sensitivity of a hybridoma cell in a continuous culture. *Biotechnol Bioeng* **1993,** 41, (4), 429-39.

43. Cain, S. J.; Chau, P. C., Transition probability cell cycle model with product formation. *Biotechnol Bioeng* **1998,** 58, (4), 387-99.

44. Arden, N.; Betenbaugh, M. J., Life and death in mammalian cell culture: strategies for apoptosis inhibition. *Trends Biotechnol* **2004,** 22, (4), 174-80.

45. al-Rubeai, M.; Singh, R. P., Apoptosis in cell culture. *Curr Opin Biotechnol* **1998,** 9, (2), 152-6.

46. Perani, A.; Singh, R. P.; Chauhan, R.; Al-Rubeai, M., Variable functions of bcl-2 in mediating bioreactor stress- induced apoptosis in hybridoma cells. *Cytotechnology* **1998,** 28, (1-3), 177-88.

47. Singh, R. P.; al-Rubeai, M., Apoptosis and bioprocess technology. *Adv Biochem Eng Biotechnol* **1998,** 62, 167-84.

CHAPTER V

Use of a Centrifugal Bioreactor for Cartilaginous Tissue Formation from Isolated Chondrocytes

Christopher J. Detzel and Bernard J. Van Wie *

Voiland School of Chemical Engineering and Bioengineering, Washington State University,

P.O. Box 642710, Pullman, Washington 99164-2710, USA

* Corresponding Author: Tel.: +1 509 335 4103; email: bvanwie@wsu.edu

Running Title: Chondrocyte Culture in a Centrifugal Bioreactor

Prepared for submission to *Biotechnology and Bioengineering*

Abstract

The centrifugal bioreactor (CCBR) is a unique system supporting high density mammalian cell culture through cell immobilization from the balance of drag and centrifugal forces. This immobilization technique also provides simultaneous application of multiple mechanical forces shown to stimulate chondrogenesis when applied individually; hydrostatic pressure and shear stress. Hydrostatic pressure can be varied from 8 kPa to 0.5 MPa, while shear rate is variable between 0.02 and 1.4 N/m^2. This manuscript presents results demonstrating the ability of the CCBR to stimulate chondrogenesis through the application of high density culture, constant shear, and intermittent hydrostatic pressure, during a 3 week culture. At 3 weeks histological results show an even distribution of glycosaminoglycan (GAG), collagen, and cell densities of 1470 ± 270 and 1890 ± 270 cells/mm^2 for pellet culture and CCBR constructs, respectively. These observations are supported by biochemical analysis showing pellet cultures at 3 weeks

contain 8.4 ± 0.9 μg/μg GAG/DNA while CCBR cultures contain 5.6 ± 1.5 and 4.1 ± 0.9 μg/μg GAG/DNA for cultures stressed at either 0.07 or 0.26 MPa, respectively. An analysis of collagen content at 3 weeks reveals similar levels for all treatment groups; 6.6 ± 1.9 for pellet, 6.8 ± 3.5 for 0.07 MPa cultures, and 5.0 ± 0.4 for 0.26 MPa cultures. Results of this study indicate mechanical stresses applied during high density CCBR cultures do not further stimulate chondrogenesis over unstressed controls. However, system advantages including continuous culture, precise medium control, and future scaffold integration may prove to further stimulate chondrogenesis.

Keywords: Chondrocyte, Hydrostatic Pressure, Centrifugal Bioreactor, High Density

1. Introduction

The limited ability for cartilage to heal following damage due to trauma or disease has facilitated tissue engineering approaches with an ultimate goal of creating an artificial tissue capable of mimicking native tissue in composition, function, and structure (Dimicco et al. 2007; Hung et al. 2004). Successful functional tissue engineering requires the use of engineering approaches to simulate both biochemical and biophysical aspects of the natural *in vivo* environment, *in vitro*. Biochemical factors encompass a myriad of bioactive molecules including but not limited to various growth factors as well as necessary nutrient concentrations, while biophysical influences on cartilage tissue development include a three-dimensional growth environment and mechanical stimulation.

A 3D culture environment prevents chondrocyte dedifferentiation (Schnabel et al. 2002), and is accomplished through a variety of methods including: gel encapsulation (Akmal et al. 2006; Dimicco et al. 2007), porous material scaffolds (Freyria et al. 2005; Wang et al. 2009), or spontaneous chondrocyte aggregation during high density suspension culture (Marlovits et al. 2003a; Marlovits et al. 2003b; Zhang et al. 2004). Additionally, mechanical stimuli such as shear, hydrostatic pressure, and direct compression have all been shown to increase incorporation of collagen and glycosaminoglycan (GAG) in the extra-cellular matrix (ECM) improving the tissues functionality (Darling and Athanasiou 2003; Li et al. 2007; Smith et al. 2004; Wang et al. 2009). The successful development of an artificial cartilage will require a precise combination of numerous external stimuli, and ultimately provide an ideal model system to study cartilage development, degeneration due to diseases such as osteoarthritis, and regeneration spurred by novel therapies.

Bioreactors systems proven to stimulate cartilage tissue development from isolated chondrocytes include a rotating wall bioreactor (RWBs) (Akmal et al. 2006; Marlovits et al. 2003b; Villanueva et al. 2009), concentric cylinder bioreactor (CBs) (Saini and Wick 2003; Williams et al. 2002), scaffold perfusion bioreactors (SPBs) (Freyria et al. 2005; Pazzano et al. 2000), and various systems facilitating nutrient distribution through efficient mixing (Vunjak-Novakovic et al. 1999). SPBs, CBs, and reactors that facilitate mixing rely on the use of scaffolds and increased nutrient transport through fluid flow which in turn provides shear forces proven to increases ECM development. RWBs have been used to stimulate chondrogenesis without the use of a scaffold when operated at initial chondrocyte densities above 5×10^5 cells/mL, a density limit above which spontaneous cell aggregation occurs resulting in the

development of a tissue construct (Marlovits et al. 2003b). The RWB provides a low shear, low gravity environment which has been proven to stimulate chondrogenesis without the use of a scaffold.

Presently novel bioreactors are being developed to investigate the possible synergistic effect of multiple mechanical forces applied simultaneously to a developing cartilage tissue *in situ*. During culture in these bioreactors shear is the result of direct perfusion of a cartilage construct and system pressurization provides hydrostatic pressure (Lagana et al. 2008; Schulz et al. 2008), while other bioreactors have proven the advantage of simultaneously applying direct compression and shear during culture (Meyer et al. 2006; Wang et al. 2009). Another novel system, heretofore only used for suspension cultures of yeast and mammalian cells, is the continuous centrifugal bioreactor (CCBR) (Detzel et al. 2009a; Van Wie et al. 1991). The CCBR has properties which appear attractive for stimulating chondrogenesis. In addition to high density chondrocyte culture, the reactor provides simultaneous application of both hydrostatic pressure and shear *in situ*.

Cells are retained in the CCBR during operation as a high density fluidized bed due to a unique method of cell immobilization relying on counter-flow centrifugation. Cell immobilization occurs when the centrifugal force is balanced by opposing drag and buoyant forces. However, due to continuous system rotation Coriolis forces must also be considered, and it has been shown they are dominant during operation without the presence of cells (Detzel et al. 2009b); however, the effect is masked and fluid dynamics are minimally impacted during cell culture.

As a result of the cell immobilization technique employed by the CCBR cells in culture are stimulated with multiple mechanical forces. Centrifugal force accelerates the fluid head in

the CCBR which pressurizes the system and results in a variable hydrostatic pressure dependant on system RPM. Similarly, a shear force is applied to the cells as culture medium must flow around individual cells imparting a drag force to suspend the cells against the increased settling force. Both of these forces are constantly applied to cells in culture during reactor operation, but the magnitudes of the forces can be individually varied through changes in system rotation rate (centrifugal force) and inlet fluid velocities (drag force) in order to accommodate a variety of cell culture applications.

In this manuscript we will present studies showing use of the CCBR as a system to stimulate chondrogenesis from isolated bovine chondrocytes seeded into the reactor chamber. We hypothesize that mechanical stimulation accompanied with high cell density culture in the CCBR will further stimulate chondrogenesis over high density control cultures lacking mechanical stimulation, specifically pellet cultures. Chondrogenesis will be assessed through histological staining as well as total GAG and collagen content normalized to DNA in order to make comparisons of cultures with differing densities of chondrocytes. Additionally, we will present the theoretical framework for understanding the pressure and shear forces applied during CCBR operation, and future possibilities for tissue culture applications using the CCBR.

2. Materials and Methods

2.1 Cell Isolation

Full thickness cartilage tissue was harvested from the carpal joint (front knee) of skeletally mature bovine animals (Potlach Pack, Potlach, ID, USA & the Washington State University/University of Idaho Center for Reproductive Biology, Pullman, WA) through joint disarticulation under aseptic conditions. Chondrocytes were released from the tissue matrix by

treatment with pronase (Sigma, St. Louis, MO) for 1 hour and collagenase (Roche, Indianapolis, IN) for an additional 16 hours at 37°C at respective concentrations of 20 U/mL and 200 U/mL (Dimicco et al. 2007). Enzymes were dissolved in digestion medium consisting of high-glucose Dulbecco's Modified Eagle Medium (DMEM) supplemented with 5% FBS (Atlanta Biologicals, Lawrenceville, GA), non-essential amino acids, 100 U/mL of penicillin, 100 μg/mL of streptomycin, and 0.4 mM proline (Sigma, St. Louis, MO). All medium ingredients were purchased from Invitrogen (Carlsbad, CA) unless otherwise specified. After the collagenase digestion period the cell suspension was filtered through a 100 μm cell strainer (BD Bioseciences, Franklin Lakes, NJ), and centrifuged. Cell pellets were washed in phosphate buffered saline three times and re-suspended in culture medium from which a cell count was determined using a Trypan Blue exclusion assay and a hemacytometer. Culture medium is similar to digestion medium except supplemented to 10% FBS and 25 mg/mL ascorbic acid (Sigma, St. Louis, MO).

2.2 Pellet Culture

Chondrocyte pellet cultures served as experimental controls for CCBR culture comparison as pellet cultures are a high density culture lacking the presence of any mechanical stimuli. Pellet cultures were prepared by adding 1 x 10^6 cells in 1 mL of culture medium to a 1.5 mL microcentrifuge tube. This suspension was then centrifuged at 500 g for 5 minutes resulting in a pellet of cells at the bottom of the tube (Zhang et al. 2004). Pellets were then cultured in a 37° C incubator with 5% CO_2. Medium was replaced twice per week throughout the entirety of pellet culture studies, after which pellets were harvested for biochemical and histological analysis.

2.3 CCBR Culture

The CCBR consists of a smooth-walled polycarbonate conical chamber (11.4 mL) machined in the WSU Engineering shops. This chamber is integrated into the Cell Purging tubing set (Gambro BCT Inc., Lakewood, CO) and connected to a COBE© Spectra™ Apheresis System (Gambro BCT Inc., Lakewood, CO). The smooth-walled chamber replaces the Gambro chamber that consists of a concentric ring staircase to form its conical shape, allowing for a more homogeneous fluidized bed of cells to be maintained in the reactor. Each tubing set is supplied sterile from the manufacturer, but after modification of the tubing lines to reflect that shown in Fig. 1 the system is re-sanitized by pumping 70% ethanol through the system for the 24 hours prior to reactor start-up. Fluid is supplied and removed from the CCBR through a flexible tubing bundle and the use of an anti-twister mechanism on the COBE© Spectra™ similar to that shown by Van Wie *et al.* (Van Wie et al. 1986). Following sanitization the system is purged of ethanol, rinsed with culture medium, and finally filled with culture medium taking care to ensure no air bubbles remain in the reactor lines, as air in the tubing lines will lead to culture disruption and failure.

Prior to inoculation the rotor speed and inlet volumetric flow rate are set at 600 RPM and 5 mL/min, respectively. A total of 2.0 - 2.5 x 10^8 chondrocytes (based on the yield of the cell isolation procedure) suspended in 10 mL of culture medium is then introduced into the system using the valve on the inoculation line shown in Fig. 1. Cell inoculation numbers and initial reactor settings were chosen based on previous experiments with hybridoma cells which resulted in a stable fluidized bed of cells during long term cultures (Detzel et al. 2009a). Following inoculation the cell suspension flows into the CCBR where cells are immobilized as a high density fluidized bed. Reactor settings remain unchanged for the initial 7 days of culture, after

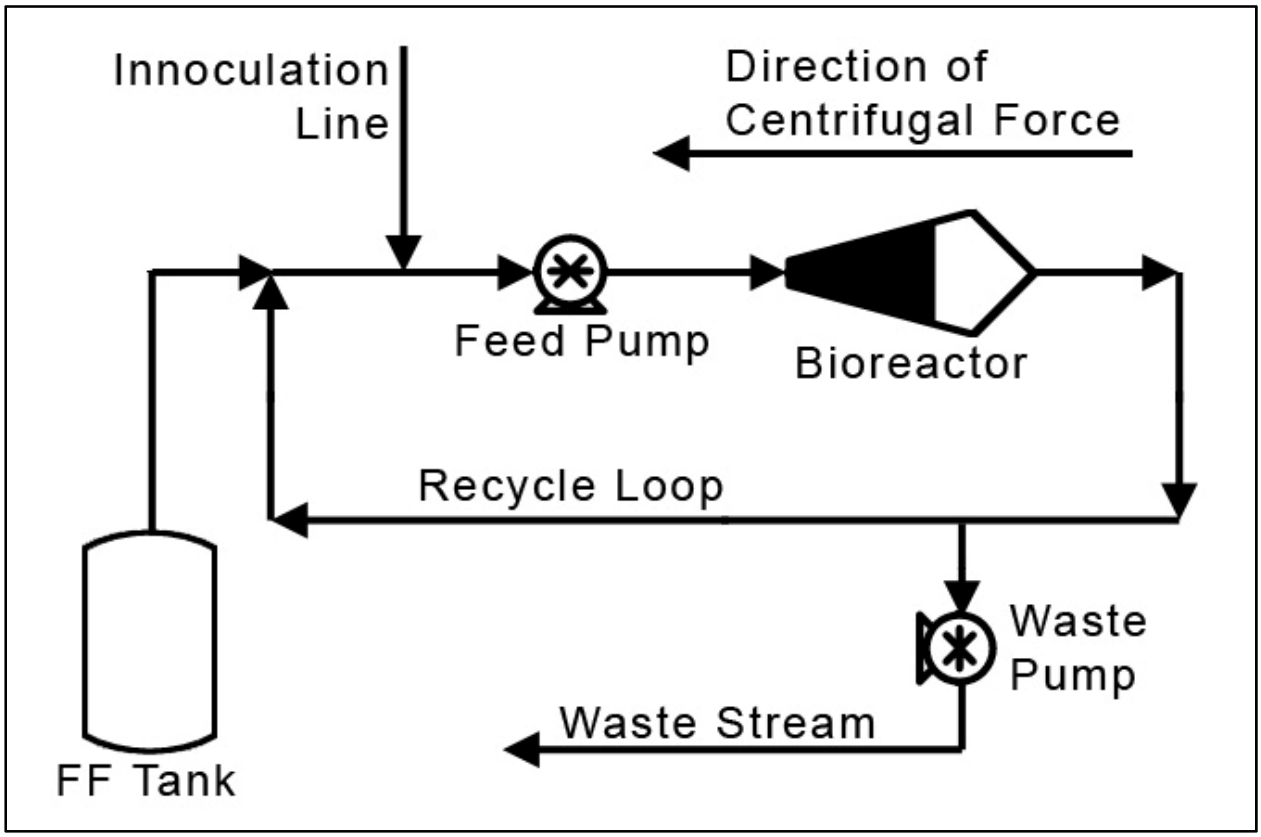

Figure 1. Cell purging tubing sets were modified to reflect the configuration shown in the schematic of the CCBR and fluid lines. Fresh medium was supplied to the reactor chamber during centrifugation with the use of flexible tubing and an anti-twister device. During the 3 week culture the waste pump was set to remove 200 mL per day which was replaced with fresh culture medium from the fresh feed (FF) tank.

which specific cultures were harvested for evaluation while others continued development in the CCBR for an additional two weeks. Over the final 14 days of 3 week cultures, the reactor settings are varied to intermittently stress the cultures with periods of increased hydrostatic pressure. The intermittent stressing regimens are carried out during 4 one hour cycles per day in which the RPM is increased to either 900 or 1650 RPM for 30 min and all rotation and pumps are stopped for the subsequent 30 minutes of the cycle. The remaining 20 hours per day the rotor speed is set at 300 RPM, while inlet flow rate of 2.5 mL/min to provide a low shear environment at all times during system rotation. Over the entire three week culture the waste pump was set such that 200 mL of fresh culture medium is exchanged per day.

2.4 Histological Analysis

Pellet or CCBR cultures harvested at the 1 and 3 week time points were immediately fixed in neutral buffered formalin for 1 hour. The tissue was then embedded in paraffin and cut into 4 μm sections. These sections were then stained with either Toluidine blue for GAG distribution or a Trichrome stain for collagen. All sectioning and staining was performed by the Washington Animal Disease Diagnostic Laboratory (WADDL) Histology Lab at Washington State University. Sections were visualized with an Olympus BH-2 optical microscope (Olympus; Center Valley, PA) and recorded digitally with a ProgRes C12plus digital microscope camera (JENOPTIK Laser, Optik, Systeme GmbH; Jena, Germany)

2.5 Biochemical Analysis

Samples for colorimetric biochemical analysis were digested overnight with proteinase K (Roche) in TE buffer at a concentration of 500 μg/mL. Sulfated GAG content was determined for each sample with a dimethylmethylene blue assay (Farndale et al. 1986), while an assay to determine hydroxyproline content (Woessner 1961) and assuming a ratio of 7.4 grams of

collagen per gram of determined hydroxyproline was used to estimate total collagen content. Finally, DNA content was estimated using a Quant-iT PicoGreen dsDNA Assay Kit (Invitrogen) allowing sample GAG and collagen content to be normalized on a per DNA basis for direct comparison of results from different experimental protocols.

2.6 Statistical Analysis

Average values of GAG/DNA (μg/μg) and Collagen/DNA (μg/μg) are calculated as arithmetic means for pellet cultures (n=7), bioreactor cultures with low intermittent stress (900 RPM cultures, n=2), and bioreactor cultures with high intermittent stresses (1650 RPM cultures, n=2). Reported error bars indicate the standard error of the mean calculated for each treatment group, and statistically significant differences between treatment groups are established at $P<0.05$ (*) level.

3. Theory

3.1 Mechanical Force Derivation

During continuous operation centrifugal force provides a hydrostatic pressure within the reactor chamber which can be varied from 8 kPa at 300 RPM to 0.5 MPa at 2300 RPM under the current configuration. These values of hydrostatic pressure are calculated by integrating the centrifugal acceleration over the radius of rotation, this is necessary as the centrifugal force and thus pressure increases with increasing distance from the center of rotation. The formula used for calculation of hydrostatic pressure is shown in Eq. 1.

$$\Delta P = \int \rho a(r) dr = \int_{r_1}^{r_2} \rho \omega^2 r dr = \rho \omega^2 \frac{r^2}{2} \qquad \text{Eq. 1}$$

Where ΔP is the pressure at any point in the reactor, ρ is the density of the fluid, and r is the radius from the center of rotation. **α**(r) is the system acceleration as a function of r which for a rotating system is equal to the square of angular velocity ω multiplied by r. Integration from the center of rotation $r_1 = 0$ to the point of interest $r_2 = r$ will result in the hydrostatic pressure at a particular distance, r, from the center of rotation. All reported pressures are found at an $r = 13.1$ cm which corresponds to the point in the CCBR where fluid enters the reactor chamber.

Also present during continuous operation is a shear force due to the flow of medium through the reactor. By equating the pressure loss per unit length for flow through a cylindrical tube (left-hand-side of Eq. 2) with the pressure loss through a fluidized bed (right-hand-side of Eq. 2) and assuming R is the hydraulic radius which corresponds to the ratio of cross-section available for flow to the wetted perimeter, the shear stress can be defined as shown in Eq. 2.

$$\tau 2\pi R = 150\left(\frac{\mu V_0}{D_P^2}\right)\frac{(1-\varepsilon)^2}{\varepsilon^3}\frac{R}{2} \qquad \text{Eq. 2}$$

Where τ is shear stress, R is the hydraulic radius - $R = \frac{\varepsilon D_P}{(1-\varepsilon)6}$, μ is the fluid viscosity, V_0 is the superficial velocity through the chamber, D_P is the particle diameter, and ε is the fluidized bed porosity. Substitution of the equation for hydraulic radius in to Eq. 2 results in an equality for the shear stress in a fluidized bed, Eq. 3.

$$\tau = \frac{150}{12}\left(\frac{\mu V_0}{D_P^2}\right)\frac{(1-\varepsilon)}{\varepsilon^2} \qquad \text{Eq. 3}$$

From Eq. 3 it can be seen that shear stress is a function of both superficial velocity and porosity. Superficial velocity is directly related to inlet velocity a key operational parameter of the CCBR while it has already been discussed that porosity, or cell density, is specifically tunable based on adjustments to either reactor RPM or inlet velocity. Hence, for an inlet volumetric flow rate

range of 1-20 mL/min shear stress will range from 0.02-0.5 N/m^2 for a porosity of 0.85. However, if porosity is reduced to 0.7 shear stress will increase to 0.07-1.4 N/m^2 over the same range of inlet fluid velocities. These values of shear stress are calculated at the centroid of the CCBR which has a diameter of 1.3 cm, but the conical shape of the reactor chamber with a continually increasing diameter from 0.25 cm at the inlet to 2.6 cm at the widest cross-section provides shear stress is differentially changing throughout the reactor chamber.

4. Results and Discussion

4.1 Magnitude of Mechanical Forces during Culture

As outlined in the Theory section the hydrostatic pressure and shear stress can be calculated for specific reactor settings. During the first week of all CCBR cultures hydrostatic pressure and shear stress are 0.03 MPa and 0.11 N/m^2, respectively. These forces correspond to operating conditions of 600 RPM and an inlet flow rate of 5 mL/min which have previously been shown to maintain a cell bed with a porosity of 0.85. Over the final two weeks of culture the reactor settings are adjusted to 300 RPM and an inlet flow rate of 2.5 mL/min corresponding to a hydrostatic pressure of 8 kPa and a shear stress of 0.08 N/m^2, respectively, again assuming a porosity of 0.85 for shear stress calculations. This assumption pertaining to the magnitude of shear stress over the final two weeks of culture is examined further in the observations of tissue formation section, where it will be shown shear stress is dramatically increased as a result of channeling through the tissue construct.

Hydrostatic pressure and shear stress were reduced over the final two weeks of culture to provide an environment with minimal mechanical stimulation allowing the culture to rest and

produce an ECM in response to the periods of increased hydrostatic pressure over the same time period. These conditions remain unchanged over the final two weeks of culture except for 4 one hour periods throughout the day when the hydrostatic pressure is cyclically increased to either 0.07 or 0.26 MPa by increasing RPM to 900 or 1650 as described in the Materials and Methods section. Each mechanical force is dependant of a reactor setting that can be varied independently to apply specific magnitudes of mechanical force on a developing tissue construct.

4.2 Observation of Bioreactor Tissue Formation

Following inoculation of the CCBR chondrocytes are suspended in the reactor chamber as a fluidized bed of cells. Assuming a void volume fraction near 0.85, a value based on previous numerical modeling and experimental work, and an average chondrocyte diameter of 13 μm (Wong et al. 1996) the cell bed will occupy approximately 2 mL of CCBR volume. This suspension of cells remains unchanged during a 48 to 72 hour lag phase as cells adjust to the new environment within the CCBR. Following the lag phase an ECM begins to develop between cells causing flocculation, ultimately disrupting the equilibrium between the drag and settling forces which results in a decrease in cell bed volume by approximately 30-50% which then remains constant for the remainder of the culture.

At the end of the three week culture period a cartilaginous tissue results and is shown inside the reactor chamber, Fig. 2 (A), and after removal from the chamber, Fig. 2 (B). The thin film shown in Fig 2 (C) is observed coating the interior of the bioreactor walls above the space containing the larger opaque tissue construct shown in Fig. 2 (B). The tissue shown in Fig. 2 is representative of that formed during either low or high hydrostatic pressure culture conditions, as gross tissue observations can not differentiate the two culture conditions.

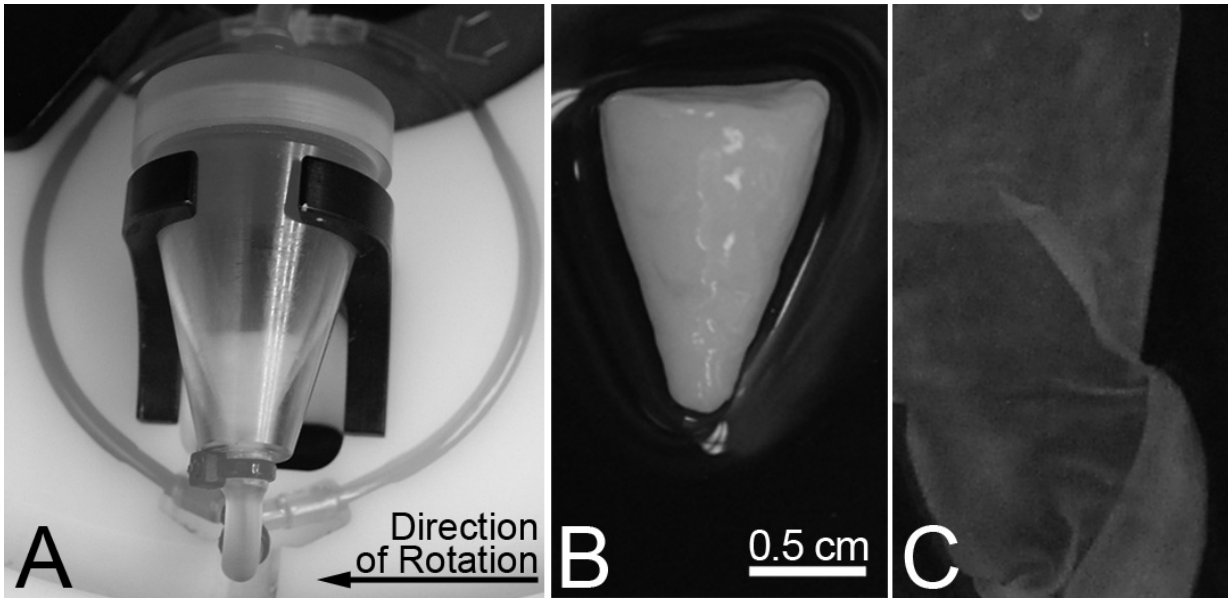

Figure 2. After 3 weeks of culture in the CCBR a cartilage construct has formed from the origional 2.5 x 10^8 isolated chondrocytes seeded into the bioreactor. The construct is observed before (A) and after (B) removal from the reactor chamber. A thin film (C) had formed on the interior walls of the reactor chamber above the major construct which appears opaque in the bottom portion of the reactor in panel (A).

Further examination of the tissue construct shows the surface near the wall of the reactor is very smooth and provides the most resistance to compression based on observations made following removal of the tissue from the reactor. However, the middle of the construct is much softer with numerous observable macro-pores, about 1 mm in diameter. Immediately following inoculation the porosity is 0.85 when all cells are individually suspended in the reactor chamber.

As the ECM forms and cells begin to "stick" together the particle effective particle size and settling velocity are both increased. Increasing settling velocity will decrease porosity and increase shear stress according to Eq. 3. At the time of tissue construct removal the ECM has undergone extensive formation; this in turn blocks liquid passage through the ECM and what is observed is the formation of numerous macro-pores or channels through which fluid flows.

Due to the formation of these macro-pores the previous analysis to determine shear stress is no longer applicable. As a fluidized bed of cells no longer exists, shear stress must be calculated assuming flow through a bundle of cylindrical pipes corresponding to the number of macro-pores. The shear stress is then equated to the pressure loss through a cylindrical tube as shown in Eq. 4

$$\tau = \frac{D}{4L}\left(-\rho g \Delta z - h_{fs}\right) = \frac{D}{4L}\left(-\frac{\rho\omega^2\left(r_2^2 - r_1^2\right)}{2} - \frac{32vL\mu}{D^2}\right) \qquad \text{Eq. 4}$$

Where ρ is the density of the fluid, g is the centrifugal acceleration integrated over the height of the tissue construct, Δz is the height of tissue construct (1 cm), and h_{fs} is the pressure loss due to friction with the wall of the pipe during laminar flow, D is the diameter of the macro-pore (1 mm), and r_1 and r_2 are the distances from the center of rotation to the top and bottom of the tissue construct (12.1 and 13.1 cm), respectively. From this analysis it can be shown that the pressure loss due to skin friction is insignificant when compared to the pressure loss due to the hydrostatic

head due to the increased gravitational force from system rotation. As a result the shear stress is increased considerably to 60 N/m^2; however, only the cells lining the pores will be subjected to this high shear environment. Due to tissue construct formation not all cells will be subjected to shear making hydrostatic pressure the primary variable examined in these experiments and its effect on stimulating chondrogenesis in the CCBR.

4.3 Histological Observations

Histological analysis can give a quantitative assessment of cell density between the two culture systems, as well as qualitative insight into GAG and collagen content and distribution throughout the construct. There is no observable difference in histological staining between bioreactor cultures stressed at 900 or 1650 RPM, and as such only sections from a single 900 RPM culture will be presented, effectively representing both bioreactor culture treatment groups.

Observation of multiple tissue sections shows pellet cultures have a significantly lower cell density, 1450 ± 120 cells/mm^2, than bioreactor constructs, 2300 ± 300 cells/mm^2, after 1 week. The same analysis after 3 weeks of culture again shows a significant difference between pellet and bioreactor culture cell density, 1480 ± 270 and 1890 ± 60 cells/mm^2, respectively. Pellet culture cell density remains unchanged over the course of a 3 week culture while cell density in the CCBR constructs significantly decreases when comparing the 1 and 3 week constructs. Finally, throughout both culture techniques cells remain round and individually embedded within their respective developing ECMs, indicating chondrocytes remain differentiated throughout the culture.

Each section in Fig. 3 (A) indicates the presence of GAG in the ECM space between cells as evidenced by the purple color preferentially taken up by GAGs. At the week 1 time point the pellet culture ECM is stained with greater intensity than the CCBR culture indicating the

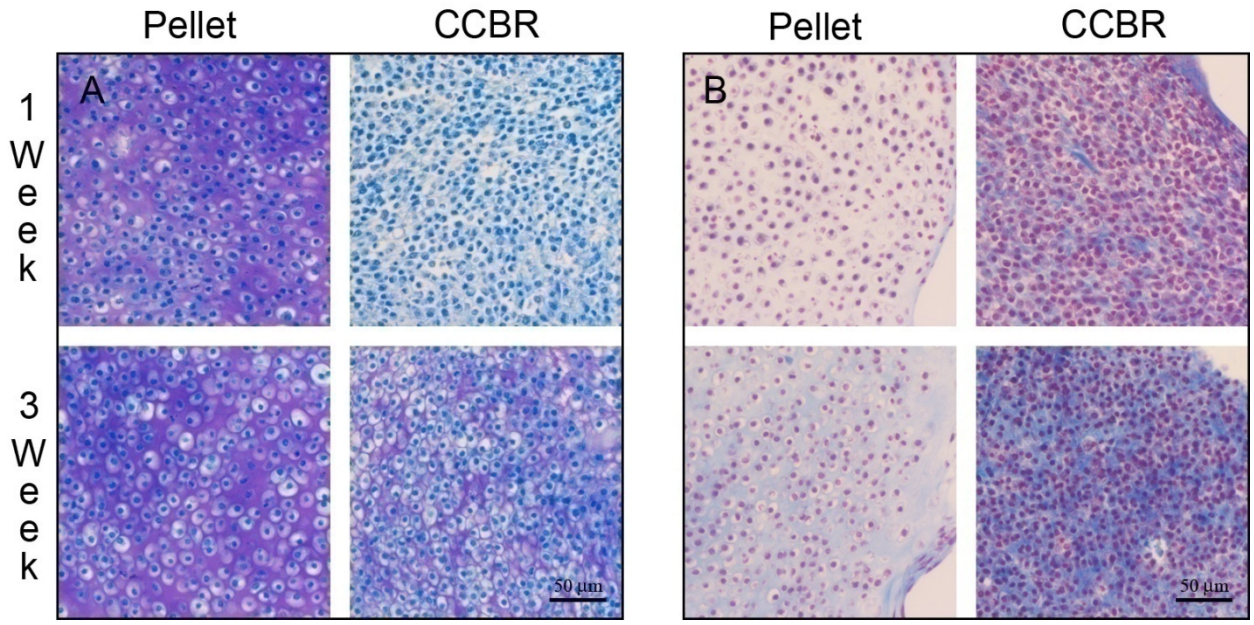

Figure 3. Histological results show cells are round and evenly distributed throughout the ECM of both the pellet and CCBR culture constructs, although the cell density is higher in the CCBR construct. Toluidine blue stain for GAG content is shown in (A) and an increase in staining intensity is difficult to discern in the pellet culture when comparing week 1 and week 3 sections, but an increase in intensity is clearly seen in sections of the CCBR construct. A trichrome stain (B) for collagen shows collagen incorporation is increased into the ECM of both constructs over time while the intensity of the CCBR tissue is greater than the pellet culture at both time points. (bar represents 50 μm)

presence of more GAG protein throughout the ECM of pellet cultures. Comparison of the week 1 and week 3 time points for pellet cultures does not appear to show an increase in intensity, but the staining intensity of the ECM has clearly increased throughout the CCBR culture when comparing the two time points. Collagen content as evidenced by blue staining of the ECM in Fig. 3 (B) appears to show the staining intensity has increased in both culture systems as the construct matures from 1 to 3 weeks, but a greater intensity is observed in bioreactor constructs than pellet cultures at each time point. However, accounting for differences in cell density collagen/DNA content is similar for each culture system as evidenced by biochemical analysis.

4.4 Biochemical Results

In contrast to histology, biochemical analysis provides a quantitative comparison of the two culture systems. Results of GAG content are shown in Fig. 4 and between the 1 and 3 week time points the average amount of GAG/DNA in pellet cultures increases, but not significantly from 7.0 ± 1.1 μg/μg to 8.4 ± 0.9 μg/μg, respectively, when evaluated using a t-test at the $P < 0.5$ level. Bioreactor tissue analyzed following the initial week of culture under constant shear and hydrostatic pressure have 1.4 ± 0.1 μg/μg GAG/DNA which is a statistically significant difference when compared to pellet cultures at the same time point. The same analysis following 3 weeks of culture indicate GAG/DNA has increased in both CCBR construct treatment groups to 6.8 ± 3.5 and 5.1 ± 0.4 μg/μg for the 900 and 1650 RPM culture conditions, respectively. In both cases the level of GAG/DNA incorporated into the CCBR tissue construct is less than that found in pellet cultures; however, only the difference between pellet cultures and CCBR cultures stressed at 1650 RPM is statistically significant at the 3 week time point.

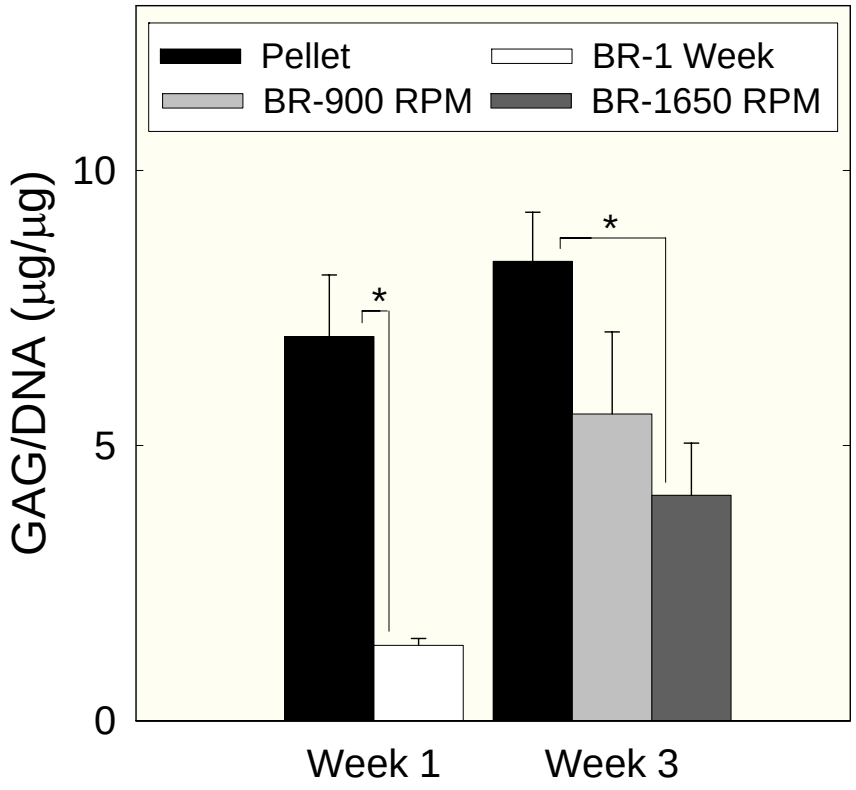

Figure 4. Biochemical results of GAG content are normalized to DNA content for comparison of CCBR cultures as cell density varies between culture systems. GAG/DNA content is significantly higher in pellet cultures (n=7) at the 1 week time point, with a value of 7.0 ± 1.1 μg/μg, when compared to the value for CCBR constructs (n=2), 1.4 ± 0.1 μg/μg. The GAG/DNA content shows an increase from week 1 to week 3 in all treatment groups, with pellet cultures containing, 8.4 ± 0.9 μg/μg GAG/DNA, and CCBR constructs containing; 5.6 ± 1.5 μg/μg at 900 RPM (n=2) and 4.1 ± 0.9 μg/μg for the 1650 RPM (n=2) culture condition. * indicates $P < 0.05$

Comparison of the two culture systems for collagen content show similar levels of collagen on a DNA basis at both the 1 and 3 week time points; results shown in Fig. 5. There is no statistical difference in the collagen/DNA content between pellet cultures, 2.8 ± 0.6 μg/μg, and bioreactor cultures, 1.8 ± 0.4 μg/μg, after 1 week of culture. After 3 weeks pellet cultures contain 6.6 ± 1.9 μg/μg of collagen/DNA as compared to bioreactor constructs containing 6.8 ± 3.5 and 5.1 ± 0.4 μg/μg for 900 and 1650 RPM culture conditions, respectively. Although there is not a statistical difference between treatment groups at individual time points, there is a significant increase in collagen/DNA content between the 1 and 3 week time points for both pellet cultures and CCBR constructs stressed at 1650 RPM. While the 900 RPM treatment group does not show a significant increase over week 1 CCBR cultures due to the large error, the average value of collagen/DNA content is consistent with that of the 1650 RPM and pellet culture treatment groups at the 3 week time point.

In addition to analyzing the major cartilage construct shown in Fig. 2 (B) the film found coating the interior wall of the CCBR chamber, shown in Fig. 2 (C), was also analyzed for both GAG and collagen. This film contained similar levels of GAG/DNA with an average value of 5.6 ± 0.8 μg/μg, but the collagen/DNA content was considerably increased by nearly 6 fold, over any other sample from either culture system with an average value of 50 ± 10 μg/μg. The error reported in the GAG and collagen content for the film is the standard deviation of three independent samples taken from various locations throughout the film.

This film is likely due to the attachment a monolayer, or a few layers, of chondrocytes directly to the polycarbonate interior surface of the CCBR which then incorporates significant levels of GAG and collagen into the ECM. Unlike the larger tissue construct the film is not

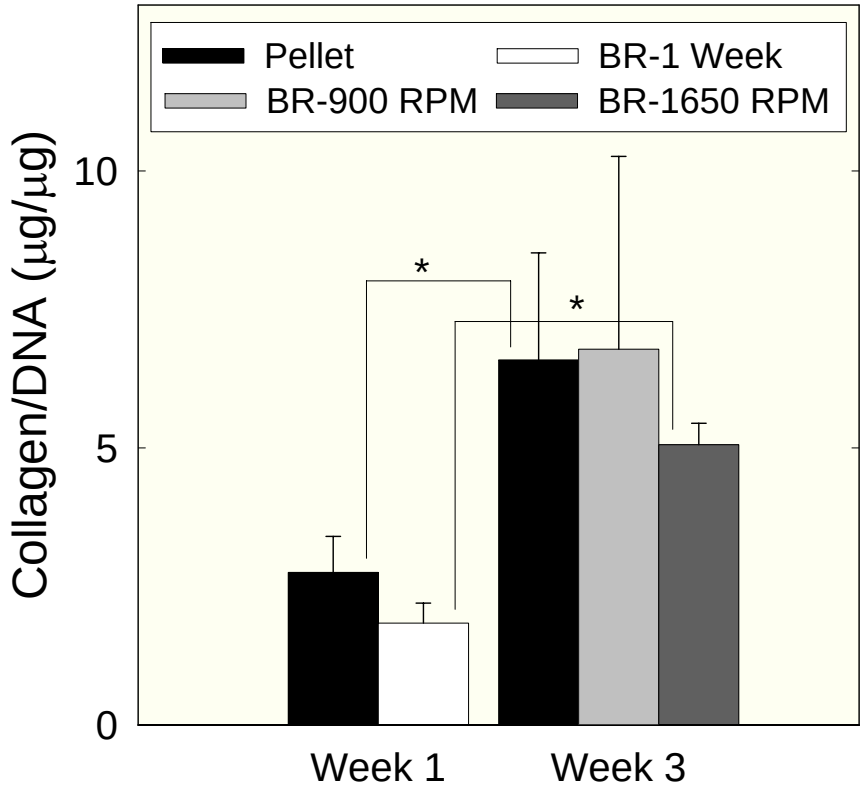

Figure 5. Collagen content normalized to DNA shows significant increases in collagen content from week 1 to week 3 for both the pellet and bioreactor culture systems. At week 1 pellet cultures contain 2.8 ± 0.6 μg/μg collagen/DNA while bioreactor cultures contain 1.8 ± 0.4 μg/μg collagen/DNA at the same time point. These values increase to 6.6 ± 1.9 μg/μg for pellet cultures at 3 weeks while bioreactor cultures increase to 6.8 ± 3.5 and 5.1 ± 0.4 μg/μg for the 900 RPM and 1650 RPM procedures, respectively. * indicates $P < 0.05$

relying as heavily on diffusion to supply all cells with necessary nutrients and may be more metabolically active than the major CCBR construct. Initially when cells are individually suspended as a fluidized bed nutrient transport is by convection, but as the ECM begins to form mass transfer will be limited by diffusion as medium is not directly perfused through the entire ECM. This is one possible explanation for the difference in GAG and collagen content between the major construct and the film.

4.5 Implications for CCBR Tissue Culture

The centrifugal bioreactor has been successfully used to create a cartilaginous tissue from isolated chondrocytes which is positive for both GAG and collagen. The tissue produced in the CCBR has similar amounts of GAG and collagen, on a per DNA basis, when compared to pellet cultures. The hypothesis driving use of the CCBR as a model system for cartilage growth is that simultaneously applying both hydrostatic pressure and shear stress to a developing tissue would further stimulate chondrogenesis over high density chondrocyte culture alone. The independent application of each of these forces has been shown to simulate chondrogenesis and current research has begun to indicate a synergistic effect on chondrogenesis from the simultaneous application of multiple forces using various bioreactors.

From this work it appears that application of hydrostatic pressure and shear using the CCBR has not improved the incorporation of GAG and collagen into the ECM of the tissue. This finding of mechanical forces not stimulating chondrogenesis is similar to that observed in fibrin gels where oscillatory dynamic compression inhibited both GAG and collagen synthesis (Hunter et al. 2004). Results from this study led to the hypothesis that the scaffold material plays a particularly significant role in determining the effect of mechanical stimuli on chondrogenesis

as similar studies using an agarose gel and mechanical compression increased matrix synthesis by chondrocytes (Buschmann et al. 1995).

The hypothesis by Hunter et al. that the scaffold material influences the effect of mechanical stimulation can be extended to include the influence mechanical stimulation has on various culture systems, such as high density chondrocyte culture. This is similar to a conclusion drawn by Elder et al. (2006) who investigated the effect of hydrostatic pressure on chondrocytes cultured in pellet cultures and alginate beads. Results showed that high density pellet cultures were more sensitive to hydrostatic pressure, but the lower density alginate bead cultures may be preferential for facilitating ECM synthesis (Elder et al. 2006). As the CCBR cultures have a higher density of cells the findings by Elder et al. would help explain the deficit in ECM incorporation of GAG and collagen when compared with pellet cultures.

We expect the CCBR will still prove to be a valuable system to study tissue development as modifications to the CCBR system can be made to exploit the unique properties of the CCBR. First, the CCBR is a continuous system where concentrations of metabolites and substrates can be precisely controlled through dilution rate manipulation. This may prove to be advantageous based on the myriad of studies showing how various growth factors can stimulate chondrogenesis both in chondrocytes and mesenchymal stem cells (Arikawa et al. 2009; Connelly et al. 2008; van der Kraan et al. 2002). Using the CCBR to culture these cells in the presence of a precisely controlled and constant concentration of a cytokine may be beneficial in studying their effect on tissue development.

Another possibility in which the CCBR could be used to stimulate chondrogenesis is to immobilize a scaffold in the reactor chamber and use the reactor to perfuse the scaffold construct and apply hydrostatic pressure to the developing tissue. However, the seeding density of the

scaffold contained in the CCBR would have to be delicately controlled as Mauck *et al.* (2002) has shown that increasing cell seeding density in agarose hydroges from 20 to 60 x 10^6 cells/mL is beneficial to both the Youngs Modulus and GAG content in free swelling cultures. However in this same study deformational loading was only beneficial to the lower density cultures (Mauck et al. 2002). It may be difficult to control scaffold seeding density in the bioreactor but it is possible to seed scaffolds and then transfer to the bioreactor where they could be stimulated with increased hyrostatic pressure and perfused in a continuous long term culture.

5. Conclusions

Various bioreactors have been developed to stimulate chondrogenesis from isolated chondrocytes with an end goal of creating functional cartilage tissue. The individual application of mechanical forces such as shear stress, hydrostatic pressure, and direct compression have all been shown to stimulate chondrogenesis, while current research has begun to investigate the possibility of a synergistic effect on cartilage development from the simultaneous application of multiple mechanical forces. A novel use of a CCBR providing independently adjustable hydrostatic pressure and shear rate to stimulate chondrogenesis from isolated chondrocytes is presented in this paper.

Results have demonstrated the feasibility of producing a cartilage-like tissue in the CCBR. When compared with pellet cultures, the ECM of tissue formed in the CCBR contains less GAG/DNA, but similar levels of collagen/DNA at both the 1 and 3 week time points. Histological results similarly confirm the development of a cartilaginous tissue pellet due to positive staining for both GAG and collagen content at both culture time points.

Although the results show mechanical stimulation of developing cartilage constructs in the CCBR does not significantly improve the quality of the tissue over high density culture alone there is still potential for the CCBR as a model system to study cartilage development. The unique nature of the CCBR reactor environment is advantageous allowing for well-mixed precise control of metabolite, substrate, and growth factor concentrations in a continuous environment. Also, with modifications to the reactor chamber it will be possible to culture scaffolds seeded with chondrocytes in a continuous environment at varying levels of hydrostatic pressure and medium perfusion.

Further studies of chondrocyte culture in the CCBR are warranted to fully realize the potential of the system to produce a tissue with the highest ECM content of GAG and collagen. Additionally, gene expression analyses to differentiate specific collagen and GAG types and identify construct similarities to articular cartilage or fibrocartilage will be undertaken. The CCBR provides a unique opportunity to investigate the simultaneous application of shear rate and hydrostatic pressure to a developing cartilage construct, and optimization of this process in future work will provide a continuous model system to study cartilage development and degeneration.

Acknowledgements

The authors would like to acknowledge the Biotechnology Training Grant (NIH 5T32-GM008336-16) and the Gene & Linda Voiland School of Chemical Engineering and Bioengineering for graduate student support and supplies. Equipment in the form of the COBE© Spectra Apheresis System and Cell Purging tubing sets in addition to corporate technical research staff consultation are a result of a donation by Gambro BCT Inc., Lakewood, CO. We

would also like to acknowledge Potlatch Pack for supply of bovine carpel joints. Mr. R. Hutchinson of the Washington State University College of Engineering and Architecture Machine Shop was instrumental in design and fabrication of the CCBR chambers used in these experiments.

References

Akmal M, Anand A, Anand B, Wiseman M, Goodship AE, Bentley G. 2006. The culture of articular chondrocytes in hydrogel constructs within a bioreactor enhances cell proliferation and matrix synthesis. J Bone Joint Surg Br 88(4):544-53.

Arikawa T, Matsukawa A, Watanabe K, Sakata KM, Seki M, Nagayama M, Takeshita K, Ito K, Niki T, Oomizu S and others. 2009. Galectin-9 accelerates Transforming Growth Factor beta3-induced differentiation of human mesenchymal stem cells to chondrocytes. Bone.

Buschmann MD, Gluzband YA, Grodzinsky AJ, Hunziker EB. 1995. Mechanical compression modulates matrix biosynthesis in chondrocyte/agarose culture. J Cell Sci 108 (Pt 4):1497-508.

Connelly JT, Wilson CG, Levenston ME. 2008. Characterization of proteoglycan production and processing by chondrocytes and BMSCs in tissue engineered constructs. Osteoarthritis Cartilage 16(9):1092-100.

Darling EM, Athanasiou KA. 2003. Articular cartilage bioreactors and bioprocesses. Tissue Eng 9(1):9-26.

Detzel CJ, Mason DJ, Davis WC, van Wie BJ. 2009a. Kinetic Simulation of a Centrifugal Bioreactor for High Population Density Hybridoma Culture. Biotechnology Progress In Press.

Detzel CJ, Thorson MR, Van Wie BJ, Ivory CF. 2009b. A Study of the Coriolis Effect on the Fluid Flow Profile in a Centrifugal Bioreactor. Biotechnology Progress In Press.

Dimicco MA, Kisiday JD, Gong H, Grodzinsky AJ. 2007. Structure of pericellular matrix around agarose-embedded chondrocytes. Osteoarthritis Cartilage 15(10):1207-16.

Elder SH, Sanders SW, McCulley WR, Marr ML, Shim JW, Hasty KA. 2006. Chondrocyte response to cyclic hydrostatic pressure in alginate versus pellet culture. J Orthop Res 24(4):740-7.

Farndale RW, Buttle DJ, Barrett AJ. 1986. Improved quantitation and discrimination of sulphated glycosaminoglycans by use of dimethylmethylene blue. Biochim Biophys Acta 883(2):173-7.

Freyria AM, Yang Y, Chajra H, Rousseau CF, Ronziere MC, Herbage D, El Haj AJ. 2005. Optimization of dynamic culture conditions: effects on biosynthetic activities of chondrocytes grown in collagen sponges. Tissue Eng 11(5-6):674-84.

Hung CT, Mauck RL, Wang CC, Lima EG, Ateshian GA. 2004. A paradigm for functional tissue engineering of articular cartilage via applied physiologic deformational loading. Ann Biomed Eng 32(1):35-49.

Hunter CJ, Mouw JK, Levenston ME. 2004. Dynamic compression of chondrocyte-seeded fibrin gels: effects on matrix accumulation and mechanical stiffness. Osteoarthritis Cartilage 12(2):117-30.

Lagana K, Moretti M, Dubini G, Raimondi MT. 2008. A new bioreactor for the controlled application of complex mechanical stimuli for cartilage tissue engineering. Proc Inst Mech Eng [H] 222(5):705-15.

Li Z, Yao S, Alini M, Grad S. 2007. Different response of articular chondrocyte subpopulations to surface motion. Osteoarthritis Cartilage 15(9):1034-41.

Marlovits S, Tichy B, Truppe M, Gruber D, Schlegel W. 2003a. Collagen expression in tissue engineered cartilage of aged human articular chondrocytes in a rotating bioreactor. Int J Artif Organs 26(4):319-30.

Marlovits S, Tichy B, Truppe M, Gruber D, Vecsei V. 2003b. Chondrogenesis of aged human articular cartilage in a scaffold-free bioreactor. Tissue Eng 9(6):1215-26.

Mauck RL, Seyhan SL, Ateshian GA, Hung CT. 2002. Influence of seeding density and dynamic deformational loading on the developing structure/function relationships of chondrocyte-seeded agarose hydrogels. Ann Biomed Eng 30(8):1046-56.

Meyer U, Buchter A, Nazer N, Wiesmann HP. 2006. Design and performance of a bioreactor system for mechanically promoted three-dimensional tissue engineering. Br J Oral Maxillofac Surg 44(2):134-40.

Pazzano D, Mercier KA, Moran JM, Fong SS, DiBiasio DD, Rulfs JX, Kohles SS, Bonassar LJ. 2000. Comparison of chondrogensis in static and perfused bioreactor culture. Biotechnol Prog 16(5):893-6.

Saini S, Wick TM. 2003. Concentric cylinder bioreactor for production of tissue engineered cartilage: effect of seeding density and hydrodynamic loading on construct development. Biotechnol Prog 19(2):510-21.

Schnabel M, Marlovits S, Eckhoff G, Fichtel I, Gotzen L, Vecsei V, Schlegel J. 2002. Dedifferentiation-associated changes in morphology and gene expression in primary human articular chondrocytes in cell culture. Osteoarthritis Cartilage 10(1):62-70.

Schulz RM, Wustneck N, van Donkelaar CC, Shelton JC, Bader A. 2008. Development and validation of a novel bioreactor system for load- and perfusion-controlled tissue engineering of chondrocyte-constructs. Biotechnol Bioeng 101(4):714-28.

Smith RL, Carter DR, Schurman DJ. 2004. Pressure and shear differentially alter human articular chondrocyte metabolism: a review. Clin Orthop Relat Res(427 Suppl):S89-95.

van der Kraan PM, Buma P, van Kuppevelt T, van den Berg WB. 2002. Interaction of chondrocytes, extracellular matrix and growth factors: relevance for articular cartilage tissue engineering. Osteoarthritis Cartilage 10(8):631-7.

Van Wie BJ, Brouns TM, Elliott ML, Davis WC. 1991. A Novel Continuous Centrifugal Bioreactor for High-Density Cultivation of Mammalian and Microbial Cells. Biotechnology and Bioengineering 38(10):1190-1202.

Van Wie BJ, Elliott ML, Lee JM. 1986. Development and Characterization of a Continuous Centrifugal Bio-Reactor. Biotechnology and Bioengineering Symp. 17:335-344.

Villanueva I, Klement BJ, von Deutsch D, Bryant SJ. 2009. Cross-linking density alters early metabolic activities in chondrocytes encapsulated in poly(ethylene glycol) hydrogels and cultured in the rotating wall vessel. Biotechnol Bioeng 102(4):1242-50.

Vunjak-Novakovic G, Martin I, Obradovic B, Treppo S, Grodzinsky AJ, Langer R, Freed LE. 1999. Bioreactor cultivation conditions modulate the composition and mechanical properties of tissue-engineered cartilage. J Orthop Res 17(1):130-8.

Wang PY, Chow HH, Tsai WB, Fang HW. 2009. Modulation of gene expression of rabbit chondrocytes by dynamic compression in polyurethane scaffolds with collagen gel encapsulation. J Biomater Appl 23(4):347-66.

Williams KA, Saini S, Wick TM. 2002. Computational fluid dynamics modeling of steady-state momentum and mass transport in a bioreactor for cartilage tissue engineering. Biotechnol Prog 18(5):951-63.

Woessner JF, Jr. 1961. The determination of hydroxyproline in tissue and protein samples containing small proportions of this imino acid. Arch Biochem Biophys 93:440-7.

Wong M, Wuethrich P, Eggli P, Hunziker E. 1996. Zone-specific cell biosynthetic activity in mature bovine articular cartilage: a new method using confocal microscopic stereology and quantitative autoradiography. J Orthop Res 14(3):424-32.

Zhang Z, McCaffery JM, Spencer RG, Francomano CA. 2004. Hyaline cartilage engineered by chondrocytes in pellet culture: histological, immunohistochemical and ultrastructural analysis in comparison with cartilage explants. J Anat 205(3):229-37.

CHAPTER VI

Conclusions and Recommendations

The objective of this dissertation has been to characterize the centrifugal bioreactor and subsequently broaden its applications in cell culture. The CCBR is a unique system with much potential for various bioprocessing applications due to cell immobilization resulting in high density culture. Cell immobilization techniques employed by other high density bioreactors rely on mechanical immobilization and consequently diffusion is the method of transport for nutrients and metabolites exchange. This leads to inactive portions of the biomass and heterogeneous product yield [1]. This limitation is circumvented during CCBR culture as convective transport results from direct suspension of individual cells against a continuous centrifugal force by drag from fluid flow, ultimately providing a homogeneous growth environment.

The forces associated with CCBR operation are centrifugal force from system rotation, drag force as a result of medium flow, and buoyancy due to a difference in density between the cells and suspending medium. When centrifugal force is balanced with opposing drag and buoyant forces cells will be immobilized in the reactor chamber and culture densities exceeding 10^8 cells/mL can be maintained. It is this one of a kind cell immobilization technique employing both system rotation and high medium flow rates which provides many unique attributes and cell culture opportunities for this system.

Resulting from the cell immobilization technique, specifically system rotation is the presence of Coriolis forces, an imaginary force which does no work on a material element. The effect of Coriolis forces on the fluid dynamics in a CCBR operated without the presence of cells is examined in Chapter II with the use of numerical simulations and experimental observations. Examination of the dimensionless Rossby number confirms the importance of considering

Coriolis forces during CCBR fluid dynamic analysis. At the widest reactor cross-section under operating conditions of 100 and 600 RPM and an inlet velocity of 4.3 cm/s Rossby numbers of 3 x 10^{-4} and 5 x 10^{-5} are found, respectively. A value much less than one indicates a significant contribution from Coriolis forces on the fluid flow profile; a result which is further confirmed through numerical simulations and dye injection experiments.

Simulation results show fluid entering the reactor, flows up the leading wall of the chamber to its widest cross-section, and at the point where the walls of the chamber begin to converge back to the outlet the fluid transverses the chamber in a skewed "N" shaped path to the opposite wall, along which fluid flows to the exit. Experimentation confirms these findings, particularly flow along the leading wall of the chamber. However, some discrepancies between simulation and experimental results appear which can be attributed to differences between dyed and un-dyed solution density and the inclusion of required artificial diffusion for simulation convergence. Furthermore, simulation and experimental results confirm the presence of a circuitous flow profile persisting for all typical cell culture operating conditions raising concerns about nutrient distribution and cell retention mechanisms during CCBR cell culture.

The subsequent chapter of this dissertation, Chapter III, investigates cell retention and the impact of cells on the previously reported flow profile in Chapter II. Dye injection experiments and simulations were performed while retaining 5 x 10^{8} total cells in the CCBR using PBS as the suspending medium. Both simulations and experiments show that for a particular reactor setting a unique cell density in the CCBR results. At a constant experimental inlet velocity of 6.5 cm/s, a 5.5 mL cell bed with a density of 9.1 x 10^{7} cells/mL results at 650 RPM, while at 920 RPM a decreased equilibrium volume of 3.4 mL and increased density of 1.5 x 10^{8} cells/mL is observed; corresponding to maximum cell volume fractions of 0.16 and 0.26 for each RPM, respectively.

Numerical simulations using COMSOL were able to predict similar cell volume fractions throughout the CCBR; 0.15 at 650 RPM and 0.22 at 920 RPM each with an inlet velocity of 6.5 cm/s.

The cell bed volume dependence on reactor settings both in simulations and experimentation is analogous to a traditional fluidized bed in which bed volume is dependent on fluid velocity, indicating cells in the CCBR behave as a high density fluidized bed. The presence of a fluidized bed of cells was further confirmed during dye injection experiments from which results showed a continual uniform darkening of the cell bed. The absence of any observable dye gradient within the cell bed indicates the region is well mixed. Simulation results similarly predicted a stable flow profile, again leading to the conclusion the cell bed is well mixed.

One prediction which could not be confirmed experimentally is that simulation results predicted an increased cell volume fraction, 10-50%, along the trailing wall of the reactor just past the inlet, corresponding to the same region shown to have little flow due to the Coriolis effect in results presented in Chapter II. This result and a similar Rossby number assessment suggest the increased cell density in this region is likely due to Coriolis forces resulting in a minimally preferential flow of fluid along the leading wall of the reactor during cell culture. Although Coriolis forces do not result in a stable skewed flow pattern during cell culture their presence must still be acknowledged even though their effect is masked by the presence of cells.

The simulation was further used to investigate varying cell size from 10-20 μm and the subsequent effect on maximum cell volume fraction and distribution throughout the reactor. It is shown that as cell size decreases the maximum cell volume fraction decreases from 0.25 to 0.1 for 20 and 10 μm cells respectively. The decrease in maximum cell volume fraction ultimately increases cell distribution throughout the reactor chamber which limits cell retention as cell size

is decreased at a particular set of operating conditions. This exercise shows that for each cell type and desired culture density, there exists a unique set of operating conditions which can be predicted with reasonable accuracy through numerical simulation and then fine-tuned during culture to reach desired densities for various applications.

The greatest shortcoming of Chapters II and III is the complicated nature of the COMSOL models developed to simulate the CCBR environment. This would not pose an issue if not for computational hardware limitations which do not allow for models to be solved with a significantly large number of nodes to eliminate necessary artificial diffusion and error. This is most apparent in the modeling in Chapter III where the fluidized bed of cells is simulated. One of the major differences between the simulation and experimental results was that a sharp interface between the top of the cell bed and the suspending medium was observed experimentally which could not be predicted with the simulation. The simulation predicted a gradient in cell volume fraction at the top of the cell bed which became steeper indicating the sharpening of the cell bed interface as the mesh density was increased; however memory limitations prevented a solution using a significantly dense mesh to predict the sharp interface. In the future as computational hardware increases in capability, revisiting this model in an attempt to simulate the cell interface may further increase the similarity between the simulation and experimental results.

During high density mammalian cell culture dilution rate is equally important as reactor setting of RPM and inlet fluid velocity. Dilution rate provides the method to maintain adequate nutrient concentrations and limits metabolite accumulation during continuous CCBR culture. Chapter IV presents the development of a kinetic model derived from low density batch cultures which may be extended to the high density continuous CCBR culture of hyrbidoma cells. A

modified Monod kinetic model was applied to the system using batch cultures and an initial rate approach. The kinetic model is capable of predicting glucose, lactate, ammonium ion, and monoclonal antibody concentrations within 13% during culture.

During high density cell culture, changes in cell concentration can lead to rapid environmental changes, namely substrate and metabolite concentrations. Using the developed kinetic model it is possible to predict and control these concentrations ensuring the maximum cellular growth rate and corresponding growth associated mAb production rate are maintained. A CCBR culture inoculated with 1×10^7 cells/mL and maintained with a dilution rate of 1.6 h^{-1} will result in a growth rate which is 90% of the maximum specific cell growth rate. If cell density increases to 2×10^8 cells/mL and the dilution rate remains unchanged the cellular growth rate will be depressed to 31% of the maximum due to substrate depletion and metabolite accumulation, likely leading to culture loss. However, use of the kinetic model predicts that 2×10^8 cells/mL can be maintained at 90% of the maximum growth rate is dilution rate is increased to 33 h^{-1}. As has been shown in the previous chapter CCBR settings lead to a specific culture density, but if environmental conditions are not maintained near optimal, loss of the entire culture are imminent. This kinetic model provides a tool with which optimal dilution rate requirements can be determined and maintained as the culture matures and cell density varies.

Use of the CCBR for suspension cultures is advantageous as cells are immobilized allowing increased culture densities accompanied by convective transport of nutrients and waste. However, CCBR culture can be extend to adherent cell types requiring mechanical stimulation as the cell immobilization technique provides both hydrostatic pressure and shear force simultaneously during culture. Hydrostatic pressure is the result of system rotation and can vary from 8 kPa to 0.5 MPa, while shear force, variable from 0.02-1.4 N/m^2, results from the flow of

fluid past immobilized cells or tissues. Each of these forces is individually adjustable to meet specific needs.

The use of the CCBR to culture isolated chondrocytes as a high density suspension culture which develops into a cartilaginous tissue over 3 weeks is presented in Chapter V. In this work isolated chondrocytes are seeded into the CCBR and stressed at a constant hydrostatic pressure, 0.03 MPa, and shear rate of 0.11 N/m^2 for the first week of culture. After the first week cultures were stressed intermittently 4 times per day by increasing RPM to either 900 or 1650 RPM corresponding to 0.07 and 0.26 MPa, respectively.

Biochemical analysis shows that bioreactor tissue constructs have less GAG/DNA, 1.4 ± 0.1 μg/μg, than pellet cultures, 6.9 ± 1.1 μg/μg, at the 1 week time point, but similar levels of collagen/DNA for both bioreactor and pellet cultures, 2.7 ± 0.6 μg/μg and 1.8 ± 0.4 μg/μg, respectively. At the 3 week time point GAG/DNA content has increased in the bioreactor tissue constructs to 5.6 ± 1.5 μg/μg for 900 RPM cultures and 4.1 ± 0.9 μg/μg for 1650 cultures, as compared to 8.3 ± 0.9 μg/μg found in pellet cultures. Again, similar levels of collagen/DNA were observed at the 3 week time point for all culture conditions; 6.6 ± 1.9 μg/μg for pellet cultures, 6.8 ± 3.5 μg/μg for 900 RPM cultures, and 5.1 ± 0.4 μg/μg for 1650 RPM cultures. Histological results similarly confirmed these findings that pellet cultures and both CCBR culture conditions produced a tissue stained similarly for both GAG and collagen while cell morphology remained rounded indicating cells remained differentiated.

Although these results do not show that the mechanical forces applied by the CCBR stimulated chondrogenesis beyond that of the high density pellet culture, a novel use of the CCBR to maintain a tissue construct for 3 weeks with a continuous supply of fresh medium has been shown. The CCBR allows for precise control of nutrients, metabolites, and growth factors

to study their effect in the dynamic CCBR environment as all have been shown to stimulate chondrogenesis [2-5]. The CCBR provides a unique opportunity to study the simultaneous application of hydrostatic pressure and shear force to a developing cartilage construct, and optimization of this process, particularly the stressing regimens, will allow for the study of cartilage development through future studies.

Potential of the CCBR system to study cartilage development remains, but some modifications in operating conditions and design may be required. Integration of a computer allowing for digital control of pump speed and RPM would allow for more elaborate stressing regimens, for instance the frequency between high and low stress settings could be increased. Another alternative may be to use a scaffold in conjunction with the bioreactor. Mechanical immobilization of scaffolds would allow for the use of the CCBR's centrifugal force to seed scaffold with chondrocytes at high densities. After seeding a scaffold at high density the CCBR could provide a long term culture environment where nutrient concentrations are precisely controlled the multiple mechanical forces are dynamically applied.

Other tissue culture opportunities employing the CCBR include the use of mesenchymal stem cells (MSC), chondrocyte precursors, to investigate how the mechanical environment may stimulate chondrocyte differentiation for cartilage repair. One other possibility may be to culture epithelial cells in an attempt to produce an artificial skin tissue with the objective to recreate the thin film of cells observed around the inside of the reactor chamber during chondrocyte culture. While tissue culture using this system has just recently been exposed as a promising avenue of research, there remains many opportunities to immobilize cells and study cell-cell interactions in a dynamic high density environment.

References

1. Yang, P.; Teo, W.-K.; Ting, Y.-P., Design and performance study of a novel immobilized hollow fiber membrane bioreactor. *Bioresource Technology* **2006,** 97, (1), 39-46.

2. Mauck, R. L.; Wang, C. C.; Oswald, E. S.; Ateshian, G. A.; Hung, C. T., The role of cell seeding density and nutrient supply for articular cartilage tissue engineering with deformational loading. *Osteoarthritis Cartilage* **2003,** 11, (12), 879-90.

3. Arikawa, T.; Matsukawa, A.; Watanabe, K.; Sakata, K. M.; Seki, M.; Nagayama, M.; Takeshita, K.; Ito, K.; Niki, T.; Oomizu, S.; Shinonaga, R.; Saita, N.; Hirashima, M., Galectin-9 accelerates Transforming Growth Factor beta3-induced differentiation of human mesenchymal stem cells to chondrocytes. *Bone* **2009**.

4. Connelly, J. T.; Wilson, C. G.; Levenston, M. E., Characterization of proteoglycan production and processing by chondrocytes and BMSCs in tissue engineered constructs. *Osteoarthritis Cartilage* **2008,** 16, (9), 1092-100.

5. van der Kraan, P. M.; Buma, P.; van Kuppevelt, T.; van den Berg, W. B., Interaction of chondrocytes, extracellular matrix and growth factors: relevance for articular cartilage tissue engineering. *Osteoarthritis Cartilage* **2002,** 10, (8), 631-7.